Department Chemie
der Technischen Universität München

ParaGauss — A Parallel Implementation of the Density Functional Method: EPR g-Tensors and Hyperfine Coupling Constants in the Douglas–Kroll–Hess Approach

Dmitri I. Ganiouchine

Vollständiger Abdruck der von der Fakultät für Chemie der Technischen Universität München zur Erlangung des akademischen Grades eines

Doktors der Naturwissenschaften (Dr. rer. nat.)

genehmigten Dissertation.

Vorsitzender: Univ.-Prof. Dr. F. H. Köhler
Prüfer der Dissertation
1. Univ.-Prof. Dr. N. Rösch
2. Univ.-Prof. Dr. M. Kleber

Die Dissertation wurde am 03.06.2004 bei der Technischen Universität München eingereicht und durch die Fakultät für Chemie am 01.07.2004 angenommen.

Contents

List of Abbreviations

AO	atomic orbital
BP	Becke–Perdew
BQ	benzoquinone
CISD	configuration interaction (with) singlets (and) doublets
DF	density functional (method)
DFT	density functional theory
DK	Douglas–Kroll (method)
DKH	Douglas–Kroll–Hess (approach)
DKS	Dirac–Kohn–Sham (equation)
DQ	duroquinone
ee	electron-electron (interaction)
EPR	electronic paramagnetic resonance
GGA	generalized gradient approximation
GHF	general Hartree-Fock (method)
GIAO	gauge including atomic orbitals
GTO	Gaussian-type orbital
IGLO	individual gauge for localized orbitals
HF	Hartree–Fock (method)
HFCC	hyperfine coupling constant
HOMO	highest occupied molecular orbital
KS	Kohn–Sham
LCGTO	linear combination of Gaussian-type orbitals
LDA	local density approximation
LUMO	lowest unoccupied molecular orbital
MRCI	multi-reference configuration interaction
NCSDF	noncollinear spin density functional
NMR	nuclear magnetic resonance
PW	Perdew-Wang
RKS	restricted Kohn-Sham
ROKS	restricted open-shell Kohn-Sham
SCF	self-consistent field
SI	self-interaction

SNSO	screened nuclear spin-orbit (interaction)
SO	spin-orbit
SOMO	singly occupied molecular orbital
SOS	sum-over-states
SR	scalar relativistic (model)
STO	Slater-type orbital
VWN	Vosko–Wilk–Nusair (*xc* functional)
UKS	unrestricted Kohn-Sham
xc	exchange-correlation (potential, functional)
ZORA	zero-order regular approximation

Chapter 1

Introduction

Electron paramagnetic resonance (EPR) spectroscopy represents one of the most powerful experimental methods for investigating electronic and structural features of systems containing unpaired electrons, such as radicals, coordination compounds and paramagnetic sites in solids [1, 2]. Also, the theoretical foundations of these methods are well established [3]. A large amount of EPR data have been collected for a large variety of open-shell systems relevant for physics, chemistry, and biology [4, 5, 6, 7, 8] since the invention of this spectroscopic technique in 1945 by the Russian physicists E. K. Zavoisky.

The EPR method deals with interactions of electrons of a molecular system with a static external magnetic field modified by the magnetic field of the nuclei of the system. These interactions can be described by a so-called effective spin Hamiltonian, chosen to reproduce the experimentally observed spectroscopic transitions.

The term $\hat{H}_Z^{eff}$ that represents the electronic Zeeman interaction (with a typical level splitting of $\backsimeq 1$ cm^{-1}) in such an effective spin Hamiltonian reads

$$\hat{H}_Z^{eff} = \mu_B \vec{B}^0 \cdot \mathbf{g} \cdot \vec{\tilde{S}} \; . \tag{1.1}$$

Here, μ_B is the Bohr magneton, $\vec{B}^0$ is the external homogeneous magnetic field, $\vec{\tilde{S}}$ is the operator of the fictitious spin, and $\mathbf{g}$ is a 3×3 matrix, commonly referred to as $\mathbf{g}$-tensor [3, 2, 1]. The latter accounts for the orientational dependence of the Zeeman splitting of the molecule under study with respect to the external field and (after diagonalization) it yields three g-values which quantify the the Zeeman interaction.

The interaction between a magnetic moment of an unpaired electron with the magnetic moments of N nuclei comprising the radical, results in another term of the effective spin Hamiltonian, the hyperfine term $\hat{H}_{hf}^{eff}$, which is characterized by a typical level splitting of $\backsimeq 10^{-1}$ cm^{-1},

$$\hat{H}_{hf}^{eff} = \sum_{\nu=1}^{N} \vec{\tilde{S}} \cdot \mathbf{a}^{\nu} \cdot \vec{I}_{\nu} \; , \tag{1.2}$$

where $\vec{I}_\nu$ is the nuclear spin operator and $\mathbf{a}^\nu$ the 3×3 hyperfine interaction tensor of nucleus ν. That tensor is commonly separated into the orientational independent (isotropic, a^ν_{iso}) and orientational dependent components (anisotropic, traceless magnetic dipolar, $\mathbf{t}^\nu$), $\mathbf{a}^\nu = a^\nu_{iso} + \mathbf{t}^\nu$ [1]. a^ν_{iso} arises from the *contact* interaction between an electron and nucleus ν and is called Fermi contact term. This term is the only one which can be detected in liquid solutions due to the spatial averaging of hyperfine interactions caused by the random and rapid tumbling of molecules. The other tensor components can be separately obtained, for instance, if the molecule in question is trapped in a matrix or a crystal [1]. The $\mathbf{a}^\nu$-tensor yields three principal values, commonly referred to as hyperfine coupling constants (HFCCs).

As we have seen, **g**- and **a**-tensors are fundamental quantities derived from EPR experiments. These parameters are very sensitive to the details of the geometric and electronic structure of an open-shell system and they often furnish unique structural-chemical information [9, 10, 11, 12]. Unfortunately, the relation of the experimentally measured data, in particular g-values, to details of the electronic structure is not straightforward [3] and calls for the application of molecular quantum mechanical methods. Due to significant complications, reliable first-principles quantum mechanical description of EPR parameters became possible essentially only in the past decade [13, 14, 15, 16].

At least two factors make the theoretical prediction of EPR parameters difficult. The first factor is connected to the fact that the spin-orbit (SO) interaction has to be treated accurately; indeed, deviations of g-values from the free-electron value g_e are inherently a relativistic SO phenomenon in systems with quenched orbital momentum [2]. Also, there are situations, where the (generally small) effect of the SO interaction on HFCCs can become significant [17, 18, 19].

The second difficulty is related to the fact that an accurate description of electron correlation is required. For transition metals systems, this condition is crucial in particular for the isotropic part of HFCCs which is proportional to the spin density at the position of a nucleus. Also, in such systems, the very delicate core-shell spin polarization should be precisely taken into account [2, 20, 18].

The first attempts to determine **g**-tensors at a high level of computation used *ab-initio* approaches, based on the Hartree-Fock (HF) method, and applied second-order static perturbation theory to the Breit-Pauli Hamiltonian [3, 21, 22, 23, 24, 25]. Later, more sophisticated wave function approaches such as restricted open-shell Hartree-Fock [26] and multireference configuration interaction (MRCI) methods [27, 28, 29, 30] were also utilized. Although the HF method can be applied to large molecules, it yields significantly less accurate results for **g**-tensors than the more demanding post-HF approaches, which are limited in application to small systems. All of these approaches are formulated as a sum-over-states (SOS) theories: their application relies on the calculation of a sufficient large number of excited state wave functions, which is often a rather time consuming task. The summation over excited states can be avoided by using a response theory treatment,

where the explicit SOS expansion is replaced by an analytical linear response function [31, 32].

Computational difficulties of HFCCs calculations are usually concerned with the isotropic Fermi contact part; at the same time, theoretical predictions of the anisotropic parts of HFCCs are generally in good agreement with experiment and not very sensitive to the choice of the computational methods and basis sets [13]. As a rule, the unrestricted Hartree-Fock (UHF) approach significantly overestimates the isotropic contribution to HFCCs [13]. This rather poor performance requires one (as in the case of **g**-tensors) to employ more sophisticated post-HF methods, such as configuration interaction [33, 34, 35, 36, 37, 38, 39], coupled cluster [40, 41, 42], and many-body perturbation theory *ab-initio* [43, 44, 45] schemes, which are not easily applicable to large complexes. Moreover, these methods demand very accurate and thus very large basis sets to obtain a satisfactory description of the electron distribution at the nuclei and in the "outer" valence regions. These requirements of large balanced basis sets and highly correlated *ab-initio* treatments again limit these kinds of studies to relatively small benchmark systems [13].

Density functional theory (DFT) provides a favorable alternative to the CPU and memory intensive correlated *ab-initio* methods for calculating magnetic properties of molecular systems, because DFT treatments allow one to account for electron correlation at a computational cost not much larger than that of the HF approach [46]. DFT methods made it possible to treat much larger systems in accurate first-principles theoretical studies [46].

Conventional one-component density functional (DF) methods for **g**-tensors calculations employ second-order perturbation theory for Zeeman and SO operators based on solutions of the unrestricted Kohn-Sham (KS) equations which are obtained with either localized (molecular) [47, 48, 49] or plane-wave basis sets [50]. The first one-component DF calculations of HFCCs used first-order perturbation theory for the non-relativistic hyperfine Hamiltonian and completely neglected SO interaction [51, 52, 53, 54]. Subsequent implementations differed by including SO effects with the help of perturbation theory applied to one-component KS solutions that were obtained in different approximations [55, 56, 18, 19].

The applicability of the above mentioned perturbational approaches can be questioned at least in two aspects. First, those methods generally require the summation over (formal) electronic excitations characterized by energies and spatial behavior of virtual (unoccupied) states; the accuracy of these features is not very high (especially in DF calculations) and the sum over states has to be truncated at some point, without guarantee of rapid convergence when exited states are ordered with respect to the energy [3]. Second, perturbation theory is accurate only for weak SO interactions. Because relativistic effects are known to grow as the square of atomic number Z [57], the deficiency of the perturbation approach can become substantial already in molecules formed by rather light atoms [47].

An alternative efficient approach was built for calculating electronic **g**-tensors by including SO interaction variationally into the equations using a formalism based on two-

component wave functions [58]. In this case, only the magnetic interaction needs to be included in the perturbation scheme by means of simple first-order perturbation theory. The idea that the scalar relativistic (SR) (mass-velocity and Darwin) contributions play a minor role for calculating molecules without rather heavy elements leads to the general Hartree-Fock (GHF) approach [58]; there, SO interaction is taken into account variationally and the SR components are neglected. The accuracy of this method is better than that of the one-component DF approach [58, 47] and it is almost as good as in demanding MRCI calculations [28]. However, for systems that contain heavy elements this promising GHF approach would need to be improved. The lack of an adequate description of SR and computationally expensive electron correlation effects significantly restricts the class of species tractable by this approach.

To combine SR effects with SO effects variationally one has to start from the four-component Dirac equation. In a fully relativistic four-component Dirac method the perturbation operator for calculating electronic Zeeman splittings and hyperfine couplings are rather simple [3]. This approach for calculating HFCCs and electronic **g**-tensors has first been implemented in the framework of the scattered-wave Xα method [59]. Of course, one can also employ a Dirac-Hartree-Fock method [60].

Switching from the four-component Dirac method with both electronic and positronic solutions to a two-component Kohn-Sham method (which describes only electronic states), one arrives at probably the most attractive formulation of the method for calculating electronic **g**-tensors and HFCCs known to date. In such a method the eigenfunctions include SO and SR effects self-consistently. This feature makes such a scheme applicable both to light and heavy (e.g. *d*- and *f*-element) molecular systems in a rather economic fashion. A DF scheme to calculate **g**-tensors and HFCCs, as just outlined, has been implemented within the zero-order regular approximation (ZORA) formalism [61, 17] and validated for radicals containing metal atoms [62] and for transition metal complexes of biological relevance [63, 64]. Along with a number of very advantageous features of this approach, one should also mention the restriction on inclusion of spin polarization effects together with two-component SO treatment, namely contributions to the calculated magnetic parameters are limited to those of a singly-occupied molecular orbital (SOMO) only [61].

One of the most reliable and efficient relativistic DF method in modern quantum chemistry is the Douglas-Kroll (DK) approach [65]. In combination with the technique for an approximate evaluation of momentum-dependent operators in a finite basis set developed by Hess et al. [66], this formalism is referred to as Douglas-Kroll-Hess (DKH) method. With the DKH approach, the relativistic linear combination of Gaussian-type orbitals DF method solves the two-component Kohn-Sham equations by means of an expansion of the orbital solutions in a Gaussian-type basis set [67, 68]; this method was recently implemented in the parallel DF package ParaGauss [69, 70, 71].

The goal of this thesis was to employ the two-component DKH method implemented in ParaGauss and to adapt it for calculating electronic **g**-tensors and HFCCs. This

thesis contains the DKH formalism modified for the case of magnetic interactions along with details of the implementation for HFCCs and **g**-tensors, benchmark calculations, and applications.

The thesis has the following structure. Chapter 2 outlines the DKH formalism, where a magnetic field is introduced by a vector potential using a gauge-invariant momentum substitution into the four-component Dirac-Kohn-Sham (DKS) equation. Application of the DK transformations to the DKS equation leads to the general two-component magnetic interaction operator, which can be used for calculating HFCCs and **g**-tensors.

In Chapter 3, the two-component hyperfine Hamiltonian is derived from the magnetic interaction operator of Chapter 2, by employing the explicit form of a vector potential taken from a classical expression for the vector potential of a magnetic nucleus. Then, the link between the quantum chemical treatment and the actual EPR spectra is illustrated by connecting the hyperfine Hamiltonian to **a**-tensor. Test HFCCs calculations of atoms and small molecules are also presented.

In Chapter 4, the Zeeman Hamiltonian is derived using the explicit form of a vector potential of a homogeneous magnetic field. The formalism to calculate experimentally observed EPR **g**-tensors is presented along with test calculations. This method is similar to the approach of Neyman et al. [72], except it is extended from the first to the second-order DKH transformation of the magnetic interaction operator.

Chapter 5 provides the details of the modifications of the integral part of the Para-Gauss code which carried out to enable calculations of HFCCs and **g**-tensors.

Chapter 6 is devoted to the application of the developed formalism to calculate **g**-tensors that reflect hydrogen-bonding effects in semiquinone anion radicals. These calculations demonstrate that the new computational scheme is able to describe very delicate effects of a hydrogen bonding. Also, general trends of how the **g**-tensor depends on the structure of hydrogen-bonded semiquinone complexes are explored. This chapter presented a work of Neyman et al. [73].

Finally, in Chapter 7 the developed method to calculate **g**-tensors is applied to the analysis of electronic g-values of surface complexes formed by probe NO molecules with Na^+ and Cu^+ cations in zeolites. A new scheme is developed and implemented to analyze g-values in terms of parameters of the electronic structure. This chapter is based on a work of Neyman et al. [74].

Part I

Theory

Chapter 2

The Magnetic Hamiltonian in the Two-Component Douglas-Kroll Kohn-Sham Method

2.1 The Douglas-Kroll Scheme

The KS approach to relativistic DFT leads to an effective four-component one-particle method [75, 76, 77]. The corresponding Hamiltonian $\hat{H}^{(4)}_{DKS}$ of this DKS problem contains an effective one-particle potential v_{eff} which describes the interactions in a many-electron system [75]:

$$\hat{H}^{(4)}_{DKS} = c\vec{\alpha} \cdot \vec{p} + \beta c^2 + v_{eff} \ . \tag{2.1}$$

Here $\vec{p}$ is the mechanical momentum, c is the speed of light, and $\vec{\alpha}$, β are the 4×4 Dirac matrices [78]

$$\vec{\alpha} = \begin{pmatrix} 0 & \vec{\sigma} \\ \vec{\sigma} & 0 \end{pmatrix}, \ \beta = \begin{pmatrix} 1 & 0 \\ 0 & -1 \end{pmatrix} \ , \tag{2.2}$$

$\vec{\sigma}$ is the vector of the 2×2 Pauli spin matrices

$$\vec{\sigma} = \begin{pmatrix} \sigma_x \\ \sigma_y \\ \sigma_z \end{pmatrix}, \ \sigma_x = \begin{pmatrix} 0 & 1 \\ 1 & 0 \end{pmatrix}, \ \sigma_y = \begin{pmatrix} 0 & -i \\ i & 0 \end{pmatrix}, \ \sigma_z = \begin{pmatrix} 1 & 0 \\ 0 & -1 \end{pmatrix} \ . \tag{2.3}$$

Throughout this work, atomic units will be used where formally Planck's constant $\hbar$, the elementary charge e, the rest mass m of the electron, and $4\pi\varepsilon_0$ are set to 1. Eigenfunctions $\varphi^{(4)}$ of the DKS equation, Eq. (2.1), are four-component spinors:

$$\varphi^{(4)} = \begin{pmatrix} \varphi_L \\ \varphi_S \end{pmatrix}, \ \varphi_L = \begin{pmatrix} \varphi_L^{\alpha} \\ \varphi_L^{\beta} \end{pmatrix}, \ \varphi_S = \begin{pmatrix} \varphi_S^{\alpha} \\ \varphi_S^{\beta} \end{pmatrix} \ . \tag{2.4}$$

For chemical systems under study here, it is convenient to separate these four-component spinors into two two-component spinors φ_L and φ_S, so-called "large" and "small" components, respectively, which describe electronic and positronic degrees of freedom. α, β indicate the usual spin components [78]. The effective potential v_{eff} is a sum of the external potential, which for a molecule is usually the potential v_{nuc} set up by the nuclei, and the electron-electron (ee) potential v_{ee}. In turn, the ee potential includes the Hartree potential v_H (the classical Coulomb potential due to the electron charge distribution) and the exchange-correlation (xc) potential v_{xc} [46],

$$v_{eff} = v_{nuc} + v_{ee} = v_{nuc} + v_H + v_{xc} \ . \tag{2.5}$$

The Hamiltonian $\hat{H}^{(4)}_{DKS}$ describes both electronic (positive energy) and positronic (negative energy) solutions. Although it is possible to treat the Hamiltonian of Eq. (2.1) in a four-component way, it causes significant complications. Because the DKS Hamiltonian has the form of a Dirac Hamiltonian, it is not bounded from below and exhibits solutions of negative energy [79]. Therefore, the corresponding four-component KS problem may not be solved directly in a finite basis set using a variational principle. The KS eigenvalue problem generates spurious solutions, which do not converge to the exact solutions; the effect is known as "variational collapse" [80, 81]. One way to overcome this problem is to employ a specially constructed "kinetically balanced" basis sets [80, 82]. This strategy makes conventional quantum chemistry calculations feasible [83, 84, 85], and can be applied for obtaining stable solutions of a four-component KS problem.

However, when dealing with most problems of chemistry, only electronic, positive energy solutions are *explicitly* needed. For them, in the regions where the potential is not extremely strong, $|\varphi_L| >> |\varphi_S|$. This suggests to search for a transformation of the four-component DKS Hamiltonian into a set of two equivalent two-component Hamiltonians, one for electrons and another for positrons [3]. One way to reduce the four-component Hamiltonian $\hat{H}^{(4)}_{DKS}$ to a an electronic two-component Hamiltonian is to perform a unitary Douglas-Kroll (DK) transformation U [65] of the DKS Hamiltonian

$$\hat{H}^{(4)}_{DK} = U\hat{H}^{(4)}_{DKS}U^{\dagger} = \begin{pmatrix} \hat{H}^{(2)}_{DK} & 0 \\ 0 & \hat{H}^{(-2)}_{DK} \end{pmatrix} \ . \tag{2.6}$$

The transformation U decouples the four-component eigenvalue problem

$$\hat{H}^{(4)}_{DKS}\varphi^{(4)} = \epsilon\varphi^{(4)} \tag{2.7}$$

into a system of two equivalent two-component eigenvalue problems, the electronic and the positronic one

$$\hat{H}^{(2)}_{DK}\varphi^{+} = \epsilon^{+}\varphi^{+} \ , \tag{2.8}$$

$$\hat{H}^{(-2)}_{DK}\varphi^{-} = \epsilon^{-}\varphi^{-} \ . \tag{2.9}$$

The eigenfunctions of $\hat{H}^{(4)}_{DK}$ and $\hat{H}^{(4)}_{DKS}$, $\varphi^{(4)}_{DK}$ and $\varphi^{(4)}$, are related to each other via the transformation U, either (for positive energy solutions)

$$\varphi^{(4)+}_{DK} = \begin{pmatrix} \varphi^{+} \\ 0 \end{pmatrix} = U \begin{pmatrix} \varphi_L \\ \varphi_S \end{pmatrix}^{+} = U\varphi^{(4)+} \; . \tag{2.10}$$

or (for negative energy solutions)

$$\varphi^{(4)-}_{DK} = \begin{pmatrix} 0 \\ \varphi^{-} \end{pmatrix} = U \begin{pmatrix} \varphi_L \\ \varphi_S \end{pmatrix}^{-} = U\varphi^{(4)-} \; . \tag{2.11}$$

Douglas-Kroll transformation U consists of series of n transformations $U = U_n ... U_1 U_0$ which decouples DKS Hamiltonian up to the n-th order in (υ_{eff}/E_p), where E_p is the relativistic energy of a free particle. In the present implementation of ParaGauss [75, 86], all terms of $\hat{H}^{(4)}_{DKS}$ are diagonal up to the second order in (υ_{eff}/E_p), except the potential υ_{xc}:

$$\hat{H}^{(4)}_{DK,1} = U_1 U_0 \hat{H}^{(4)}_{DKS} U_0^{\dagger} U_1^{\dagger} = \begin{pmatrix} \hat{H}^{(2)}_{DK,1} & \mathcal{O}\left[(\upsilon_{eff}/E_p)^2\right] \\ \mathcal{O}\left[(\upsilon_{eff}/E_p)^2\right] & \hat{H}^{(-2)}_{DK,1} \end{pmatrix} \; . \tag{2.12}$$

In ParaGauss, the relativistic transformation of the potential υ_{ee} [87, 77, 71], Eq. (2.5), is currently restricted to the Hartree potential term to exploit the advantage connected with the analytical density-fit approach to this term [88]. A relativistic transformation of the *xc* potential, which is evaluated numerically on a grid, would be too demanding. Fortunately, this restriction of the relativistic treatment to the Hartree term can often be justified because commonly υ_{xc} is much smaller than υ_H [89]. Introduction of an analytic representation of the *xc* term via a fitting technique [88] would make a relativistic transformation of υ_{xc} feasible.

2.2 Introduction of a Magnetic Field "Picture Change" Effect

To calculate magnetic properties, such as electronic **g**-tensors and hyperfine coupling constants (HFCCs), we need to introduce a magnetic field into the field-free Hamiltonian, Eq. (2.1). One can achieve this by making the common minimal substitution to a gauge-invariant momentum [57]. As a result, the electronic momentum operator $\vec{p}$ is substituted by $\vec{\pi}$ defined as:

$$\vec{p} \rightarrow \vec{\pi} = \vec{p} + \vec{A}/c \; . \tag{2.13}$$

Here, $\vec{A}$ is the vector potential of the magnetic field. Thus, the DKS Hamiltonian, which includes a magnetic field, reads:

$$\hat{H}^{(4)}_{DKS,A} = c\vec{\alpha} \cdot \vec{p} + \beta c^2 + \upsilon_{eff} + \vec{\alpha} \cdot \vec{A} \; . \tag{2.14}$$

The term $\vec{\alpha} \cdot \vec{A}$ is assumed to be small and can be considered as a perturbation to the DKS Hamiltonian Eq. (2.1). Therefore, first-order perturbation theory can be applied for obtaining the first-order energy change of the Hamiltonian $\hat{H}^{(4)}_{DKS,A}$.

If the magnetic perturbation $\hat{H}^{(4)}_A = \vec{\alpha} \cdot \vec{A}$ is introduced into the unperturbed problem

$$\hat{H}^{(4)}_{DKS} \varphi^{(4)}_0 = \epsilon_0 \varphi^{(4)}_0 \ , \tag{2.15}$$

one needs to solve

$$\left(\hat{H}^{(4)}_{DKS} + \hat{H}^{(4)}_A \right) \varphi^{(4)} = \left(\epsilon_0 + \epsilon_A \right) \varphi^{(4)} \ . \tag{2.16}$$

In first-order perturbation theory, the resulting energy change ϵ_1 of the unperturbed system can be expressed as expectation value of the perturbation operator in the unperturbed state $\varphi^{(4)}_0$ [90]:

$$\epsilon_1 = \left\langle \varphi^{(4)}_0 \left| \hat{H}^{(4)}_A \right| \varphi^{(4)}_0 \right\rangle \ . \tag{2.17}$$

In terms of the DK unitary transformed eigenvalue problem

$$\hat{H}^{(4)}_{DK} \varphi^{(4)}_{0,DK} = \epsilon_0 \varphi^{(4)}_{0,DK} \ , \tag{2.18}$$

the corresponding expression becomes

$$\epsilon_1 = \left\langle \varphi^{(4)}_0 \left| U U^\dagger \hat{H}^{(4)}_A U U^\dagger \right| \varphi^{(4)}_0 \right\rangle \tag{2.19}$$

$$= \left\langle \varphi^{(4)}_0 U^\dagger \left| U \hat{H}^{(4)}_A U^\dagger \right| U \varphi^{(4)}_0 \right\rangle \tag{2.20}$$

$$= \left\langle \varphi^{(4)}_{0,DK} \left| U \hat{H}^{(4)}_A U^\dagger \right| \varphi^{(4)}_{0,DK} \right\rangle \ . \tag{2.21}$$

Thus, the calculation of the expectation value requires the transformation of the perturbation operator. Such a transformation of other operators than the Hamiltonian in the Douglas-Kroll approach is referred to as "picture change" [91, 92].

For calculations of the properties that can be described by a spin-independent operator, e.g. dipole moment, effects of the "picture change" may be neglected [93]; resulting errors are of the order of α^2, where $\alpha = e^2/\hbar c = c^{-1}$ (in atomic units) is the fine structure constant [91]

$$\epsilon_1 \simeq \left\langle \varphi^{(4)}_{0,DK} \left| \hat{H}^{(4)}_A \right| \varphi^{(4)}_{0,DK} \right\rangle \ . \tag{2.22}$$

However, this strategy is not acceptable for calculating magnetic properties. An approach based on the DK wave function $\varphi^{(4)}_{0,DK}$, which has a vanishing "small" component, and on an untransformed perturbation operator would lead to an erroneous result:

$$\epsilon_1 = \left\langle \varphi^{(4)}_{0,DK} \left| \hat{H}^{(4)}_A \right| \varphi^{(4)}_{0,DK} \right\rangle \simeq 0 \ . \tag{2.23}$$

This reflects the fact that the operator of magnetic interactions

$$\hat{H}^{(4)}_A = \begin{pmatrix} 0 & \vec{\sigma} \cdot \vec{A} \\ \vec{\sigma} \cdot \vec{A} & 0 \end{pmatrix} \ , \tag{2.24}$$

which perturbs the field-free Hamiltonian $\hat{H}^{(4)}_{DKS}$, is *odd* [75], i.e. is has only off-diagonal non-zero matrix elements. Therefore, a finite result can only appear as matrix element between electronic and positronic solutions.

Note that the wave functions in practical calculations do not correspond *exactly* to any particular picture because not all terms of the total DK Hamiltonian are treated on the same footing.

It is possible to calculate the energy change ϵ_1 using Eq. (2.17) and back-transformed wave function $\varphi^{(4)}_{0,DK}$. However, evaluation of ϵ_1 according to Eq. (2.21) is preferable because one can profit from the analytical transformations of the magnetic Hamiltonian and identify well-known individual contributions, see Sections 3.1, 4.1.

2.3 Douglas-Kroll Transformations of the Magnetic Hamiltonian

In the following, Douglas-Kroll transformations will be performed by considering the components of the vector potential $\vec{\alpha} \cdot \vec{A}$ as an external potential υ_{eff} and jointly expanding the DK Hamiltonian in powers of the external potential $\vec{\alpha} \cdot \vec{A}$ and υ_{eff}. This strategy was first suggested by Fukuda et al. [94].

Calculations of the magnetic properties require a magnetic Hamiltonian which is linear in $\vec{A}$, but at the same time the transformed Hamiltonian should be accurate up to the second order with respect to the two potentials. The required Douglas-Kroll transformations needs to be applied in two steps. First, the free-particle Fouldy-Wouthuysen transformation U_0 is applied [95]:

$$U_0 = A_p(1 + \beta R_p) = A_p(1 + K_p \beta \vec{\alpha} \cdot \vec{p}) = A_p \begin{pmatrix} \mathbf{1} & K_p \vec{\sigma} \cdot \vec{p} \\ -K_p \vec{\sigma} \cdot \vec{p} & \mathbf{1} \end{pmatrix} , \tag{2.25}$$

which can be expressed in a simple analytical form using the relativistic kinematic factors

$$A_p = \sqrt{\left(E_p + c^2\right)/2E_p} , \tag{2.26}$$

$$K_p = c/\left(E_p + c^2\right) , \tag{2.27}$$

$$R_p = K_p(\vec{\alpha} \cdot \vec{p}) , \tag{2.28}$$

and the relativistic generalization of the kinetic energy

$$E_p = c\sqrt{p^2 + c^2} . \tag{2.29}$$

The transformation U_0 decouples the free-particle Dirac Hamiltonian exactly; it is also useful when applied to the DKS Hamiltonian. The transformed Hamiltonian reads:

$$U_0 \hat{H}^{(4)}_{DKS,A} U_0^\dagger = \beta E_p + E_1^V + E_1^A + O_1^V + O_1^A . \tag{2.30}$$

Here the *odd* terms O_1^V and O_1^A couple large and small components of a four-component spinor $\varphi^{(4)}$, Eq. (2.4). The terms E_1^V and E_1^A are referred to as *even*: they are diagonal in a representation of large and small components, and thus do not couple large and small components of $\varphi^{(4)}$. For first-order *even* operators in the potentials v_{eff} and $\vec{\alpha}\cdot\vec{A}$ we obtain:

$$E_1^V = A_p v_{eff} A_p + A_p R_p v_{eff} R_p A_p \tag{2.31}$$

and

$$E_1^A = \beta A_p \left[R_p \left(\vec{\alpha}\cdot\vec{A} \right) + \left(\vec{\alpha}\cdot\vec{A} \right) R_p \right] A_p \ , \tag{2.32}$$

whereas the *odd* contributions are

$$O_1^V = \beta A_p \left(R_p v_{eff} - v_{eff} R_p \right) A_p \tag{2.33}$$

and

$$O_1^A = A_p \left[\vec{\alpha}\cdot\vec{A} - R_p \left(\vec{\alpha}\cdot\vec{A} \right) R_p \right] A_p \ . \tag{2.34}$$

The first-order DK transformation requires application of a unitary transformation [65, 77]

$$U_1 = \sqrt{1+\hat{W}^2} + \hat{W} = 1 + \hat{W} + \frac{1}{2}\hat{W} + O\left(\hat{W}^3\right) \ , \tag{2.35}$$

with the anti-Hermitian generator $\hat{W} = -\hat{W}^\dagger$ which is assumed to be small. The four-component generator $\hat{W}$ depends on the potential v_{eff} in the first order of (v_{eff}/E_p). Introducing two generators, $\hat{W}^V$ for the potential v_{eff} and $\hat{W}^A$ for the potential $\vec{\alpha}\cdot\vec{A}$, we obtain

$$\begin{aligned} U_1 &= \sqrt{1+\left(\hat{W}^V+\hat{W}^A\right)^2} + \left(\hat{W}^V+\hat{W}^A\right) \\ &= 1 + \left(\hat{W}^V+\hat{W}^A\right) + \frac{1}{2}\left(\hat{W}^V+\hat{W}^A\right)^2 + O\left(\left(\hat{W}^V\right)^3\right) + O\left(\left(\hat{W}^A\right)^3\right) \ . \end{aligned} \tag{2.36}$$

With the notations $[X,Y] = XY - YX$ for commutators, and $\{X,Y\} = XY + YX$ for anticommutators, the transformation U_1 of any operator C can be written as

$$\begin{aligned} U_1 C U_1^\dagger &= C + \left[\hat{W}, C\right] + \frac{1}{2}\left[\hat{W}, \left[\hat{W}, C\right]\right] + O\left(\hat{W}^3\right) \\ &= C + \left[\hat{W}, C\right] + \frac{1}{2}\left\{\hat{W}^2, C\right\} - \hat{W}C\hat{W} + O\left(\hat{W}^3\right) \ . \end{aligned} \tag{2.37}$$

Therefore, assuming operator C equals to the right part of Eq. (2.30) and omitting the second-order operators in the potentials v_{eff} and $\vec{\alpha}\cdot\vec{A}$, the transformed Hamiltonian can

be written as

$$\begin{aligned} U_1U_0\hat{H}^{(4)}_{DKS,A}U_0^\dagger U_1^\dagger &= \beta E_p + E_1^V + E_1^A + O_1^V + O_1^A \\ &+ \left[\left(\hat{W}^V + \hat{W}^A\right), \beta E_p\right] \\ &+ \left[\left(\hat{W}^V + \hat{W}^A\right), \left(E_1^V + E_1^A\right)\right] \\ &+ \left[\left(\hat{W}^V + \hat{W}^A\right), \left(O_1^V + O_1^A\right)\right] \\ &+ \frac{1}{2}\left[\left(\hat{W}^V + \hat{W}^A\right), [\left(\hat{W}^V + \hat{W}^A\right), \beta E_p]\right] + \dots \ . \end{aligned} \tag{2.38}$$

To eliminate the *odd* terms, the operators O_1^A and O_1^V have to satisfy the relations

$$O_1^V + [\hat{W}^V, \beta E_p] = 0 \ , \tag{2.39}$$

$$O_1^A + [\hat{W}^A, \beta E_p] = 0 \ . \tag{2.40}$$

With the help of Eq. (2.39) and Eq. (2.40) the commutator

$$\left[\left(\hat{W}^V + \hat{W}^A\right), \left(O_1^V + O_1^A\right)\right] \tag{2.41}$$

can be expanded as

$$-\left[\left(\hat{W}^V + \hat{W}^A\right), \left[\left(\hat{W}^V + \hat{W}^A\right), \beta E_p\right]\right] \ . \tag{2.42}$$

The term $\left[\left(\hat{W}^V + \hat{W}^A\right), \left(E_1^V + E_1^A\right)\right]$ of Eq. (2.38) is *odd* and neglected in the transformed second-order Hamiltonian.

Finally, $\hat{H}^{(4)}_{DKS,A}$ accurate up to second order can be written as

$$\begin{aligned} U_1U_0\hat{H}^{(4)}_{DKS,A}U_0^\dagger U_1^\dagger &= \beta E_p + E_1^V + E_1^A \\ &- \frac{1}{2}\left[\left(\hat{W}^V + \hat{W}^A\right), [\left(\hat{W}^V + \hat{W}^A\right), \beta E_p]\right] \\ &= \beta E_p + E_1^V + E_1^A \\ &+ \left(\hat{W}^V + \hat{W}^A\right)\beta E_p\left(\hat{W}^V + \hat{W}^A\right) - \frac{1}{2}\left\{\left(\hat{W}^V + \hat{W}^A\right)^2, \beta E_p\right\} \ . \end{aligned} \tag{2.43}$$

To fulfil conditions Eq. (2.39) and (2.40), one expresses the anti-Hermitian operators W^V and W^A in a plane-wave basis of eigenfunctions $|p\rangle$ of the momentum operator [65]:

$$W^V = \int d^3p d^3p' \, |p\rangle \, W^V_{p,p'} \, \langle p'| \ , \tag{2.44}$$

$$W^A = \int d^3p d^3p' \, |p\rangle \, W^A_{p,p'} \, \langle p'| \ . \tag{2.45}$$

Then operators $W^V_{p,p'}$ and $W^A_{p,p'}$ can be written as integral kernels [65]

$$\hat{W}^V_{p,p'} = \beta \frac{O^V_{1;p,p'}}{E_p + E_{p'}} \tag{2.46}$$

and

$$\hat{W}^A_{p,p'} = \beta \frac{O^A_{1;p,p'}}{E_p + E_{p'}} \ . \tag{2.47}$$

Collecting terms up to second order in the external potential υ_{eff} and up to first order in the vector potential $\vec{\alpha} \cdot \vec{A}$, one obtains the Hamiltonian $\hat{H}^{(4)}_{mag}$ which describes various magnetic interactions:

$$\begin{aligned} \hat{H}^{(4)}_{mag} &= E^A_1 + \hat{W}^A \beta E_p \hat{W}^V + \hat{W}^V \beta E_p \hat{W}^A \\ &- \frac{1}{2}\left(\hat{W}^V \hat{W}^A \beta E_p + \beta E_p \hat{W}^V \hat{W}^A + \hat{W}^A \hat{W}^V \beta E_p + \beta E_p \hat{W}^A \hat{W}^V\right) \ . \end{aligned} \tag{2.48}$$

Combination of Eqs. (2.33, 2.34) with Eqs. (2.46, 2.47) yields:

$$\hat{W}^V = \begin{pmatrix} 0 & W^V \\ W^V & 0 \end{pmatrix}, \ \hat{W}^A = \begin{pmatrix} 0 & W^A \\ -W^A & 0 \end{pmatrix} \ . \tag{2.49}$$

Here the two-component operator W^V in the momentum space representation reads:

$$W^V_{p,p'} = A_p \left(K_p \left(\vec{\sigma} \cdot \vec{p}\right) \tilde{\upsilon}_{p,p'} - \tilde{\upsilon}_{p,p'} \left(\vec{\sigma} \cdot \vec{p}\right) K_{p'}\right) A_{p'} \ , \tag{2.50}$$

with

$$\tilde{\upsilon}_{p,p'} = \frac{\upsilon_{eff;p,p'}}{E_p + E_{p'}} \ , \tag{2.51}$$

where $\upsilon_{eff;p,p'}$ is the momentum space representation of the effective potential υ_{eff}. W^A is a two-component operator

$$W^A_{p,p'} = A_p \left(\vec{\sigma} \cdot \vec{\tilde{A}}_{p,p'}\right) A_{p'} - A_p K_p \left(\vec{\sigma} \cdot \vec{p}\right) \left(\vec{\sigma} \cdot \vec{\tilde{A}}_{p,p'}\right) \left(\vec{\sigma} \cdot \vec{p}\right) K_{p'} A_{p'} \tag{2.52}$$

with

$$\vec{\tilde{A}}_{p,p'} = \frac{\vec{A}_{p,p'}}{E_p + E_{p'}} \ , \tag{2.53}$$

where $\vec{A}_{p,p'}$ is a momentum space representation of the vector potential $\vec{A}$.

The two-component Hamiltonian $\hat{H}^{(2)}_{mag}$ can be obtained by projecting out the electronic part of the 4×4 matrix from Eq. (2.48).$\hat{H}^{(2)}_{mag}$ includes a first-order term $\hat{H}^{(2)}_{mag,1}$ and a second-order term $\hat{H}^{(2)}_{mag,2}$:

$$\hat{H}^{(2)}_{mag} = \hat{H}^{(2)}_{mag,1} + \hat{H}^{(2)}_{mag,2} \equiv \hat{H}^{(2)}_{mag,DK2} \tag{2.54}$$

with

$$\hat{H}^{(2)}_{mag,1} = A_p \left(K_p \left(\vec{\sigma} \cdot \vec{p}\right) \left(\vec{\sigma} \cdot \vec{A}\right) + \left(\vec{\sigma} \cdot \vec{A}\right) \left(\vec{\sigma} \cdot \vec{p}\right) K_p\right) A_p \tag{2.55}$$

$$\begin{aligned} \hat{H}^{(2)}_{mag,2} &= \frac{1}{2}[\left(W^V W^A - W^A W^V\right) E_p + 2\left(W^V E_p W^A - W^A E_p W^V\right) \\ &+ E_p \left(W^V W^A - W^A W^V\right)] \ . \end{aligned} \tag{2.56}$$

The first-order term $\hat{H}^{(2)}_{mag,1}$depends only on one term $\vec{\sigma}\cdot\vec{A}$, the second-order term $\hat{H}^{(2)}_{mag,2}$ comprises cross terms between the two potential contributions $\vec{\sigma}\cdot\vec{A}$ and υ_{eff}. This level of calculations will be referred latter as "DK_2".

The evaluation of the matrix $W^V_{p,p'}$ is quite expensive because it depends on the effective potential which includes the *ee* interaction and the *xc* potential. To avoid the resource consuming procedure of building matrix $W^V_{p,p'}$ using the full effective potential, matrix $W^V_{p,p'}$ is constructed approximately only with the dominating contribution to the effective potential, namely the nuclear potential υ_{nuc}. This popular approximation, which is referred to as DK transformation *"in the nuclear field only"* [75, 96, 97], was implemented in the ParaGauss code for evaluating the DK Hamiltonian [70, 71].

One may discuss two further approximations for the magnetic Hamiltonian. In the first one, the second-order term is ignored, leaving only the first-order term, referred as "DK_1"

$$\hat{H}^{(2)}_{mag,DK1} = A_p\left(K_p\left(\vec{\sigma}\cdot\vec{p}\right)\left(\vec{\sigma}\cdot\vec{A}\right)+\left(\vec{\sigma}\cdot\vec{A}\right)\left(\vec{\sigma}\cdot\vec{p}\right)K_p\right)A_p \tag{2.57}$$

At this level of accuracy, only a mass-velocity correction is taken into account in the operators A_p and K_p. The second approximation addresses the case of small momenta, $p/c << 1$; in this limit, the second-order term vanishes, and the magnetic Hamiltonian turns to the approximation "DK_0"

$$\hat{H}^{(2)}_{mag,DK0} = \frac{1}{2c}\left(\left(\vec{\sigma}\cdot\vec{p}\right)\left(\vec{\sigma}\cdot\vec{A}\right)+\left(\vec{\sigma}\cdot\vec{A}\right)\left(\vec{\sigma}\cdot\vec{p}\right)\right)\ . \tag{2.58}$$

It is difficult to judge in general whether and when these approximations are sufficient. Therefore, they will be tested for the calculations of HFCCs in Chapter 3, and for the calculations of electronic **g**-tensors in Chapter 4.

The purely relativistic nature of magnetic interactions follows immediately from Eq. (2.54) and the definitions of E_p, A_p, and K_p, Eqs. (2.26, 2.27, 2.29). Indeed, $\hat{H}^{(2)}_{mag}$ vanishes in the limit where the speed of light is formally considered infinitely large. This result emphasizes the necessity of a relativistic treatment of magnetic interactions.

2.4 Computation of Relativistic Matrix Elements

The second-order term $\hat{H}^{(2)}_{mag,2}$ of the magnetic Hamiltonian, Eq. (2.54), exhibits a complicated form. The required matrix elements of relativistic operators are complicated functions of momentum p and can not be easily evaluated in position space. However, in momentum space all operators, which are functions of p^2, e.g. E_p, A_p, K_p, have a diagonal form and thus can be calculated in straightforward fashion. Hess et al. [66, 98] suggested to evaluate such relativistic operators in an approximate momentum space, namely in the space of eigenvectors of the matrix that represents the nonrelativistic kinetic energy operator $p^2/2$ in a finite set of (Gaussian-type) basis functions. In combination with such a technique, the DK formalism was developed into the practical DKH computational method [75, 99, 77].

In the program ParaGauss, basis functions are employed which are represented as product of a harmonic polynomial and a Gaussian – in coordinates relative a center, usually an atom (see Chapter 5) [100, 101]. The evaluation of relativistic matrix elements with such basis functions has been described in detail in Refs. [70, 71].

The actual implementation of the DKH scheme in ParaGauss [75] comprises the following steps. First, the non-orthogonal basis set is subjected to a canonical orthogonalization [102] to obtain an uncontracted orthonormal basis set. Then, the eigenvalue problem is solved for the matrix which represents the nonrelativistic kinetic energy operator $p^2/2$ in this orthonormal basis. This unitary transformation of the basis set is also used to transform operators into momentum space $|p_i\rangle$. For instance, the operators E_p, A_p, and K_p are represented by diagonal matrices. In the next step, the relativistic operators are transformed back to the orbital space. Finally, if desired, the orbital basis set is contracted; in many cases, calculations with ParaGauss are carried out with so-called generalized contractions, with coefficients derived from atomic KS or DKS eigenvectors.

In the momentum representation, the operators $W^V W^A$ and $W^A W^V$ can be obtained following the multiplication procedure of two operators Eqs. (2.44, 2.45)

$$W^V W^A = \sum_{p,p',p''} |p\rangle \, W^V_{p,p'} W^A_{p',p''} \, \langle p''| \ , \tag{2.59}$$

$$W^A W^V = \sum_{p,p',p''} |p\rangle \, W^A_{p,p'} W^V_{p',p''} \, \langle p''| \ . \tag{2.60}$$

The kernels are expanded according to Eqs. (2.50, 2.52) as

$$\begin{aligned} W^V_{p,p'} W^A_{p',p''} = & \left[A_p \left(R_p \tilde{v}_{p,p'} - \tilde{v}_{p,p'} R_{p'}\right) A_{p'}\right] \cdot \\ & \left[A_{p'} \left(\vec{\sigma} \cdot \vec{\tilde{A}}_{p',p''}\right) A_{p''} - A_{p'} R_{p'} \left(\vec{\sigma} \cdot \vec{\tilde{A}}_{p',p''}\right) R_{p''} A_{p''}\right] \end{aligned} \tag{2.61}$$

and

$$\begin{aligned} W^A_{p,p'} W^V_{p',p''} = & \left[A_p \left(\vec{\sigma} \cdot \vec{\tilde{A}}_{p,p'}\right) A_{p'} - A_p R_p \left(\vec{\sigma} \cdot \vec{\tilde{A}}_{p,p'}\right) R_{p'} A_{p'}\right] \cdot \\ & \left[A_{p'} \left(R_{p'} \tilde{v}_{p',p''} - \tilde{v}_{p',p''} R_{p''}\right) A_{p''}\right] \ . \end{aligned} \tag{2.62}$$

Rearrangement of terms produces a convenient identity:

$$A_p \left(R_p \tilde{v}_{p,p'} - \tilde{v}_{p,p'} R_{p'}\right) A_{p'} = A_p R_p \tilde{v}_{p,p'} R_{p'} A_{p'} \frac{R_{p'}}{R^2_{p'}} - \frac{R_p}{R^2_p} A_p R_p \tilde{v}_{p,p'} R_{p'} A_{p'} \ . \tag{2.63}$$

Eqs. (2.61, 2.62) combined with Eq. (2.63) yield:

$$\begin{aligned} W^V_{p,p'}W^A_{p',p''} - W^A_{p,p'}W^V_{p',p''} &= A_pR_p\tilde{\upsilon}_{p,p'}R_{p'}A_{p'}\frac{R_{p'}}{R^2_{p'}}A_{p'}\left(\vec{\sigma}\cdot\vec{\tilde{A}}_{p',p''}\right)A_{p''} \\ &- A_pR_p\widetilde{\upsilon}_{p,p'}R_{p'}A_{p'}\frac{R_{p'}}{R^2_{p'}}A_{p'}R_{p'}\left(\vec{\sigma}\cdot\vec{\tilde{A}}_{p',p''}\right)R_{p''}A_{p''} \\ &- \frac{R_p}{R^2_p}A_pR_p\tilde{\upsilon}_{p,p'}R_{p'}A_{p'}A_{p'}\left(\vec{\sigma}\cdot\vec{\tilde{A}}_{p',p''}\right)A_{p''} \\ &+ \frac{R_p}{R^2_p}A_pR_p\tilde{\upsilon}_{p,p'}R_{p'}A_{p'}A_{p'}R_{p'}\left(\vec{\sigma}\cdot\vec{\tilde{A}}_{p',p''}\right)R_{p''}A_{p''} \\ &- A_p\left(\vec{\sigma}\cdot\vec{\tilde{A}}_{p,p'}\right)A_{p'}A_{p'}R_{p'}\tilde{\upsilon}_{p',p''}R_{p''}A_{p''}\frac{R_{p''}}{R^2_{p''}} \\ &+ A_p\left(\vec{\sigma}\cdot\vec{\tilde{A}}_{p,p'}\right)A_{p'}\frac{R_{p'}}{R^2_{p'}}A_{p'}R_{p'}\tilde{\upsilon}_{p',p''}R_{p''}A_{p''} \\ &+ A_pR_p\left(\vec{\sigma}\cdot\vec{\tilde{A}}_{p,p'}\right)R_{p'}A_{p'}A_{p'}R_{p'}\tilde{\upsilon}_{p',p''}R_{p''}A_{p''}\frac{R_{p''}}{R^2_{p''}} \\ &- A_pR_p\left(\vec{\sigma}\cdot\vec{\tilde{A}}_{p,p'}\right)R_{p'}A_{p'}\frac{R_{p'}}{R^2_{p'}}A_{p'}R_{p'}\tilde{\upsilon}_{p',p''}R_{p''}A_{p''}\ . \end{aligned} \tag{2.64}$$

We use the notations

$$\left(AR\tilde{V}RA\right)_{p,p'} = A_pR_p\tilde{\upsilon}_{p,p'}R_{p'}A_{p'} \tag{2.65}$$

and

$$\left(A\tilde{V}A\right)_{p,p'} = A_p\tilde{\upsilon}_{p,p'}A_{p'} \tag{2.66}$$

together with

$$h = (\vec{\sigma}\cdot\vec{p})\left(\vec{\sigma}\cdot\vec{A}\right) \tag{2.67}$$

and

$$\tilde{h}_{p,p'} = \frac{A_pK_ph_{pp'}A_{p'}}{E_p+E_{p'}}\ . \tag{2.68}$$

Then Eq. (2.64) can be rewritten as

$$\begin{aligned} W^V_{p,p'}W^A_{p',p''} - W^A_{p,p'}W^V_{p',p''} &= \left(AR\tilde{V}RA\right)_{p,p'}\frac{1}{K^2_{p'}p'^2}\tilde{h}_{p',p''} + \tilde{h}^\dagger_{p,p'}\frac{1}{K^2_{p'}p'^2}\left(AR\tilde{V}RA\right)_{p',p''} \\ &- \left(AR\tilde{V}RA\right)_{p,p'}\tilde{h}^\dagger_{p',p''} - \tilde{h}_{p,p'}\left(AR\tilde{V}RA\right)_{p',p''} \\ &- \left(A\tilde{V}A\right)_{p,p'}\tilde{h}_{p',p''} - \tilde{h}^\dagger_{p,p'}\left(A\tilde{V}A\right)_{p',p''} \\ &+ \left(A\tilde{V}A\right)_{p,p'}K^2_{p'}p'^2\tilde{h}^\dagger_{p',p''} + \tilde{h}_{p,p'}K^2_{p'}p'^2\left(A\tilde{V}A\right)_{p',p''}\ . \end{aligned} \tag{2.69}$$

The term $\left(AR\tilde{V}RA\right)_{p,p'}$ is obtained as

$$\left(AR\tilde{V}RA\right)_{p,p'} = \frac{A_pK_pK_{p'}A_{p'}}{E_p+E_{p'}}\left\langle\vec{p}\right|(\vec{\sigma}\vec{p})\,\upsilon_{nuc}\,(\vec{\sigma}\vec{p})\left|\vec{p}'\right\rangle \tag{2.70}$$

and the term $\left(A\tilde{V}A\right)_{p,p'}$ as

$$\left(A\tilde{V}A\right)_{p,p'} = \frac{A_p A_{p'}}{E_p + E_{p'}} \langle \vec{p} | \upsilon_{nuc} | \vec{p}' \rangle \ . \tag{2.71}$$

Using the Pauli relation

$$(\vec{\sigma}\vec{a})\left(\vec{\sigma}\vec{b}\right) = \left(\vec{a}\vec{b}\right) + i\vec{\sigma}\left(\vec{a}\times\vec{b}\right) \tag{2.72}$$

one can rearrange the term $(\vec{\sigma}\vec{p})\,\upsilon_{nuc}\,(\vec{\sigma}\vec{p})$ to read

$$(\vec{\sigma}\vec{p})\,\upsilon_{nuc}\,(\vec{\sigma}\vec{p}) = \vec{p}\upsilon_{nuc}\vec{p} + i\vec{\sigma}\vec{p}\upsilon_{nuc}\times\vec{p}\,. \tag{2.73}$$

The matrices $\left(A\tilde{V}A\right)_{p,p'}$ and $\left(AR\tilde{V}RA\right)_{p,p'}$, implemented previously [70, 71], are required when building of the DK Hamiltonian which accounts for scalar relativistic and spin-orbit (SO) effects. Therefore, they were available for evaluating the matrix elements of Eq. (2.69).

One can reduce the number of terms and the computational effort for Eq. (2.69) by precalculating the following quantities [94]:

$$\tilde{U}_{pp'} = \left(A\tilde{V}A\right)_{p,p'} - \left(AR\tilde{V}RA\right)_{p,p'} \frac{1}{K_{p'}^2 p'^2}\ , \tag{2.74}$$

$$\tilde{T}_{pp'} = K_p^2 p^2 \left(A\tilde{V}A\right)_{p,p'} - \left(AR\tilde{V}RA\right)_{p,p'}\ . \tag{2.75}$$

Then, rewriting expression of Eq. (2.69) as

$$\begin{aligned} W^V_{p,p'}W^A_{p',p''} - W^A_{p,p'}W^V_{p',p''} = &-\left(\left(A\tilde{V}A\right)_{p,p'} - \left(AR\tilde{V}RA\right)_{p,p'}\frac{1}{K_{p'}^2 p'^2}\right)\tilde{h}_{p',p''} \\ &- \tilde{h}^\dagger_{p,p'}\left(\left(A\tilde{V}A\right)_{p',p''} - \frac{1}{K_{p'}^2 p'^2}\left(AR\tilde{V}RA\right)_{p',p''}\right) \\ &+ \left(\left(A\tilde{V}A\right)_{p,p'} K_{p'}^2 p'^2 - \left(AR\tilde{V}RA\right)_{p,p'}\right)\tilde{h}^\dagger_{p',p''} \\ &+ \tilde{h}_{p,p'}\left(K_{p'}^2 p'^2\left(A\tilde{V}A\right)_{p',p''} - \left(AR\tilde{V}RA\right)_{p,p'}\right)\ . \end{aligned} \tag{2.76}$$

one obtains:

$$\begin{aligned} W^V_{p,p'}W^A_{p',p''} - W^A_{p,p'}W^V_{p',p''} = &-\tilde{U}_{p,p'}\tilde{h}_{p',p''} - \tilde{h}^\dagger_{p,p'}\tilde{U}^\dagger_{p',p''} \\ &+ \tilde{T}^\dagger_{p,p'}\tilde{h}^\dagger_{p,p'} + \tilde{h}_{p,p'}\tilde{T}_{p',p''}\ . \end{aligned} \tag{2.77}$$

Finally, collecting various terms and using Eq. (2.52, 2.50), one can express the first- and second-order magnetic contributions to the DK Hamiltonian as

$$\hat{H}^{(2)}_{mag,1} = A_p\left(K_p h + h^\dagger K_p\right)A_p\ , \tag{2.78}$$

$$\begin{aligned}\hat{H}^{(2)}_{mag,2,ij} = &\frac{1}{2}\left\langle p_i\right| \left(W^V W^A - W^A W^V\right) E_p \left|p_j\right\rangle \\ &+ \left\langle p_i\right| \left(W^V E_p W^A - W^A E_p W^V\right) \left|p_j\right\rangle \\ &+ \frac{1}{2}\left\langle p_i\right| E_p \left(W^V W^A - W^A W\right) \left|p_j\right\rangle \ .\end{aligned} \tag{2.79}$$

The matrix elements of $\hat{H}^{(2)}_{mag,2}$ are obtained in a three-fold loop over all $i \leq j$, and k [103, 70, 71]:

$$\begin{aligned}\hat{H}^{(2)}_{mag,2,ij} = &\frac{1}{2}\sum_k \left(-\tilde{U}_{p_i p_k}\tilde{h}_{p_k,p_j} - \tilde{h}^\dagger_{p_i,p_k}\tilde{U}^\dagger_{p_k p_j} + \tilde{T}^\dagger_{p_i p_k}\tilde{h}^\dagger_{p_k,p_j} + \tilde{h}_{p_i,p_k}\tilde{T}_{p_k p_j}\right)\cdot \\ &\left(E_{p_i} + 2E_{p_j} + E_{p_k}\right) \ .\end{aligned} \tag{2.80}$$

However, this three-fold loop evaluation is computationally quite demanding. For practical calculations, one can profit from very efficient implementations of matrix algebra operations, and rewrite equivalently the term $\hat{H}^{(2)}_{mag,2}$ [94]:

$$\begin{aligned}\hat{H}^{(2)}_{mag,2} = -\frac{1}{2}(&\left\{\tilde{U}_{p,p'}, E_p\right\}\tilde{h}_{p,p'} + \tilde{U}_{p,p'}\left\{\tilde{h}_{p,p'}, E_p\right\} \\ &+ \tilde{h}^\dagger_{p,p'}\left\{\tilde{U}^\dagger_{p,p'}E_p\right\} + \left\{\tilde{h}^\dagger_{p,p'}, E_p\right\}\tilde{U}^\dagger_{p,p'}) \\ &+ \frac{1}{2}(\tilde{h}_{p,p'}\left\{\tilde{T}_{p,p'}, E_p\right\} + \left\{\tilde{h}_{p,p'}, E_p\right\}\tilde{T}_{p,p'} \\ &+ \left\{\tilde{T}^\dagger_{p,p'}, E_p\right\}\tilde{h}_{p,p'} + \tilde{T}^\dagger_{p,p'}\left\{\tilde{h}^\dagger_{p,p'}, E_p\right\}) \ .\end{aligned} \tag{2.81}$$

2.5 Douglas-Kroll Transformations Including a Magnetic Field

As an alternative to the procedure just described, one can derive the operator of magnetic interactions (which depends on the vector potential $\vec{A}$) within the DK formalism by applying a field-dependent DK transformation to the DKS Hamiltonian, where the vector potential $\vec{A}$ is introduced via the gauge invariant mechanical momentum $\vec{\pi}$, Eq. (2.13). This way to define the magnetic interactions operator has the advantage of eliminating the inconsistency of the previous approach, which is connected with the application of a DK transformation *independent* of a magnetic field to obtain a magnetic operator which *depends* on the magnetic field [94, 72].

In the case of an external magnetic field, one obtains the kinetic energy operator as

$$\begin{aligned}E_\pi\left(\vec{A}\right) &= c\sqrt{\left(\vec{\sigma}\cdot\vec{\pi}\right)^2 + c^4} \\ &= c\left[\left(c^2 + p^2\right)^2 + \left(\vec{p}\cdot\vec{A} + \vec{A}\cdot\vec{p} + A^2\right) + \vec{\alpha}\left(\vec{p}\times\vec{A} + \vec{A}\times\vec{p}\right)\right]^{\frac{1}{2}} \ .\end{aligned} \tag{2.82}$$

This operator reproduces exactly the relativistic positive energy of free particles in a magnetic field. Other kinematic operators, A_p, K_p, and R_p, are changed to their field-dependent analogues accordingly:

$$A_\pi\left(\vec{A}\right) = \sqrt{\frac{E_\pi + c^2}{2E_\pi}} \ , \tag{2.83}$$

$$K_\pi\left(\vec{A}\right) = \frac{c}{(E_\pi + c^2)} \ , \tag{2.84}$$

$$R_\pi\left(\vec{A}\right) = K_\pi\left(\vec{\alpha}\vec{\pi}\right) \ . \tag{2.85}$$

When calculating magnetic properties, one has to expand Eq. (2.82) in powers of $\vec{A}$. This expansion is not obvious because individual terms do not commute. Invoking a momentum space representation in which E_p is diagonal, Eq. (2.82) can be expanded in powers of $\vec{A}$ [94]

$$(a+b)^{1/2} = < p|a|p > + \frac{< p|b|p' >}{< p|a|p > + < p'|a|p' >} + ... \ , \tag{2.86}$$

where

$$a = p^2 + c^2 \tag{2.87}$$

and

$$b = \left(\vec{p}\cdot\vec{A} + \vec{A}\cdot\vec{p} + A^2\right) + \vec{\alpha}\cdot\left(\vec{p}\times\vec{A} + \vec{A}\times\vec{p}\right) \ . \tag{2.88}$$

However, this approach based on a DK transformation which depends on a magnetic field seems to be more complicated because the kinetic operator E_π appears everywhere in the DK Hamiltonian. Thus far, this latter formalism has been developed only for the limiting case $p << c$ [72]. Nevertheless, for practical calculations of magnetic properties of molecular systems, one expects that the two methods give rather similar results [94].

2.6 Conclusions

We have described the DK transformations of magnetic operators for an arbitrary external vector potential $\vec{A}$. Depending on the specific form of $\vec{A}$, it is possible to calculate different magnetic interactions. In particular, taking the vector potential of nuclear magnetic dipoles, one obtains an expression for HFCCs, as will be shown in Chapter 3. By considering the vector potential $\vec{A}$ of a homogeneous external magnetic field, one can arrive at expressions for calculating electronic **g**-tensors as will be done in Chapter 4. The same DK transformed magnetic Hamiltonian has previously been employed for calculating magnetic (NMR) shielding constants [94].

Chapter 3

Calculation of Hyperfine Coupling Constants Using the Relativistic Density Functional Douglas-Kroll-Hess Method

3.1 Hyperfine Hamiltonian

3.1.1 Point Nucleus Model

Hyperfine coupling constants describe the interaction of electrons with nuclear spins in a paramagnetic molecule. The magnetic field created by the point nucleus ν located at $\vec{R}_\nu$ can be described by the vector potential (in atomic units)

$$\vec{A}_\nu(\vec{r}) = \frac{\vec{\mu}_\nu \times \vec{r}_\nu}{r_\nu^3} \ , \tag{3.1}$$

where $\vec{r}_\nu = \vec{r} - \vec{R}_\nu$ and $\vec{\mu}_\nu$ is the magnetic dipole moment of nucleus ν [104, p. 186]. A magnetic field created by N nuclei in a molecule is described by the sum of such potentials

$$\vec{A}(\vec{r}) = \sum_{\nu=1}^{N} \vec{A}_\nu(\vec{r}) \ . \tag{3.2}$$

The magnetic field $\vec{B}_\nu = \nabla \times \vec{A}_\nu$ of nucleus ν reads [104, p. 188]:

$$\vec{B}_\nu = -\frac{\vec{\mu}_\nu}{r_\nu^3} + 3\frac{\vec{r}_\nu(\vec{\mu}_\nu \cdot \vec{r}_\nu)}{r_\nu^5} + \frac{8\pi}{3}\delta(\vec{r}_\nu)\vec{\mu}_\nu \ . \tag{3.3}$$

Employing the explicit form of the vector potential $\vec{A}_\nu$, Eq. (3.1), and the magnetic Hamiltonian, Eq. (2.54), one can derive the Hamiltonian for this particular type of magnetic

interaction – the hyperfine Hamiltonian $\hat{H}^{hf}$. With the help of the Pauli relation, Eq. (2.72), the quantity h of Eq. (2.67) can be rewritten as

$$h = (\vec{\sigma}\cdot\vec{p})\left(\vec{\sigma}\cdot\vec{A}\right) = \vec{p}\cdot\vec{A} + i\vec{\sigma}\cdot\left(\vec{p}\times\vec{A}\right) \equiv h_1 \ . \tag{3.4}$$

Note that this operator is not Hermitian. Its Hermitian conjugate is [105]

$$h^\dagger = \left(\vec{\sigma}\cdot\vec{A}\right)(\vec{\sigma}\cdot\vec{p}) \ \equiv h_2. \tag{3.5}$$

We follow the approach suggested by Pyper [105] for evaluating matrix elements of Eqs. (2.55, 2.56), which corresponds to the so-called Gordon decomposition [79, p. 123]. We demonstrate the procedure for the first term of the magnetic operator, Eq. (2.55), and note that the second term, Eq. (2.56), can be transformed in analogous fashion: way):

$$\begin{aligned}\hat{H}^{(2)}_{mag,1} &= \frac{1}{2}A_p\left(K_p h_1 + h_2 K_p\right)A_p \\ &+ \frac{1}{2}A_p\left(K_p h_2 + h_1 K_p\right)A_p\end{aligned} \tag{3.6}$$

Recalling that $\vec{p} = -i\nabla$, for any wave function φ we have

$$h_1\varphi = \vec{p}\cdot\vec{A}\varphi + i\vec{\sigma}\cdot\left(\vec{p}\times\vec{A}\right)\varphi \tag{3.7}$$

$$\begin{aligned}&= \left[\vec{p}\cdot\vec{A}\right]\varphi + \vec{A}\cdot\vec{p}\varphi \\ &+ i\vec{\sigma}\cdot\left[\vec{p}\times\vec{A}\right]\varphi - i\vec{\sigma}\cdot\left(\vec{A}\times\vec{p}\right)\varphi \ .\end{aligned} \tag{3.8}$$

For the operator h_2 we obtain

$$h_2\varphi = \vec{A}\cdot\vec{p}\varphi + i\vec{\sigma}\cdot\left(\vec{A}\times\vec{p}\right)\varphi \tag{3.9}$$

Therefore, we obtain for Eq. (3.6)

$$h_A = \left[\vec{p}\cdot\vec{A}\right] + \vec{A}\cdot\vec{p} + i\vec{\sigma}\cdot\left[\vec{p}\times\vec{A}\right] \ , \tag{3.10}$$

$$\hat{H}^{(2)}_{mag,1} = A_p\left(K_p h_A + h_A K_p\right)A_p \ . \tag{3.11}$$

Here square brackets restrict the action of the gradient and indicate that it does not act on the wave function. We employ the vector rule [57, Appendix B] for the term $\left[\vec{p}\cdot\vec{A}\right]$ of Eq. (3.10),

$$\nabla\cdot\left(\vec{a}\times\vec{b}\right) = \vec{b}\cdot(\nabla\times\vec{a}) - \vec{a}\cdot\left(\nabla\times\vec{b}\right) \ , \tag{3.12}$$

and obtain using Eq. (3.1):

$$\vec{p}\cdot\left(\vec{\mu}_\nu\times\frac{\vec{r}_\nu}{r_\nu^3}\right) = \frac{\vec{r}_\nu}{r_\nu^3}\cdot(\vec{p}\times\vec{\mu}_\nu) - \vec{\mu}_\nu\cdot\left(\vec{p}\times\frac{\vec{r}_\nu}{r_\nu^3}\right) \ . \tag{3.13}$$

The first term of Eq. (3.13) vanishes because the magnetic moment $\vec{\mu}_\nu$ is a constant. It is convenient to introduce the unit antisymmetric tensor ϵ_{ijk} [57, p. 18], referring here to

Cartesian components i, j, $k = x$, y, z, and to rewrite the vector product of the second term as

$$-\vec{\mu}_\nu \cdot \left(\vec{p} \times \frac{\vec{r}_\nu}{r_\nu^3}\right) = -\mu_{\nu i}\epsilon_{ijk} p_j \frac{r_{\nu k}}{r_\nu^3} \,, \tag{3.14}$$

Here, the summation is assumed over indices that occur twice. Latin letters which refer to the Cartesian components should not be confused with the Greek letter ν which refers to a specific nucleus. Using the notation $\partial_i \equiv \partial/\partial r_i$ and the relation [57, Appendix B]

$$\partial_i \left(\frac{r_j}{r^3}\right) = \left(\frac{4\pi}{3}\delta_{ij}\delta\left(\vec{r}\right) + \frac{\delta_{ij}}{r^3} - \frac{3r_i r_j}{r^5}\right) \,, \tag{3.15}$$

where δ_{ij} is the Kronecker delta, and $\delta\left(\vec{r}\right)$ is the Dirac delta function, we can rewrite Eq. (3.14) as

$$-\vec{\mu}_\nu \cdot \left(\vec{p} \times \frac{\vec{r}_\nu}{r_\nu^3}\right) = -\mu_{\nu i}\epsilon_{ijk} \left(\frac{4\pi}{3}\delta_{jk}\delta\left(\vec{r}_\nu\right) + \frac{\delta_{jk}}{r_\nu^3} - \frac{3r_{\nu j}r_{\nu k}}{r_\nu^5}\right) \,. \tag{3.16}$$

The first two terms of this equation vanish because the unit antisymmetric tensor with two identical indices is zero. The third term vanishes because it is proportional to the vector product $\vec{r} \times \vec{r}$. Hence, the first term of Eq. (3.10) vanishes.

The second term $\vec{A} \cdot \vec{p}$ of Eq. (3.8) reads explicitly

$$\vec{A} \cdot \vec{p} = \left(\vec{\mu}_\nu \times \frac{\vec{r}_\nu}{r_\nu^3}\right) \cdot \vec{p} \,. \tag{3.17}$$

Employing the vector rule [57, Appendix B]

$$\left(\vec{a} \times \vec{b}\right) \cdot \vec{c} = \vec{a} \cdot \left(\vec{b} \times \vec{c}\right) \,, \tag{3.18}$$

we obtain

$$\vec{A} \cdot \vec{p} = \vec{\mu}_\nu \cdot \frac{\vec{L}_\nu}{r_\nu^3} \equiv h_{point}^{orb}. \tag{3.19}$$

Here, the orbital angular momentum $\vec{L}_\nu$ is defined as $\vec{r}_\nu \times \vec{p}$ and computed with respect to the origin $\vec{R}_\nu$. The term h_{point}^{orb} represents the *orbital* contribution to the hyperfine interaction for the point nucleus model [3, p. 57].

Applying the relation [57, Appendix B]

$$\nabla \times \left(\vec{a} \times \vec{b}\right) = \vec{a}\left(\nabla \cdot \vec{b}\right) - \left(\vec{a} \cdot \nabla\right)\vec{b} + \left(\vec{b} \cdot \nabla\right)\vec{a} - \vec{b}\left(\nabla \cdot \vec{a}\right) \tag{3.20}$$

and taking the vector potential of Eq. (3.1), the third term of Eq. (3.10) reads:

$$\begin{aligned} i\vec{\sigma} \cdot \left[\vec{p} \times \vec{A}_\nu\right] &= i\vec{\sigma} \cdot \left[\vec{p} \times \left(\vec{\mu}_\nu \times \frac{\vec{r}_\nu}{r_\nu^3}\right)\right] \\ &= i\vec{\sigma} \cdot \left[\vec{\mu}_\nu\left(\vec{p} \cdot \frac{\vec{r}_\nu}{r_\nu^3}\right) - \left(\vec{\mu}_\nu \cdot \vec{p}\right)\frac{\vec{r}_\nu}{r_\nu^3} + \left(\frac{\vec{r}_\nu}{r_\nu^3} \cdot \vec{p}\right)\vec{\mu}_\nu - \frac{\vec{r}_\nu}{r_\nu^3}\left(\vec{p} \cdot \vec{\mu}_\nu\right)\right] \,. \end{aligned} \tag{3.21}$$

Obviously, the last two terms vanish because $\vec{\mu}_\nu$ is a constant. Combination of the first and the second terms of Eq. (3.21) yields:

$$i\vec{\sigma}\cdot\left[\vec{p}\times\vec{A}_\nu\right] = i\vec{\sigma}\cdot\left[\frac{2}{3}\vec{\mu}_\nu\left(\vec{p}\cdot\frac{\vec{r}_\nu}{r_\nu^3}\right) - \left(\left(\vec{\mu}_\nu\cdot\vec{p}\right)\frac{\vec{r}_\nu}{r_\nu^3} - \frac{1}{3}\vec{\mu}_\nu\left(\vec{p}\cdot\frac{\vec{r}_\nu}{r_\nu^3}\right)\right)\right] \ . \tag{3.22}$$

With the identity $\vec{r}_\nu/r_\nu^3 = -\nabla r_\nu^{-1}$, one can write the first term of Eq. (3.22) as

$$-\frac{2}{3}\vec{\sigma}\cdot\vec{\mu}_\nu\left(\nabla^2\frac{1}{r_\nu}\right) \ . \tag{3.23}$$

Using the relation [57, Appendix B]

$$\nabla^2\frac{1}{r} = -4\pi\delta\left(\vec{r}\right) \ , \tag{3.24}$$

one arrives at:

$$h_{point}^{iso} = \frac{8\pi}{3}\delta\left(\vec{r}_\nu\right)\vec{\sigma}\cdot\vec{\mu}_\nu \ . \tag{3.25}$$

This latter quantity represents the *Fermi contact* interaction term which arises from the direct contact interaction between an electron and a magnetic nucleus [3, p. 59]. Using Eq. (3.15), the second term of Eq. (3.22) can be transformed to

$$h_{point}^{dip} = -\frac{\vec{\sigma}\cdot\vec{\mu}_\nu}{r_\nu^3} + 3\frac{\left(\vec{\sigma}\cdot\vec{r}_\nu\right)\left(\vec{\mu}_\nu\cdot\vec{r}_\nu\right)}{r_\nu^5} \ . \tag{3.26}$$

This so-called *dipolar hyperfine* interaction term [3, p. 58] describes the dipole-dipole interaction between an electron and nucleus ν.

Collecting the terms h_{point}^{orb}, h_{point}^{iso}, and h_{point}^{dip} from Eqs. (3.19), (3.25), and (3.26), we obtain:

$$\begin{aligned} h_{point} &= h_{point}^{iso} + h_{point}^{dip} + h_{point}^{orb} \\ &= \frac{8\pi}{3}\delta\left(\vec{r}_\nu\right)\vec{\sigma}\cdot\vec{\mu}_\nu - \frac{\vec{\sigma}\cdot\vec{\mu}_\nu}{r_\nu^3} + 3\frac{\left(\vec{\sigma}\cdot\vec{r}_\nu\right)\left(\vec{\mu}_\nu\cdot\vec{r}_\nu\right)}{r_\nu^5} + \frac{\vec{L}_\nu}{r_\nu^3}\cdot\vec{\mu}_\nu \ . \end{aligned} \tag{3.27}$$

Finally, one has to substitute the latter operator into Eqs. (2.78) and (2.79) to obtain the hyperfine Hamiltonian $\hat{H}^{hf}$. For systems consisting of light atoms, such as organic radicals, the contributions of the Fermi contact and dipole hyperfine terms in Eq. (3.27) dominate. Moreover, for a rapidly tumbling molecule, e.g. a molecule in solution, one has to account for a rotational averaging of the Hamiltonian. In such a case, only the isotropic Fermi contact term yields a non-vanishing contribution [3, p. 63]. The last term of Eq. (3.27) appears to be important only for systems features strong SO interaction [17].

Fermi-contact and dipolar hyperfine interaction terms have to be multiplied by a correction factor, which arises from a treatment of the interaction between an electron and the electromagnetic field according to quantum electrodynamics [3, Section 1.3]. This interaction modifies the g-factor of a free electron from the integer value $g = 2$, predicted by Dirac theory, to the experimentally observed value [3, Section 1.3]

$$g_e = 2.002319778 \ . \tag{3.28}$$

One can approximately take this modification into account by multiplying the terms which are proportional to $\vec{\sigma}$ in Eq. (3.27) by $g_e/2$ [3, Section 1.3]. For similar reason, the orbital hyperfine interaction term is multiplied by a quantum electrodynamics correction factor g', the so-called electronic spin-orbit g-factor [3, Section 1.3]

$$g' = 2.0046385556 \ . \tag{3.29}$$

These two g-factors are connected to each other as [3, Section 1.3]:

$$g' = 2\left(1 + 2g_1\right) \ , \tag{3.30}$$

where

$$g_1 = \frac{1}{2}\left(g_e - 2\right) \ . \tag{3.31}$$

The factors g_e and g' differ only very slightly. Therefore, the commonly used approximation $g_e = g'$ seems to be sufficiently accurate for practical purposes [47, 61].

3.1.2 Finite Nucleus Model

All operators for calculations of HFCCs, Eq. (3.27), were derived in the approximation that a nucleus can be represented by a point charge or a point dipole. However, the finite size of a nucleus can also affect the hyperfine coupling constants in a relativistic formalism. For instance, the finite nucleus size of heavy atoms is known to be reflected in the hyperfine structures [106] and in the magnetic shielding constants [94]. Recent relativistic calculations of nuclear magnetic shielding constants showed that the effect of a finite nucleus size for atoms with a nuclear charge $Z > 90$ is 10% or more [94].

Moreover, the point nucleus model is known to fail in the Dirac-Hartree-Fock approach because the one-particle Dirac-Coulomb equation for the external potential of a point nucleus exhibits a weak singularity at the origin [107, 108]. This singularity is connected to the fact that radial solutions of the Dirac equation for the case $j = 1/2$ and the Coulomb potential diverge at the origin. The asymptotic behavior of the large and small components of the wave function at the nucleus is (in atomic units) [79, p. 243]:

$$\varphi^D\left(r\right) \sim r^{\sqrt{1-Z^2\alpha^2}-1} \exp\left(-Zr\right) \ . \tag{3.32}$$

This radial solution diverges weakly at the origin (weaker than r^{-1}), but it remains square-integrable.

Problems with the singularity are particularly obvious in the Roothaan approach to the solutions of the relativistic equations. A basis set optimization, for example, when using Gaussian-type basis functions, requires functions with very tight exponents that are trying to mimic the divergence of the wave function at the origin [107].

Obviously, this singularity at the origin affects the isotropic Fermi-contact contribution which is proportional to a δ-function and represents a *local* property at the position of

the nucleus, Eq. (3.25). Indeed, let us consider for simplicity a one-component (scalar) relativistic calculation of the isotropic hyperfine term of a hydrogen atom located at the origin and an solution of the relativistic equation, approximated as a linear combination of normalized Gaussian-type basis functions χ_α and coefficients c_α [109, p. 65]:

$$\psi\left(\vec{r}\right) = \sum_\alpha c_\alpha \chi_\alpha \ , \tag{3.33}$$

$$\chi_\alpha\left(\vec{r}\right) = \left(\frac{2\alpha}{\pi}\right)^{3/4} \exp\left(-\alpha r^2\right) \ . \tag{3.34}$$

Since the numerical solution tries to simulate the divergence of the exact wave function at the origin (Eq. (3.32)), the coefficients c_α will remain finite even for the steepest basis functions. Then, the Fermi contact term of Eq. (3.25) will give rise to a term proportional to $\langle\psi|\,\delta\left(\vec{r}\right)|\psi\rangle$, which will be determined by matrix elements between basis set functions with exponents α_1 and α_2 and coefficients c_{α_1}, c_{α_2}:

$$\langle\psi|\,\delta\left(\vec{r}\right)|\psi\rangle = \sum_{\alpha_1,\alpha_2} c_{\alpha_1} c^*_{\alpha_2} \left\langle\chi_{\alpha_1}\right|\delta\left(\vec{r}\right)\left|\chi_{\alpha_2}\right\rangle \tag{3.35}$$

$$= \sum_{\alpha_1,\alpha_2} c_{\alpha_1} c^*_{\alpha_2} \left(\frac{4\alpha_1\alpha_2}{\pi^2}\right)^{3/4} \ . \tag{3.36}$$

Numerical calculations demonstrate that the latter quantity does not reach a limit with increasing exponent size of steep Gaussian basis functions (Section 3.3.2). Thus, it seems plausible that one is not able to reach basis set saturation with respect to the isotropic part of HFCCs when using the point nucleus model. In other words, the point nucleus model is not suitable for calculating of isotropic HFCCs using a relativistic scheme. Therefore, it is necessary to introduce a finite-nucleus approach for the isotropic term of the magnetic interaction operator, Eq. (3.25).

The latter can by realized in the most obvious way by substituting the δ-function in the isotropic term, Eq. (3.25), by a Gaussian distribution, using the well known property [110, p. 69]

$$\lim_{\eta\to 0^+} \left(\frac{\eta}{\pi}\right)^{3/2} \exp\left(-\eta r^2\right) = \delta\left(\vec{r}\right) \ . \tag{3.37}$$

For a better motivation, one can adopt a model in which the entire classical nuclear magnetic moment is distributed in a small volume [94, 105] and described in terms of macroscopic bulk magnetization or a magnetic moment density [104, p. 192]. It is convenient to represent the magnetic moment $\vec{\mu}_\nu$ of a finite nucleus ν at point $\vec{R}_\nu$ by a normalized magnetic density distribution ω with Gaussian shape (employing $r'_\nu = \left|\vec{r}' - \vec{R}_\nu\right|$):

$$\omega\left(r'_\nu\right) = \left(\frac{\eta_\nu}{\pi}\right)^{3/2} \exp\left(-\eta_\nu r'^2_\nu\right) \ . \tag{3.38}$$

The exponent η_ν in the Gaussian distribution of Eq. (3.38) may be defined, for instance, using the root mean square radius ρ_ν of a nucleus of atomic mass M_ν (in atomic units)

given as [111]

$$\rho_\nu = 2.27 \times 10^{-5} M_\nu^{1/3} \ . \tag{3.39}$$

Then, η_ν reads

$$\eta_\nu = (3/2)\, \rho_\nu^{-2} \ . \tag{3.40}$$

This estimate of the nuclear radius ρ_ν is obtained from the nuclear charge distribution and of course not unique. For example, ρ_ν can be obtained from the distribution of the nuclear mass-density [112, p. 911]. Although the mass-density distribution of heavy nuclei may deviate slightly from the charge-density distribution [112, p. 911], any such realistic estimate would be sufficient for the present study because the calculated HFCCs are not very sensitive to the radius of the finite nucleus (see Section 3.3.2).

The vector potential of a (macroscopic) magnetic moment distribution can be expressed without approximations as [104, p. 192, p. 153]:

$$\vec{A}_{finite}\left(\vec{r}\right) = \int \omega\left(r'_\nu\right) \vec{\mu}_\nu \times \nabla' \frac{1}{|\vec{r} - \vec{r}'|} d^3\vec{r}' \ , \tag{3.41}$$

where ∇' is the gradient with respect to $\vec{r}'$. One can derive all non-vanishing terms of Eq. (3.27) for the case of the latter vector potential. However, we are interested only in the expression for the isotropic term; therefore, it is sufficient to apply the vector rule of Eq. (3.20) to the term $i\vec{\sigma} \cdot \left[\vec{p} \times \vec{A}_{finite}\right]$ and combine the terms as done in Eq. (3.22). Then, the isotropic contribution becomes

$$h_{finite}^{iso} = i\frac{2}{3} \left(\vec{\sigma} \cdot \vec{\mu}_\nu\right) \left(\vec{p} \cdot \int \omega\left(r'_\nu\right) \nabla' \frac{1}{|\vec{r} - \vec{r}'|} d^3\vec{r}'\right) \ .$$

Employing $\vec{p} = -i\nabla$ we obtain

$$h_{finite}^{iso} = \frac{2}{3} \left(\vec{\sigma} \cdot \vec{\mu}_\nu\right) \int \omega\left(r'_\nu\right) \nabla \cdot \nabla' \frac{1}{|\vec{r} - \vec{r}'|} d^3\vec{r}' \ . \tag{3.42}$$

In the preceding equation one can change the gradient with respect to $\vec{r}$ for the gradient with respect to $\vec{r}'$ if we use

$$\nabla \left(\frac{1}{|\vec{r} - \vec{r}'|}\right) = -\nabla' \left(\frac{1}{|\vec{r} - \vec{r}'|}\right) \ . \tag{3.43}$$

Then, with Eq. (3.25), one gets

$$\begin{aligned} h_{finite}^{iso} &= \frac{8\pi}{3} \vec{\sigma} \cdot \vec{\mu}_\nu \int \omega\left(r'_\nu\right) \delta\left(\vec{r} - \vec{r}'\right) d^3\vec{r}' \\ &= \frac{8\pi}{3} \vec{\sigma} \cdot \vec{\mu}_\nu \omega\left(r_\nu\right) \ . \end{aligned} \tag{3.44}$$

Substitution of the distribution function of the magnetic moment, Eq. (3.38), into preceding relation yields:

$$h_{finite}^{iso} = \frac{8\pi}{3} \left(\frac{\eta_\nu}{\pi}\right)^{3/2} \vec{\sigma} \cdot \vec{\mu}_\nu \exp\left(-\eta_\nu r_\nu^2\right) \ . \tag{3.45}$$

Finally, one has to exchange h^{iso}_{point} for h^{iso}_{finite} in Eq. (3.27) and substitute Eq. (3.27) to Eq. (2.78, 2.79) in order to obtain the hyperfine Hamiltonian used in the calculations of this work (Section 3.3).

A matrix element of this operator for two normalized Gaussian-type basis functions χ_{α_1}, χ_{α_2}, Eq. (3.34), is proportional to

$$\left\langle \chi_{\alpha_1} \right| \left(\frac{\eta_\nu}{\pi}\right)^{3/2} \exp\left(-\eta_\nu r_\nu^2\right) \left| \chi_{\alpha_2} \right\rangle = \left(\frac{4\alpha_1\alpha_2\eta_\nu^2}{\pi^2\left(\alpha_1+\alpha_2+\eta_\nu\right)^2}\right)^{3/4} . \tag{3.46}$$

Using this model, basis set saturation can be achieved as will be demonstrated in Section 3.3.2. To be fully consistent, one has to use wave functions of a DK Hamiltonian which takes the finite charge distribution of the nuclei into account. This can conveniently be realized by modeling the nuclei as Gaussian charge distributions [107, 113]. However, in the present work, we refrained from applying these finite nucleus corrections.

3.1.3 The Problem of Gauge Origin

Calculations of magnetic properties exhibit one notable complication compared to calculations of other molecular properties. One has to consider the so-called gauge problem, i.e. the dependence of the calculated results on the choice of the origin of the coordinate system (the "gauge") of the vector potential $\vec{A}$ of a magnetic field [109, p. 252]. The vector potential is not uniquely defined, because the gradient of any scalar function may by added (the curl of a gradient vanishes) [104, p. 240]:

$$\nabla \times \nabla f\left(\vec{r}\right) = 0 , \tag{3.47}$$

$$\vec{A} = \vec{A}' + \nabla f\left(\vec{r}\right) . \tag{3.48}$$

Such a change of vector potential is called a gauge transformation [104, p. 240]. We restrict the choice of the vector potential further by adopting the Coulomb gauge, namely we choose the vector potential to be divergence free [104, p. 241]:

$$\nabla \cdot \vec{A}\left(\vec{r}\right) = 0 . \tag{3.49}$$

For the case of a homogeneous magnetic field $\vec{B} = \nabla \times \vec{A}$, it is convenient to define the vector potential as

$$\vec{A}\left(\vec{r}\right) = \frac{1}{2}\vec{B} \times \left(\vec{r} - \vec{R}_o\right) , \tag{3.50}$$

where $\vec{R}_o$ is referred to as "gauge origin". Variation of $\vec{R}_o$ can be considered as a particular gauge transformation of Eq. (3.48) with

$$f\left(\vec{r}\right) = -\frac{1}{2}\left(\vec{B} \times \vec{R}_o\right) \cdot \vec{r} . \tag{3.51}$$

Inclusion of this vector potential into the Hamiltonian with a magnetic perturbation renders extra terms dependent on an *arbitrary* vector $\vec{R}_o$. For an exact wave function, which is

an eigenfunction of the Hamiltonian without magnetic field, these additional terms cancel exactly, yielding an origin-independent result [114, p. 44]. Indeed, any additional gauge term like in Eq. (3.48) to the vector potential of Eq. (3.1) leaves the matrix element of the operator h_A of Eq. (3.10) invariant. An additional term of the form $\vec{p} \cdot \nabla f(\vec{r})$ vanishes because we invoked the Coulomb gauge; an additional term of the form $\vec{p} \times \nabla f(\vec{r})$ is the curl of a gradient which is always zero. Also, matrix elements of the type $[\nabla f(\vec{r})] \cdot \vec{p}$ vanish [114, Appendix 5].

An exact wave function φ^{exact} of a system in a magnetic field transforms under change of the gauge origin accordingly to [57, p. 107]

$$\varphi_o^{exact} = \exp\left[\frac{i}{2}\left(\vec{B} \times \vec{R}_o\right) \cdot \vec{r}\right] \varphi^{exact} \ . \tag{3.52}$$

However, this relationship is not guaranteed for a Roothan approximation of the wave function [109, 61]:

$$\varphi_o^{approx} \neq \exp\left[\frac{i}{2}\left(\vec{B} \times \vec{R}_o\right) \cdot \vec{r}\right] \varphi^{approx} \ , \tag{3.53}$$

different gauge origins give different results. Hence, the gauge dependence vanishes only in the limit of a complete basis set, but not for the commonly used finite basis sets. As a result, the total value of a magnetic property may depends on the gauge origin $\vec{R}_o$ [109, p. 252].

The gauge error depends on the distance between the region where the electrons of a molecule are most probably located and the origin of the coordinate system. Therefore, the center of mass is usually chosen as gauge origin [109, p. 252], but this is not a unique choice, of course. Calculations of **g**-tensors and NMR shielding constants have been shown to approximate effectively the results of fully gauge-invariant calculations if one chooses the center of the electronic charge as gauge origin [115].

Several approaches have been suggested to eliminate or minimize the gauge origin dependence [116, 117, 118]. One procedure relies on *Gauge Including Atom Orbitals* (GIAO) [119, 117]; it completely eliminates the gauge dependence by rendering the basis functions explicitly dependent on the magnetic field via a complex-valued phase factor which refers to the origin position of a basis function located at the nucleus [109, p. 252]:

$$\chi_\nu\left(\vec{B}, \vec{r} - \vec{R}_\nu\right) = \exp\left[-\frac{i}{2}\left(\vec{B} \times \vec{R}_\nu\right) \cdot \vec{r}\right] \chi_\nu\left(\vec{r} - \vec{R}_\nu\right) \ . \tag{3.54}$$

Here $\vec{R}_\nu$ is the position of the nucleus at which a field-free basis function $\chi_\nu(\vec{r})$ is centered. The field-dependent phase factor assures gauge-invariant expectation values [109, p. 252]. Another commonly used technique minimizes the gauge-dependence by choosing separate gauges for each localized molecular orbital; this method is known as *Individual Gauge for Localized Orbital* (IGLO) [116].

Fortunately, if the size of the basis set is sufficiently large (as is generally the case in our calculations), the results obtained with different gauges may vary far less than their

inherent accuracy due to other approximations of the formalism. In this case, the gauge dependence may be neglected, provided that the gauge origin is chosen close to the center of electronic charge of the system under study. Consequently, each series of calculations with a certain basis set requires a sensitivity study regarding the gauge origin dependence.

When magnetic filed is induced by a nucleus, to avoid additional terms in the hyperfine Hamiltonian it is convenient to choose the vector potential so, that the nuclear position is a gauge origin, although other choices are also possible. Then (neglecting for the moment the magnetic moment distribution due to a finite size nucleus) the vector potential induced by a magnetic nucleus is defined by Eq. (3.1):

$$\vec{A}_\nu\left(\vec{r}\right) = \frac{\vec{\mu}_\nu \times \left(\vec{r} - \vec{R}_\nu\right)}{\left|\vec{r} - \vec{R}_\nu\right|^3} \ .$$

In summary, there is no gauge dependence in calculations of HFCCs. However, a dependence arises when the magnetic interaction in question is that of a homogeneous magnetic field with an electron spin or a nuclear spin, in particular, in calculations of **g**-tensors (Chapter 4) and NMR shielding constants [109, p. 252].

3.2 Spin Hamiltonian for Hyperfine Interaction

One can calculate the first-order energy change in a molecular system due to the presence of magnetic nuclei with the help of the hyperfine Hamiltonian derived in Section 3.1. However, the results of such calculations will be of limited use until one is able to compare them with experimental data. Therefore, the concepts widely used in the experimental determination of HFCCs have to be adapted to connect the quantities calculated theoretically using the hyperfine Hamiltonian and the values obtained in electronic paramagnetic resonance (EPR) experiments. Such a connection will be established in this Section.

3.2.1 Effective Spin

Magnetic hyperfine interactions, studied by magnetic spectroscopy, are of the order of 10^{-1} cm^{-1} [2, p. 7]. Hence, one is directly interested only in transitions within a group of levels which are (nearly) degenerate without a magnetic field. A convenient method is needed to represent the behavior of such a group of levels when the interaction of the electron spins in the field of the nuclear magnetic moments is studied or when an external magnetic field is applied.

For this purpose, a suitable method has been developed based on the concept of an "effective spin" $\vec{\tilde{S}}$ (a fictitious angular momentum). It is defined such that the degeneracy of the group of levels involved is equal to $(2\tilde{S}+1)$, the same as in an ordinary spin multiplet [2, p. 134]. Furthermore, the matrix elements between various states determined by the

full Hamiltonian that describes the system are required to be proportional to those of the effective spin. Then, it becomes possible to describe the behavior of the group of levels by an "effective spin Hamiltonian" employing only the effective electron spin and the nuclear spin operators [3, p. 111]. This concept is useful because it enables one to reproduce the behavior of the group of levels in a concise form, similar to that of a free atom or an ion. In some cases a theoretical justification of the effective spin Hamiltonian can be given [3, p. 111]; if the local symmetry of the system is known, the effective spin Hamiltonian is expected to reflect this symmetry, and suitable restrictions on its form have to be imposed. If the observed EPR spectrum does not conform to the assumed spin Hamiltonian, other forms can be tried empirically until a good fit is obtained.

The most general form of the spin Hamiltonian contains many terms, representing (a) the Zeeman interaction of electrons with an external magnetic field, (b) the level splittings due to indirect effects of the crystal field (fine structure), (c) the hyperfine structure due to the presence of a nuclear magnetic dipole and electric quadrupole moments in molecules, and (d) the Zeeman interaction of the nuclear moment with the external magnetic field (which may be modified by induced electronic moments – equivalent to a "paramagnetic shift") [2, p. 134].

Of course, real molecular systems studied by EPR experiment may possess a very complicated level structure. As first step, we consider in the following the simplest case when the system under study features only two degenerate levels in the absence of a magnetic field. For this case, known as a Kramers doublet, we will obtain the effective spin Hamiltonian in the next Subsection.

3.2.2 Spin Hamiltonian for a Kramers Doublet

Suppose we have a radical with an odd number of electrons. Then, according to Kramers theorem, in the absence of a magnetic field the energy eigenstates must remain at least two-fold degenerate [2, p. 650]. Such a pair of states Φ and $\bar{\Phi}$, forming a Kramers doublet, are in general n-electron wave functions, connected to each other by the time-reversal operator K so that $\bar{\Phi} = K\Phi$ [2, p. 647],

$$K = \prod_{p=1}^{n} -i\sigma_y(p)\, K_0(p)\,, \;\; K^2 = -1\;. \tag{3.55}$$

Here $p = 1, 2, ..., n$ refers to the action of the operator on the p-th electron; K_0 is the operator which converts a wave function ψ into its complex conjugate ψ^*. In particular, a Kramers pair of two spinors φ and $\bar{\varphi}$, connected by time-reversal symmetry, may be written as

$$\varphi = \begin{pmatrix} \varphi^{\alpha} \\ \varphi^{\beta} \end{pmatrix},\; \bar{\varphi} = \begin{pmatrix} -\varphi^{\alpha *} \\ \varphi^{\beta *} \end{pmatrix}\;, \tag{3.56}$$

where φ^{α} and φ^{α} indicate the usual spin-up and spin-down components. In fact, one can represent a Kramers pair of states Φ and $\bar{\Phi}$ by eigenfunctions of an effective spin $\vec{\tilde{S}}$ with

$\tilde{S} = \frac{1}{2}$, i.e. spin states $\left|\frac{1}{2}\right\rangle$ and $\left|-\frac{1}{2}\right\rangle$. Therefore, assuming that these spin states oriented along the axis z, the effective spin operator $\vec{\tilde{S}}$ can be defined via the Pauli matrices, Eq. (2.3):

$$\tilde{S}_x = \frac{1}{2}\sigma_x,\ \tilde{S}_y = \frac{1}{2}\sigma_y,\ \tilde{S}_z = \frac{1}{2}\sigma_z\ . \tag{3.57}$$

The degeneracy of a Kramers doublet can only be lifted by a magnetic field, which may be either an applied external field or a field generated by the non-zero magnetic moment of a nucleus. For a magnetic field induced by a nucleus, the energy splitting can be written as $-\vec{\mu}_\nu \cdot \vec{B}_e$, where $\vec{\mu}_\nu$ is the magnetic moment of the nucleus ν and $\vec{B}_e$ is the magnetic field produced by electrons of the radical at the position of nucleus ν [2, p. 651]. We assume the magnetic interactions to be much smaller than the energy difference between the doublet and other levels. Therefore, only matrix elements within the ground state are required for an adequate description of the energy levels of the doublet. Because each component of the magnetic field $\vec{B}_e$ is *odd* under time reversal $\left(K\hat{C}K^{-1} = -\hat{C}^\dagger\right)$, i.e. it changes sign [2, p. 647], we have

$$\langle\Phi|\,\vec{\mu}_\nu \cdot \vec{B}_e\,|\Phi\rangle = -\left\langle\bar{\Phi}\right|\vec{\mu}_\nu \cdot \vec{B}_e\left|\bar{\Phi}\right\rangle\ , \tag{3.58}$$

$$\langle\Phi|\,\vec{\mu}_\nu \cdot \vec{B}_e\left|\bar{\Phi}\right\rangle = \left\langle\bar{\Phi}\right|\vec{\mu}_\nu \cdot \vec{B}_e\,|\Phi\rangle^*\ . \tag{3.59}$$

Then, the matrix representation of the operator $-\vec{\mu}_\nu \cdot \vec{B}_e$ within the space $\left\{\Phi, \bar{\Phi}\right\}$ can be written as

$$\begin{pmatrix} \tau & \xi - i\zeta \\ \xi + i\zeta & -\tau \end{pmatrix} \tag{3.60}$$

with real numbers ξ, ζ, τ [114, p. 332]. For an effective spin $\tilde{S} = \frac{1}{2}$ and the corresponding eigenstates $\left|\frac{1}{2}\right\rangle$ and $\left|-\frac{1}{2}\right\rangle$, the operator

$$2\xi\tilde{S}_x + 2\zeta\tilde{S}_y + 2\tau\tilde{S}_z \tag{3.61}$$

has exactly the same matrix representation as the operator $-\vec{\mu}_\nu \cdot \vec{B}_e$ within the space $\left\{\Phi, \bar{\Phi}\right\}$ [114, p. 333]. In other words, the matrix elements of the magnetic interactions within the Kramers doublet state can be completely represented by a linear form in the components of the effective spin $\vec{\tilde{S}}$ with real coefficients, if one correlates $\left|\frac{1}{2}\right\rangle$ with Φ and $\left|-\frac{1}{2}\right\rangle$ with $\bar{\Phi}$ [114, p. 333]. One can represent the coefficients ξ, ζ, and τ of Eq. (3.61) as linear forms in the components of nuclear spin $\vec{I}_\nu$ and represent in this way the interaction of the electrons with the magnetic moments of the nuclei. Nuclear spin $\vec{I}_\nu$ is connected to the the magnetic moments of the nucleus $\vec{\mu}_\nu$ by the relation [3, p. 95]:

$$\vec{\mu}_\nu = \gamma_\nu \vec{I}_\nu\ . \tag{3.62}$$

Thus, one arrives at an operator equivalent representation of the interactions of the electrons and the magnetic moments of the nuclei within the ground state multiplet (doublet). Such a linear form can be written as an effective spin Hamiltonian $\hat{H}^{eff}$ for the

hyperfine interactions [2, p. 26],[3, p. 136]:

$$\hat{H}^{eff} = \sum_{\nu=1}^{N} \vec{\tilde{S}} \cdot \mathbf{a}^{\nu} \cdot \vec{I}_{\nu} \ . \tag{3.63}$$

Here $\vec{I}_{\nu}$ couples with the effective electron spin $\vec{\tilde{S}}$ and the summation runs over N nuclei present in the system. Matrix $\mathbf{a}^{\nu}$ represents a real 3×3 matrix which includes the orientations of the effective spin vector $\vec{\tilde{S}}$, nuclear spin $\vec{I}_{\nu}$ [2, pp. 13, 26]. The quantity $\mathbf{a}^{\nu}$ (no confusion should arise between the index ν of a nucleus and a power) is often called **a**-tensor, although its components do not transform like tensor components [2, p. 26]. The notation $\vec{\tilde{S}} \cdot \mathbf{a}^{\nu} \cdot \vec{I}_{\nu}$ stands for

$$\begin{aligned} \vec{\tilde{S}} \cdot \mathbf{a}^{\nu} \cdot \vec{I}_{\nu} = {} & a^{\nu}_{xx}\tilde{S}_x I_{\nu x} + a^{\nu}_{yy}\tilde{S}_y I_{\nu y} + a^{\nu}_{zz}\tilde{S}_z I_{\nu z} \\ & + a^{\nu}_{xy}\tilde{S}_y I_{\nu x} + a^{\nu}_{yx}\tilde{S}_x I_{\nu y} + a^{\nu}_{yz}\tilde{S}_z I_{\nu y} \\ & + a^{\nu}_{zy}\tilde{S}_y I_{\nu z} + a^{\nu}_{zx}\tilde{S}_x I_{\nu z} + a^{\nu}_{xz}\tilde{S}_z I_{\nu x} \ . \end{aligned} \tag{3.64}$$

Having established the form of the effective spin Hamiltonian, one can finally define the values obtained in EPR experiments and relate them to solutions of the hyperfine Hamiltonian derived in Section 3.1.

3.2.3 Hyperfine Coupling Tensor

The effective spin Hamiltonian of Eq. (3.63) operates on the basis of direct product of normalized electron and nuclear spin functions [3, p. 113]

$$|m_s; m_1, ..., m_\nu, ..., m_N\rangle = \left|\tilde{S}\tilde{m}_s\right\rangle \otimes |I_1 m_{z1}\rangle \otimes \cdots \otimes |I_\nu m_{z\nu}\rangle \otimes \cdots \otimes |I_N m_{zN}\rangle \ . \tag{3.65}$$

Here the effective spin functions $\left|\tilde{S}\tilde{m}_s\right\rangle$ represents the electronic states defined by a Kramers pair Φ or $\bar{\Phi}$, Eq. (3.56), and $|I_\nu m_{z\nu}\rangle$ the spin state of the nucleus ν with quantum number I_ν and spin projection $I_{\nu z}$ so that

$$I_{\nu z}\,|m_s; m_1..., m_\nu, ...m_N\rangle = m_{\nu z}\,|m_s; m_1..., m_\nu, ...m_N\rangle \ . \tag{3.66}$$

Transitions between energy levels, considered in magnetic spectroscopy, involve various combinations of flips of electron and nuclear spins. In other words, we are interested only in transitions which do not change the orientations of nuclear spins. The corresponding selection rules read [2, p. 27]:

$$\Delta m_s = \pm 1; \ \Delta m_{I,\nu} = 0 \ . \tag{3.67}$$

The latter condition corresponds to the so-called strong field approximation which implies that the interaction energy among nuclear spins is much less than between the spins and

the external magnetic field. Therefore, a state of the system can be presented as a product of the individual nuclear states. It is convenient to separate the contributions from different nuclei and focus in the following on finding matrix $\mathbf{a}^\nu$ of a particular nucleus ν. Applying the selection rules of Eq. (3.67), the splitting between two energy levels in the presence of nucleus ν is:

$$\begin{aligned}\Delta E = &\left\langle \frac{1}{2}; m_1, ..., m_N \middle| \vec{\tilde{S}} \cdot \mathbf{a}^\nu \cdot \vec{I}_\nu \middle| \frac{1}{2}; m_1, ..., m_N \right\rangle \\ &- \left\langle -\frac{1}{2}; m_1, ..., m_N \middle| \vec{\tilde{S}} \cdot \mathbf{a}^\nu \cdot \vec{I}_\nu \middle| -\frac{1}{2}; m_1, ..., m_N \right\rangle \ .\end{aligned} \tag{3.68}$$

Because $\vec{\tilde{S}}$ and $\vec{I}_\nu$ are not coupled in our approximation, then $\vec{\mu}_\nu$ can be considered as a classical quantity. The classical magnetic moment $\vec{\mu}_\nu$ associated with the spin of the nucleus ν can be written for our purposes as [120, p. 381]

$$\mu_{\nu k} = \gamma_\nu \left\langle m_\nu \right| I_{\nu k} \left| m_\nu \right\rangle \ , \tag{3.69}$$

where $k = x$, y, z are Cartesian components. Employing Eqs. (3.64, 3.62, 3.68), we obtain

$$\Delta E = \frac{1}{\gamma_\nu} \left(\left\langle \frac{1}{2} \middle| \vec{\tilde{S}} \cdot \mathbf{a}^\nu \cdot \vec{\mu}_\nu \middle| \frac{1}{2} \right\rangle - \left\langle -\frac{1}{2} \middle| \vec{\tilde{S}} \cdot \mathbf{a}^\nu \cdot \vec{\mu}_\nu \middle| -\frac{1}{2} \right\rangle \right) \ . \tag{3.70}$$

ΔE can be obtained from diagonalization of the matrix $\vec{\tilde{S}} \cdot \mathbf{a}^\nu \cdot \vec{\mu}_\nu$. We use the fact that the operator

$$\lambda_x \sigma_x + \lambda_y \sigma_y + \lambda_z \sigma_z \tag{3.71}$$

has the eigenvalues (see Section 3.5):

$$\pm \left(\lambda_x^2 + \lambda_y^2 + \lambda_z^2 \right)^{1/2} \ . \tag{3.72}$$

Application of this relation yields the following result for Eq. (3.70):

$$\begin{aligned}\Delta E^2 = &\frac{1}{\gamma_\nu^2} [(\mu_{\nu x} a^\nu_{xx} + \mu_{\nu y} a^\nu_{yx} + \mu_{\nu z} a^\nu_{zx})^2 \qquad (3.73)\\ &+ (\mu_{\nu x} a^\nu_{xy} + \mu_{\nu y} a^\nu_{yy} + \mu_{\nu z} a^\nu_{zy})^2 \\ &+ (\mu_{\nu x} a^\nu_{xz} + \mu_{\nu y} a^\nu_{yz} + \mu_{\nu z} a^\nu_{zz})^2] \\ = &\frac{1}{\gamma_\nu^2} \sum_{k,l} \mu_{\nu k} \mu_{\nu l} \sum_\alpha a^\nu_{k\alpha} a^\nu_{l\alpha} \ . \qquad (3.74)\end{aligned}$$

The latter expression is a compact representation of the energy difference between the electronic levels in the presence of a nuclear magnetic moment. It is useful to introduce the quantities

$$A^\nu_{kl} = \sum_\alpha a^\nu_{\alpha k} a^\nu_{\alpha l} \ , \text{ or } \mathbf{A}^\nu = \mathbf{a}^{\nu T} \mathbf{a}^\nu \ , \tag{3.75}$$

which form the components of a *true* tensor, namely the hyperfine coupling tensor $\mathbf{A}^\nu$ [2, p. 652]. This symmetric tensor can *always* be transformed to diagonal form by a proper choice of coordinate system. Moreover, the coordinate system in which tensor $\mathbf{A}^\nu$ is diagonal is identical to that in which matrix $\mathbf{a}^\nu$ is diagonal.

Indeed, matrix $\mathbf{a}^\nu$ can be altered by two separate transformations. The first one is a change of the coordinate system. As a result, the components of $\vec{I}_\nu$ are replaced with another set $\vec{I}'_\nu$

$$I'_\nu = \sum_{q=1}^{3} R_{kq} I_{\nu q} \ , \tag{3.76}$$

where R_{kq} are components of a real orthogonal matrix ($\mathbf{R}^T = \mathbf{R}^{-1}$), or in matrix form

$$\vec{I}'_\nu = \mathbf{R}\vec{I}_\nu \ , \ \vec{I}_\nu = \mathbf{R}^{-1}\vec{I}'_\nu = \mathbf{R}^T\vec{I}'_\nu \ . \tag{3.77}$$

The second possible transformation of $\mathbf{a}$ is a convenient choice of two Kramers partners from the subspace spanned by the degenerate Kramers functions $\left\{\Phi, \bar{\Phi}\right\}$. The corresponding unitary transformation $D^{(1/2)}$ in that subspace [2, p. 652]

$$\Phi' = D^{(1/2)}\Phi \tag{3.78}$$

defines a transformation of the corresponding effective spin $\vec{\tilde{S}}$ [3, Appendix C],

$$\vec{\tilde{S}}' = D^{(1/2)}\vec{\tilde{S}}D^{(1/2)\dagger} \ , \tag{3.79}$$

similar to any operator corresponding to an observable. Because $D^{(1/2)}$ is unitary, $D^{(1/2)\dagger} = D^{(1/2)-1}$, we obtain

$$\vec{\tilde{S}}' = D^{(1/2)}\vec{\tilde{S}}D^{(1/2)-1} \ . \tag{3.80}$$

The transformed effective spin operator $\vec{\tilde{S}}'$ is related to the origin spin operator $\vec{\tilde{S}}$ by a linear transformation (see Section 3.5),

$$\tilde{S}'_k = \sum_{q=1}^{3} Q_{kq}\tilde{S}_q \ , \ \tilde{S}_q = \sum_{k=1}^{3} \left(Q^{-1}\right)_{qk} \tilde{S}'_k = \sum_{k=1}^{3} Q_{kq}\tilde{S}'_k \ , \tag{3.81}$$

where Q_{kq} are components of a real orthogonal matrix ($\mathbf{Q}^T = \mathbf{Q}^{-1}$) [2, p. 652].

Thus, for the transformed effective spin Hamiltonian we obtain

$$\vec{\tilde{S}}^T\mathbf{a}^\nu\vec{I}_\nu = \vec{\tilde{S}}'^T\mathbf{Q}\mathbf{a}^\nu\mathbf{R}^T\vec{I}'_\nu = \vec{\tilde{S}}'^T\mathbf{a}^{\nu\prime}\vec{I}'_\nu \ , \tag{3.82}$$

where the matrix $\mathbf{a}^{\nu\prime} = \mathbf{Q}\mathbf{a}^\nu\mathbf{R}^T$ defines the transformed matrix $\mathbf{a}^\nu$. We now specialize the matrices $\mathbf{Q}$ and $\mathbf{R}$ such that they accomplish a *singular value decomposition* of $\mathbf{a}^\nu$ [121, pp. 70-71],

$$\mathbf{a}^\nu = \mathbf{Q}^T\mathbf{a}^{\nu\prime}\mathbf{R} \ , \tag{3.83}$$

where $\mathbf{a}^{\nu\prime}$ exhibits diagonal form. As a result, we have

$$\mathbf{A}^{\nu\prime} = \mathbf{a}^{\nu\prime T}\mathbf{a}^{\nu\prime} = \mathbf{R}\mathbf{a}^{\nu}\mathbf{Q}^T\mathbf{Q}\mathbf{a}^{\nu}\mathbf{R}^T = \mathbf{R}\mathbf{A}^{\boldsymbol{\nu}}\mathbf{R}^T \tag{3.84}$$

Therefore, matrix $\mathbf{R}$ also diagonalizes $\mathbf{A}^{\boldsymbol{\nu}}$. Moreover, the diagonal elements of $\mathbf{a}^{\nu\prime}$ are the square roots of the elements of $\mathbf{A}^{\nu\prime}$:

$$a^{\nu}_{xx} = \sqrt{A^{\nu}_{xx}},\ a^{\nu}_{yy} = \sqrt{A^{\nu}_{yy}},\ a^{\nu}_{zz} = \sqrt{A^{\nu}_{zz}}\ . \tag{3.85}$$

Strictly speaking, these relations hold for the primed quantities, but it is convenient to return to the original designators after having applied transformations $\mathbf{Q}$ and $\mathbf{R}$.

The components of $\mathbf{A}^{\nu}$ are related to the experimental energy splitting ΔE due to the presence of the nucleus ν as follows, Eq. (3.74):

$$A^{\nu}_{kl} = \frac{\gamma^2_{\nu}}{2}\left.\frac{\partial^2\left(\Delta E\right)^2}{\partial\mu_{\nu k}\mu_{\nu l}}\right|_{\vec{\mu}_{\nu}=0}\ . \tag{3.86}$$

The connection between theory and experiment is established by assuming that ΔE of Eq. (3.86) is the energy difference calculated theoretically with the hyperfine Hamiltonian of the n-electron system

$$\hat{H}^{hf}_{total} = \sum_{i=1}^{n}\hat{h}^{hf}\left(i\right)\ , \tag{3.87}$$

where $\hat{h}^{hf}\left(i\right)$ is the one-electron Hamiltonian for electron i derived in Section 3.1. The energy difference between two degenerated levels corresponding to n-electron wave functions Φ and $\bar{\Phi}$ in the magnetic field induced by a nucleus

$$\Delta E^{hf} = E_1 - E_2 \tag{3.88}$$

can be obtained in terms of the standard first-order perturbation treatment for a pair of degenerate states [90, p. 175]

$$\det\begin{pmatrix} \langle\Phi|\hat{H}^{hf}_{total}|\Phi\rangle - E & \langle\Phi|\hat{H}^{hf}_{total}|\bar{\Phi}\rangle \\ \langle\bar{\Phi}|\hat{H}^{hf}_{total}|\Phi\rangle & \langle\bar{\Phi}|\hat{H}^{hf}_{total}|\bar{\Phi}\rangle - E \end{pmatrix} = 0\ . \tag{3.89}$$

At this point it is helpful to introduce further approximations. Without a magnetic field, a two-component KS calculation with self-consistent treatment of SO interaction on an open-shell system yields two degenerate solutions, represented by KS determinants which can be chosen as Kramers partners; in other words, after suitable adjustment of phases, the determinants are formally connected by time-reversal symmetry. If those KS determinants are obtained from a restricted open-shell Kohn-Sham calculation (ROKS), the spinors of the paired electrons are also connected by time-reversal symmetry. Such a KS determinant of $2M+1$ normalized spin orbitals φ_i, where M spin orbitals are "paired", can be written as

$$\Phi_{KS} = \mathcal{A}\left\{\varphi_1\cdots\varphi_M\varphi_{M+1}\bar{\varphi}_1\cdots\bar{\varphi}_M\right\}\ , \tag{3.90}$$

where the antisymmetrizing operator $\mathcal{A}$ comprises the normalization factor [109, p. 59]. However, in the present work, we use a Kramers pair of KS determinants which are of this general form, but with orbitals determined by the so-called "half-electron method". In this method, two "half" electrons of opposite spins occupy the orbital of the open shell and this system is then treated in the framework of the restricted Kohn-Sham (RKS) formalism [109, p. 71], [122].

The expectation value of the total hyperfine Hamiltonian $\hat{H}^{hf}_{total}$, Eq. (3.87), reads ($n = 2M + 1$) [109, p. 60]:

$$\langle \Phi_{KS}|\hat{H}^{hf}_{total}|\Phi_{KS}\rangle = \sum_{i=1}^{M+1}\langle\varphi_i|\hat{h}^{hf}|\varphi_i\rangle + \sum_{i=1}^{M}\langle\bar{\varphi}_i|\hat{h}^{hf}|\bar{\varphi}_i\rangle \ . \tag{3.91}$$

The various terms of the operator $\hat{H}^{hf}$ are proportional to either $\vec{\sigma}$ or $\vec{L}$ operators [Eq. (3.27)], which are time-odd; therefore, they change signs with time reversal [3, Appendix C], and we have

$$\langle\varphi_i|\hat{h}^{hf}|\varphi_i\rangle = -\langle\bar{\varphi}_i|\hat{h}^{hf}|\bar{\varphi}_i\rangle \ . \tag{3.92}$$

Thus, according to Eq. (3.91), the paired spin orbitals do not contribute to the matrix elements of the corresponding KS determinants of the hyperfine Hamiltonian:

$$\langle \Phi_{KS}|\hat{H}^{hf}_{total}|\Phi_{KS}\rangle = \langle\varphi_{M+1}|\hat{h}^{hf}|\varphi_{M+1}\rangle \ . \tag{3.93}$$

According to Eq. (3.55), Kramers conjugation of Φ_{KS} yields:

$$\bar{\Phi}_{KS} = \mathcal{A}\left\{\bar{\varphi}_1\cdots\bar{\varphi}_M\bar{\varphi}_{M+1}\varphi_1\cdots\varphi_M\right\} \ . \tag{3.94}$$

Interchanging the first M columns of the latter determinant with the last M columns, we have:

$$\bar{\Phi}_{KS} = (-1)^M\,\mathcal{A}\left\{\varphi_1\cdots\varphi_M\bar{\varphi}_{M+1}\bar{\varphi}_1\cdots\bar{\varphi}_M\right\} \ . \tag{3.95}$$

Then, the matrix element $\langle\Phi_{KS}|\hat{H}^{hf}|\bar{\Phi}_{KS}\rangle$ reads:

$$\langle \Phi_{KS}|\hat{H}^{hf}_{total}|\bar{\Phi}_{KS}\rangle = (-1)^M\left[\sum_{i=1}^{M}\langle\varphi_i|\hat{h}^{hf}|\varphi_i\rangle + \sum_{i=1}^{M}\langle\bar{\varphi}_i|\hat{h}^{hf}|\bar{\varphi}_i\rangle + \langle\varphi_{M+1}|\hat{h}^{hf}|\bar{\varphi}_{M+1}\rangle\right] \ . \tag{3.96}$$

Employing Eq. (3.92), we have

$$\langle \Phi_{KS}|\hat{H}^{hf}_{total}|\bar{\Phi}_{KS}\rangle = (-1)^M\,\langle\varphi_{M+1}|\hat{h}^{hf}|\bar{\varphi}_{M+1}\rangle \ . \tag{3.97}$$

The matrix element $\langle\bar{\Phi}_{KS}|\hat{H}^{hf}|\bar{\Phi}_{KS}\rangle$ and $\langle\bar{\Phi}_{KS}|\hat{H}^{hf}|\Phi_{KS}\rangle$ can be obtained as

$$\langle\bar{\Phi}_{KS}|\hat{H}^{hf}|\bar{\Phi}_{KS}\rangle = -\langle\Phi_{KS}|\hat{H}^{hf}_{total}|\Phi_{KS}\rangle \ , \tag{3.98}$$

$$\langle\bar{\Phi}_{KS}|\hat{H}^{hf}|\Phi_{KS}\rangle = \langle\Phi_{KS}|\hat{H}^{hf}_{total}|\bar{\Phi}_{KS}\rangle^* \ . \tag{3.99}$$

because $\hat{H}^{hf}$ is a time-odd operator.

Employing Eq. (3.91, 3.97), Eq. (3.89) can be reduced to:

$$\det \begin{pmatrix} \langle\varphi|\hat{h}^{hf}|\varphi\rangle - E & (-1)^M \langle\varphi|\hat{h}^{hf}|\bar{\varphi}\rangle \\ (-1)^M \langle\bar{\varphi}|\hat{h}^{hf}|\varphi\rangle & \langle\bar{\varphi}|\hat{h}^{hf}|\bar{\varphi}\rangle - E \end{pmatrix} = 0 \ . \tag{3.100}$$

Here, we denoted the spin orbital φ_{M+1} of the unpaired electron (the orbital where the half-electrons are located) by φ, for simplicity. Then, the square of the energy difference ΔE^{hf} of Eq. (3.88) reads:

$$(\Delta E^{hf})^2 = \left[\langle\varphi|\hat{h}^{hf}|\varphi\rangle - \langle\bar{\varphi}|\hat{h}^{hf}|\bar{\varphi}\rangle\right]^2 + 4\langle\varphi|\hat{h}^{hf}|\bar{\varphi}\rangle\langle\bar{\varphi}|\hat{h}^{hf}|\varphi\rangle \ . \tag{3.101}$$

With Eq. (3.86), we can obtain the **A**-tensor of nucleus ν by taking second derivatives with respect to Cartesian components of the magnetic moment $\mu_{\nu k}$ of nucleus ν:

$$A^{\nu}_{kl} = \frac{\gamma_\nu^2}{2} \left.\frac{\partial^2 \left(\Delta E^{hf}\right)^2}{\partial\mu_{\nu k}\partial\mu_{\nu l}}\right|_{\vec{\mu}_\nu=0} \tag{3.102}$$

$$= \gamma_\nu^2 \left[\left(\Phi_{11}^{\nu k} - \Phi_{22}^{\nu k}\right)\left(\Phi_{11}^{\nu l} - \Phi_{22}^{\nu l}\right) + 2\Phi_{12}^{\nu k}\Phi_{21}^{\nu l} + 2\Phi_{12}^{\nu l}\Phi_{21}^{\nu k}\right] \ . \tag{3.103}$$

Because $\hat{H}^{hf}$ is linear in $\vec{\mu}_\nu$, Eq. (3.27), second derivatives of matrix elements of $\hat{h}^{hf}$ with respect to the components of $\vec{\mu}_\nu$ vanish. To derive Eq. (3.102), we used the Hellmann-Feynman theorem [109, p. 241]:

$$\Phi_{11}^{\nu k} \equiv \frac{\partial}{\partial\mu_{\nu k}} \langle\varphi|\hat{h}^{hf}|\varphi\rangle\Big|_{\vec{\mu}_\nu=0} = \langle\varphi| \left.\frac{\partial\hat{h}^{hf}}{\partial\mu_{\nu k}}\right|_{\vec{\mu}_\nu=0} |\varphi\rangle \ , \tag{3.104}$$

$$\Phi_{22}^{\nu k} \equiv \frac{\partial}{\partial\mu_{\nu k}} \langle\bar{\varphi}|\hat{h}^{hf}|\bar{\varphi}\rangle\Big|_{\vec{\mu}_\nu=0} = \langle\bar{\varphi}| \left.\frac{\partial\hat{h}^{hf}}{\partial\mu_{\nu k}}\right|_{\vec{\mu}_\nu=0} |\bar{\varphi}\rangle \ ,$$

$$\Phi_{12}^{\nu k} \equiv \frac{\partial}{\partial\mu_{\nu k}} \langle\varphi|\hat{h}^{hf}|\bar{\varphi}\rangle\Big|_{\vec{\mu}_\nu=0} = \langle\varphi| \left.\frac{\partial\hat{h}^{hf}}{\partial\mu_{\nu k}}\right|_{\vec{\mu}_\nu=0} |\bar{\varphi}\rangle \ ,$$

$$\Phi_{21}^{\nu k} \equiv \frac{\partial}{\partial\mu_{\nu k}} \langle\bar{\varphi}|\hat{h}^{hf}|\varphi\rangle\Big|_{\vec{\mu}_\nu=0} = \langle\bar{\varphi}| \left.\frac{\partial\hat{h}^{hf}}{\partial\mu_{\nu k}}\right|_{\vec{\mu}_\nu=0} |\varphi\rangle \ .$$

These expressions are valid for a Kramers pair $\{\varphi, \bar{\varphi}\}$ of orbitals (independent of $\vec{\mu}_\nu$) as solutions of the DK Hamiltonian without magnetic field. Then, using matrix elements of Eqs. (3.104), one can construct tensor $\mathbf{A}^\nu$ according to Eq. (3.102) which has to be diagonalized as described above, Eq. (3.85).

Other approaches to establish an effective spin Hamiltonian for magnetic interactions are available in the literature [59, 58, 17]. We will use here the method of van Lenthe et al. for derivation of expressions for a-values [17] to demonstrate that it gives the same results, Eq. (3.102). When a molecular electronic system is affected by a perturbation $\vec{X}$, its Hamiltonian changes to first order as

$$\hat{H}\left(\vec{X}\right) = \hat{H}^{(0)} + \left.\frac{d\hat{H}}{d\vec{X}}\right|_{\vec{X}=0} \cdot \vec{X} \ . \tag{3.105}$$

Accordingly, one can write the linear approximation of the hyperfine Hamiltonian $\hat{H}^{hf}$ of a molecular system perturbed by the magnetic field induced by the nucleus ν – reduced to the subspace spanned by a Kramers pair $\left\{\Phi, \bar{\Phi}\right\}$ – as the following 2×2 matrix:

$$\hat{H}^{hf}_{red} = \sum_k \frac{\partial}{\partial \mu_{\nu k}} \left(\begin{array}{cc} \langle \Phi | \hat{H}^{hf}_{total} | \Phi \rangle & \langle \Phi | \hat{H}^{hf}_{total} | \bar{\Phi} \rangle \\ \langle \bar{\Phi} | \hat{H}^{hf}_{total} | \Phi \rangle & \langle \bar{\Phi} | \hat{H}^{hf}_{total} | \bar{\Phi} \rangle \end{array} \right) \Bigg|_{\vec{\mu}_\nu = 0} \mu_{\nu k} \ , \tag{3.106}$$

where $\mu_{\nu k}$ are the Cartesian components of the nuclear magnetic moment $\vec{\mu}_\nu$. The matrix elements $\langle \Phi | \hat{H}^{hf}_{total} | \Phi \rangle$, $\langle \bar{\Phi} | \hat{H}^{hf}_{total} | \bar{\Phi} \rangle$, $\langle \Phi | \hat{H}^{hf}_{total} | \bar{\Phi} \rangle$, and $\langle \bar{\Phi} | \hat{H}^{hf}_{total} | \Phi \rangle$ can be obtained using a KS determinant Φ_{KS} from ROKS or half-electron RKS calculation as described earlier in this section. Then, employing Eqs. (3.91, 3.97) one can reduce Eq. (3.106) to the form

$$\hat{H}^{hf}_{red} = \sum_k \frac{\partial}{\partial \mu_{\nu k}} \left(\begin{array}{cc} \langle \varphi | \hat{h}^{hf} | \varphi \rangle & \langle \varphi | \hat{h}^{hf} | \bar{\varphi} \rangle \\ \langle \bar{\varphi} | \hat{h}^{hf} | \varphi \rangle & \langle \bar{\varphi} | \hat{h}^{hf} | \bar{\varphi} \rangle \end{array} \right) \Bigg|_{\vec{\mu}_\nu = 0} \mu_{\nu k} \ , \tag{3.107}$$

where φ is the orbital occupied by the unpaired electron and $\bar{\varphi}$ its Kramers partner. In notations of Eqs. (3.104), the preceding equation reads:

$$\hat{H}^{hf}_{red} = \sum_k \left(\begin{array}{cc} \Phi^{\nu k}_{11} & \Phi^{\nu k}_{12} \\ \Phi^{\nu k}_{21} & \Phi^{\nu k}_{22} \end{array} \right) \mu_{\nu k} \ , \tag{3.108}$$

This 2×2 Hamiltonian is of the same form as an effective Hamiltonian $\hat{H}^{eff} = \vec{\tilde{S}} \cdot \mathbf{a}^\nu \cdot \vec{I}_\nu$ with $\vec{I}_\nu = \gamma_\nu^{-1} \vec{\mu}_\nu$, Eq. (3.62), and $\vec{\tilde{S}} = \frac{1}{2}\vec{\sigma}$, Eq. (3.57), which reads explicitly:

$$\hat{H}^{eff} = \frac{1}{2\gamma_\nu} \sum_k \left(\begin{array}{cc} a^\nu_{zk} & a^\nu_{xk} - i a^\nu_{yk} \\ a^\nu_{xk} + i a^\nu_{yk} & -a^\nu_{zk} \end{array} \right) \mu_{\nu k} \ . \tag{3.109}$$

Comparing the coefficients of the components $\mu_{\nu k}$ of Eqs. (3.108) and (3.109), the values a^ν_{kl} can be directly expressed in terms of the matrix elements $\Phi^{\nu k}_{ij}$:

$$\begin{aligned} a^\nu_{kx} &= 2\gamma_\nu \operatorname{Re} \Phi^{\nu k}_{12} = 2\gamma_\nu \operatorname{Re} \Phi^{\nu k}_{21} \ , \\ a^\nu_{ky} &= -2\gamma_\nu \operatorname{Im} \Phi^{\nu k}_{12} = 2\gamma_\nu \operatorname{Im} \Phi^{\nu k}_{21} \ , \\ a^\nu_{kz} &= 2\gamma_\nu \Phi^{\nu k}_{11} = -2\gamma_\nu \Phi^{\nu k}_{22} \ . \end{aligned} \tag{3.110}$$

Note, that the matrix $\mathbf{A}^\nu = \mathbf{a}^{\nu T} \mathbf{a}^\nu$, Eq. (3.75), coincides with that obtained above, Eq. (3.102), i.e. both derivations lead to the same expressions for a-values.

3.3 Results and Discussion

3.3.1 Computational Details

Adequate account of correlation effects is crucial for accurate calculations of HFCCs [13]. Furthermore, these calculations require carefully selected extended basis sets [13] and, in

a DF approach, a proper choice of the *xc* functional. Isotropic HFCCs are also known to be very sensitive to the geometry of a molecular system [13]. Thus, for benchmarking purposes, atomic calculations offer the advantage that no geometry effects are involved.

A wave function should represent the region near a nucleus, that basically defines the HFCC, with high accuracy. Thus, as mentioned in Section 3.2, a well-known problem arises when Gaussian-type basis functions are employed, which do not satisfy the correct cusp conditions of the wave function at the nucleus [41]. Fortunately, one can partly overcome this drawback by using extended basis sets augmented by tight *s*-type exponents [123]. In general, it has been recommended to calculate HFCCs with basis sets of triple-ζ quality (or better), extended by functions with very large *s*-type exponents and by polarization functions [13].

The formalism to calculate *a*-values outlined in Sections 3.1 and 3.2 was implemented in the program ParaGauss for parallel computers [75, 86], which is based on the LCGTO-FF-DF (linear combination of Gaussian-type orbitals fitting-functions density functional) method [88]. Details of the implementation can be found in Chapter 5. We calculated HFCCs with two-component relativistic wave functions [86, 87] of a Kramers doublet representing an unpaired electron which resulted from a self-consistent two-component treatment including the SO interaction (Section 3.2). The SO interaction was treated in two different variants: at DKnuc level (with non-relativistic treatment of *ee* interaction) and at DKee1 level which takes first-order *ee*-correction due to relativistic transformations of the Hartree term into account [87]. Non-relativistic *xc* potentials have been used without DK transformations. The spin orbitals were generated in the spin-restricted half-electron fashion described in Section 3.2.2, using the gradient-corrected (GGA) exchange [124] and correlation [125] functionals as suggested by Becke and Perdew (BP). For comparison with the present BP results and DF data from the literature, HFCCs were also calculated in the local density approximation (LDA) with the *xc* functional by Vosko-Wilk-Nusair (VWN) [126]. Whenever available, the radicals were studied in their experimental geometries.

Two different Gaussian-type basis sets are used in the LCGTO-FF-DF method: one to expand the KS orbitals and another one to represent the electron density when calculating the classical Coulomb (Hartree) interaction between electrons [127]. Very flexible basis sets are required for accurate relativistic transformations of the Hartree interaction [87]. Therefore, standard basis sets have to be augmented with functions of angular momentum l+1 or even l+2 functions, where l is the maximum angular momentum of the occupied atomic orbitals. We will demonstrate in Chapter 4 that such transformations are obligatory for an adequate accuracy of **g**-tensor calculations. For HFCCs calculations, we used these extended basis sets as starting point for specific further extensions.

Large and flexible uncontracted orbital basis sets were constructed for our test HFCC calculations to essentially eliminate basis set incompleteness effects. To improve the description of the region near the nuclei, these basis sets were augmented with several steep exponents, chosen as $\alpha_{n+1} = \alpha_n^2/\alpha_{n-1}$ etc., where α_n and α_{n+1} are the two largest ex-

ponents of a shell; in other words, the series of exponents was extended as a geometric progression.

The auxiliary fitting basis sets of the LCGTO-DF-FF method were constructed in a standard fashion by doubling the s- and p-exponents of orbital basis functions of standard basis sets [88]; these basis sets were augmented by standard sets of 5 p- and 5 d-type polarization functions [88].

All orbital and Coulomb fitting basis sets employed are listed in Appendix A. For convenience, we list in Appendix B the values of the nuclear spins and nuclear magnetic moments, taken from Ref. [128].

3.3.2 Hyperfine Coupling Constants for Cu, Ag, and Au Atoms

We chose copper, silver, and gold atoms as first tests for our DKH-based approach to the calculation of HFCCs. According to ZORA SR calculations, spin polarization effects play a minor role for these atoms [17]. This makes them suitable for examining the accuracy at which relativistic effects have to be accounted for. At the same time, these atoms, exhibiting an unpaired electron in the s shell, are very convenient for testing basis set saturation in the framework of the finite nucleus model (Section 3.1.2).

In Table 3.1, we compare isotropic absolute a-values of atomic Cu, Ag, and Au obtained with the VWN xc potential using various basis sets and different representations of the hyperfine Hamiltonian. The columns denoted as DK_0, DK_1, and DK_2 display the results obtained with the corresponding approximations of the hyperfine Hamiltonian, Eq. (2.54, 2.57, 2.58), see Chapter 2. The HFCC values calculated in both the point and finite nucleus models are presented. The standard basis sets, referred to as *std*, were chosen as follows (not augmented with steep s-type exponents): $(15s,11p,6d,6f)$ for Cu, constructed from the basis set $(14s,9p,5d)$ of Ref. [131], $(18s,13p,9d,9f)$ for Ag obtained from a $(17s,11p,8d)$ basis set of Ref. [132], and $(19s,15p,10d,6f,6g)$ for Au taken from Ref. [70] (see Appendix A). Basis sets labeled as "$+2s$", "$+4s$", "$+6s$" and "$+8s$" comprised in addition 2, 4, 6, or 8 tight s-type exponents, respectively. The *ee* interaction was treated in the economic DKnuc model because test calculations with DKnuc and DKee1 models gave HFCCs which differ by as little as $\sim$1 MHz for all atoms considered

One can see from Table 3.1 that the point nucleus model reveals an obvious instability of HFCCs with respect to an extension of the basis set. In fact, it is impossible to reach basis set saturation by adding tight s-type exponents. The absolute isotropic a-values do not convergence for any of the atoms studied; by extending the basis set, basically any value could be obtained in the point nucleus approach.

At variance with the point nucleus model, the finite nucleus model provides a-values that are essentially converged with respect to the basis set extension after addition of four tight s-type exponents in all inspected atoms (Table 3.1): basis set saturation can be reached in this model. Therefore, all HFCCs of this work discussed in the following were

Table 3.1: VWN absolute isotropic a-values (in MHz) calculated with point and finite nucleus models using different representations of the hyperfine Hamiltonian. Also shown are results calculated with the ZORA method and experimental data.

		Point nucleus model			Finite nucleus model			ZORA[b]	Exp.[c]
	Basis[a]	DK_0	DK_1	DK_2	DK_0	DK_1	DK_2		
^{63}Cu	*std*	10463	6813	6395	10454	6810	6393		
	$+2s$	15060	7954	7481	14664	7863	7394		
	$+4s$	20815	9093	8586	15899	8121	7644		
	$+6s$	28047	10308	9768	15894	8121	7644		
	$+8s$	36993	11600	11028	15890	8121	7644	6701	5867
^{107}Ag	*std*	4493	2105	1949	4474	2100	1945		
	$+2s$	8023	2728	2543	7166	2590	2411		
	$+4s$	13326	3414	3204	7439	2628	2448		
	$+6s$	21106	4198	3964	7441	2628	2448		
	$+8s$	32195	5092	4830	7440	2631	2446	1905	1713
^{197}Au	*std*	17455	4061	3783	16832	3979	3706		
	$+2s$	49581	6749	6365	27581	5022	4704		
	$+4s$	124359	10491	9985	27663	5025	4707		
	$+6s$	288601	15769	15096	27663	5025	4707		
	$+8s$	126139	10563	10054	27682	5025	4708	3143	3053

a) The standard basis set (see text) is denoted as *std*; extensions of this basis set by n steep s-type exponents are noted as $+ns$.
b) Zero-order regular approximation including spin orbit interaction, Ref. [17]
c) Gas phase experiment, Refs. [129, 130]

calculated with the finite nucleus model and the orbital basis sets extended with four steep s-type exponents.

Comparing the a-values in Table 3.1 for the approximations DK_0, DK_1, and DK_2, one concludes that "picture change" effects are essential for the calculation of HFCCs (see Chapter 2). At the DK_0 level, the calculated a-values notably overestimate the experimental data. This overestimation increases rapidly with nuclear charge Z as it is typical for relativistic effects [78]; the overestimation, a factor of ∼2 for Cu, increases to factors of ∼4 for Ag and ∼9 for Au. At the DK_1 level, the effect a mass-velocity correction notably reduces the a-values compared to those obtained at the $\mathbf{DK_0}$ level; errors are now ∼40% for Cu, ∼55% for Ag, and 65% for Au. Switching to the DK_2 level further reduces the calculated a-values toward the experimental data, but the calculated HFCCs still significantly overestimate the experimental values: 30% for Cu, 43% for Ag, and 54% for Au. Hence, only the DK_2 scheme as the most reliable one has been applied in this work to calculate HFCCs discussed in the following.

For comparison, we also list in Table 3.1 isotropic HFCCs calculated with the two-component DF ZORA SO method [17]; that method also provides a self-consistent treatment of the SO interaction in the RKS approximation. Similarly to the present DKH method, the ZORA SO scheme overestimates atomic a-values, although the results are closer to the experimental values. Note, that ZORA SO results were obtained with the point nucleus model with unsaturated basis sets [17], which are not complete with respect to the a-values as has been demonstrated later on [62]. Therefore, the close agreement of the ZORA results with experiment appears to be merely the result of a "lucky" choice of the basis set.

There are several sources of inaccuracy in the present calculations of atomic a-values. One of them is the lack of spin polarization effects. However, the results obtained from the spin restricted and spin unrestricted ZORA SR calculations for the atoms under scrutiny deviate at most by 1% [17]. Moreover, switching from the VWN to BP xc functionals alters the calculated a-values less than 3% [17]. Therefore, one of the dominating sources of inaccuracy in the present calculations of atomic a-values is probably approximations of the implemented finite nucleus model. Indeed, as described in Section 3.1.2, our finite nucleus model accounts for the isotropic part of the magnetic operator only, but the finite size of the nucleus is neglected in the nuclear attraction operator of the DK Hamiltonian [70, 71].

3.3.3 Hyperfine Interactions in Selected Test Molecules

The present DKH approach for calculating hyperfine constants was also tested on a few small molecules of light elements: NO_2 (Table 3.2), HCO (Table 3.3), and TiF_3 (Table 3.4). These molecules were chosen because for them detailed benchmark calculations have been reported [53, 55, 17]. In the Tables 3.2–3.4 a_{iso} stands for the isotropic part of a-matrix;

the notation t_{kk} refers to the anisotropic part of a-matrix which is computed by subtraction of the a_{iso} values from the eigenvalues of matrix a (Section 3.2.3).

The following saturated orbital basis sets were employed, augmented as outlined in Section 3.3.1: $(17s,8p,7d)$ for N, O, C; $(18s,5p,1d)$ for H; $(19s,8p,7d)$ for F; $(21s,11p,6d,5f)$ for Ti (Appendix A). The radicals NO_2 and HCO were computed at their experimental geometries [61]. The NO_2 molecule was oriented in the yz-plane with the z direction as C_2 symmetry axis; the experimental N-O distance is 1.194 Å and the angle 133.9°. For the HCO molecule, the C-H bond length is 1.152 Å, the C-O distance is 1.177 Å, and the angle H-C-O is 123°; the z-axis was oriented perpendicular to the molecular plane. For the planar molecule TiF_3, the HFCCs calculations have been performed with the Ti-F bond length optimized at the BP ZORA SR level, 1.784 Å [55], and at the BP DK SR level, 1.802 Å, obtained in the present work; apparently, there is no experimental value available so far.

The results in Tables 3.2 and 3.3 are given in Gauss which are common units for a-values of molecules featuring small g-tensor shifts, like organic radicals [5, p. 20]. HFCCs in Table 3.4 are presented in MHz as usually done for molecular systems manifesting large g-tensor shifts, in particular for transition metal complexes. The a-values calculated in atomic units are converted to MHz with the help of the factor 6.57968374×10^9; to obtain the a-values in Gauss, the values in MHz are to be multiplied by $0.71447/g$, where g-factors of the radicals under study are sufficiently close to g_e to use the latter for the purposes of conversion [5, p. 20].

We compare our VWN and BP HFCC results for NO_2 and HCO with corresponding ZORA SO data obtained with a Slater-type orbitals (STO) basis set [17] and with results of non-relativistic unrestricted Kohn-Sham (UKS) and *ab initio* GTO calculations [53]. The GGA PW86 *xc* used in Ref. [53] contains the correction of exchange by Perdew and Wang [133] and the correction for correlation suggested by Perdew [133]. Results of configuration interaction calculations performed with inclusion of singlets and doublets (CISD) [53], are also displayed in Table 3.2. In the above mentioned non-relativistic approaches, a-values were computed using Fermi contact and dipole hyperfine operators, Eqs. (3.25, 3.26) with $\vec{s} = \frac{1}{2}\vec{\sigma}$ [53].

Relativistic effects are expected to be small for the molecules NO_2 and HCO; therefore, calculations with relativistic and non-relativistic wave functions should give very similar a-values [17]. The the NO_2 radical, both isotropic and anisotropic a-values of N and O, calculated with the present method, agree well with experiment; VWN and BP results are very close to each other, as already reported in the ZORA SO study [17]. The difference between the present results and those of PW86 study is partly is due to different *xc* potentials and the UKS approach [53], which includes spin-polarization effects. Moreover, since basis set effects are known to be one of the major source of error in calculations of HFCCs [13], they should be another reason for the difference. Indeed, the considerably more compact IGLO-III basis sets [134] were employed in the PW86 calculation [53] and

the results are less satisfactory.

Finally, for a one-to-one comparison of computed HFCCs with experiment, one has to take into account the influence of environmental effects. In experiment, NO_2 radicals have been trapped in a sulfur hexafluoride matrix [135] at low temperature, which may slightly polarize the radical and hence result in experimental a-values that differ slightly from the unknown (experimental) gas-phase reference. At the CISD/(14s,7p,1d) level, the oxygen isotropic a-value is significantly underestimated compared to the experimental one, but for nitrogen atom good agreement with experimental isotropic a-value has been achieved [53].

For the H atom of the radical HCO (Table 3.3) the difference between VWN and BP HFCCs is more significant than for the atoms C and O and the radical NO_2. BP calculations agree well with the available experimental ^{1}H and ^{13}C a_{iso}-values. Our a_{iso}-values for ^{1}H and ^{13}C are larger than the corresponding ZORA SO values which is not unexpected due to different quality of the basis set: a saturated basis with respect to a_{iso}-values in the present finite nucleus description and an ad-hoc unsaturated basis employed at the point nucleus approximation level of ZORA SO calculations (see Section 3.3.2). In comparison with experiment, all anisotropic HFCCs parameters are well reproduced, except t_{xx} of the atom ^{13}C. However, all our calculated anisotropic a-values are in good agreement with those of other calculations. The present somewhat larger difference between VWN and BP a_{iso}-values for an H atom may partly be rationalized by different self-interaction (SI) errors of VWN and BP xc functionals, namely the lack of the exact cancellation of the Coulomb and xc energy in a one-electron system [46, p. 86]. SI corrected DF calculations of atoms and molecules have been shown to yield a much improved description of core orbitals and isotropic HFCCs [138, 139] and isotropic contribution to NMR shielding tensor [140]. In other words, isotropic HFCCs clearly exhibit a dependence on the SI error of a particular xc functional. Because the BP functional yields a much less SI error for the H atom (-0.0001 Hartree) than VWN (0.0314 Hartree), the difference between BP and VWN a_{iso}-values is large. For the atoms C, O, and N, which are many-electron systems, that effect is smaller. Both the CISD and PW86 calculations yield too large anisotropic carbon couplings. The CISD a_{iso} (H) value is underestimated, whereas PW86 calculations give overestimated isotropic carbon coupling.

HFCCs calculations of molecules containing transition metal atoms are often less precise, because both relativistic effects and very delicate polarization effects of core orbitals should be simultaneously represented with high accuracy. The results of our calculations of TiF_3 are displayed in Table 3.4 together with the data of ZORA SO, unrestricted ZORA SR calculations, RKS and UKS approaches [55, 56] which include SO interactions as a perturbation.

The ^{47}Ti hyperfine splittings are defined by the character of SOMO. The latter is a mixture of the Ti 4s orbital, a dominating Ti 3d contribution, and a small contribution of F 2p orbitals. The Ti 4s orbital makes a *direct* contribution to the isotropic a-value. Ti 3d orbitals cannot directly contribute to the isotropic a-value because they possesses a node

Table 3.2: Calculated hyperfine structure of NO_2 compared with results of other theoretical methods and experiment (in Gauss).

Method	^{14}N				^{17}O			
	a_{iso}	t_{xx}	t_{yy}	t_{zz}	a_{iso}	t_{xx}	t_{yy}	t_{zz}
VWN[a]	52.3	−6.3	−5.7	12.0	−17.6	18.2	17.0	−35.3
BP[a]	51.4	−6.2	−5.6	11.8	−16.3	18.3	17.0	−35.3
VWN[b]	49.7	−6.3	−5.8	12.1	−17.0	18.2	17.8	−36.0
BP[b]	48.9	−6.2	−5.7	11.9	−15.8	18.2	17.9	−36.1
PW86[c]	58.8	−7.3	−6.1	13.4	−21.1	19.5	18.0	−37.4
CISD[d]	50.2	−8.8	−8.1	16.7	−12.0	17.3	16.4	−33.7
Exp.[e]	54.7	−7.8	−5.4	13.8	−20.3	18.6	16.3	−34.6
Exp.[f]	54.2				−22.2			
Exp.[g]	54.0							

a) Present work.
b) ZORA SO, Ref. [17].
c) UKS Ref. [53].
d) Ref. [53].
e) Ref. [136].
f) Ref. [135].
g) Ref. [137].

Table 3.3: Calculated hyperfine structure of HCO molecule compared with results of other theoretical methods and experiment (in Gauss).

Method	^{1}H				^{13}C			
	a_{iso}	t_{xx}	t_{yy}	t_{zz}	a_{iso}	t_{xx}	t_{yy}	t_{zz}
VWN[a]	116.7	−5.0	8.5	−3.4	131.1	−14.4	27.3	−12.9
BP[a]	125.1	−4.9	8.3	−3.4	134.1	−14.1	26.5	−12.4
VWN[b]	108.2	−5.9	9.1	−3.2	121.7	−13.4	28.2	−14.8
BP[b]	115.7	−5.8	9.0	−3.1	124.6	−13.0	27.5	−14.5
PW86[c]	128.3	−5.2	7.3	−2.1	145.3	−14.2	31.4	−17.3
CISD[d]	101.7	−6.2	8.9	−2.7	139.5	−15.2	32.0	−16.9
Exp.[e]	126.4				130.4	−4.2	18.0	−13.8
Exp.[f]	135.8	−4.9	9.0	−3.2	134.6	−8.6	25.7	−17.1
	^{17}O							
	a_{iso}	t_{xx}	t_{yy}	t_{zz}				
VWN[a]	−5.3	18.6	−37.5	18.9				
BP[a]	−5.3	18.5	−37.3	18.9				
VWN[b]	−5.3	19.1	−37.6	18.5				
BP[b]	−5.2	18.8	−37.3	18.4				
PW86[c]	−10.9	20.6	−37.4	17.4				
CISD[d]	−10.8	17.0	−31.6	14.6				

a) Present work.
b) ZORA SO, Ref. [17].
c) UKS, Ref. [53].
d) Ref. [53].
e) Ref. [141].
f) Ref. [142].

Table 3.4: Calculated hyperfine structure of TiF_3 molecule compared with results of other theoretical methods and experiment (in MHz).

Method	^{47}Ti				^{19}F			
	a_{iso}	t_{xx}	t_{yy}	t_{zz}	a_{iso}	t_{xx}	t_{yy}	t_{zz}
VWN[a]	−298.7	15.5	15.5	−31.0	19.7	29.4	−13.8	−15.5
VWN[b]	−286.3	16.0	16.0	−32.0	16.4	28.9	−13.8	−15.1
BP[a]	−289.8	15.3	15.3	−30.6	15.4	32.3	−15.2	−17.1
BP[b]	−277.6	15.7	15.7	−31.4	12.0	31.9	−15.1	−16.8
VWN[c]	−283.3	18.5	18.5	−23.0	31.0	31.0	−10.2	−12.2
VWN[d]	−289.3	13.6	13.6	−17.9	−42.7	31.9	10.1	−36.3
VWN, SO[e]	−284.5	14.5	14.5	−28.9	38.8	22.8	−11.1	−11.7
BP, SO[e]	−260.8	14.8	14.8	−29.6	26.1	24.4	−11.9	−12.5
BP, SR[f]	−259.2	12.5	12.5	−25.0	20.4	32.3	−18.3	−14.0
BP, SR[g]	−227.9	8.4	8.4	−16.8	1.9	27.7	8.7	−36.4
Exp.[h]	−184.8	8.1	8.1	−16.2	|23.6|	|24.3|	|12.5|	|12.5|

a) Present work, d(Ti-F)=1.784 Å, taken from Ref. [55].
b) Present work, d(Ti-F)=1.802 Å, optimized at the BP DK SR level.
c) RKS Refs. [55, 56].
d) UKS Refs. [55, 56].
e) ZORA SO Ref. [17].
f) Restricted ZORA SR Ref. [17].
g) Unrestricted ZORA SR Ref. [17].
h) Ref. [143], Ne matrices.

at the position of the nucleus. However, they contribute *indirectly* due to spin-polarization effects. Such effects arise because paired s electrons of lower-lying shells interact differently with the unpaired electron: assuming the latter is a spin-up electron, the spin-up electrons experience both the Coulomb and the exchange interaction with the unpaired electron, while the spin-down electrons are only subject to the Coulomb interaction alone [13]. Since the presented method does not account for spin polarization effects, it fails to describe the indirect contribution to calculated a-values, which leads to some discrepancies with experimental a-values.

The anisotropic a-values for ^{47}Ti, obtained with the present method, agree well with the data of all other reported spin-restricted calculations, ZORA SO [17] and RKS [55, 56]. As follows from a comparison of calculated results in Table 3.4 with experiment, none of the contemporary DF methods is able to simultaneously describe both spin-polarization and relativistic effects for this molecule with sufficient accuracy. Another conceivable rationalization of the disagreement between DF and experimental a-values of the TiF_3 radical can be related to the deficiency in description of localization of KS states using common xc functionals; this holds in particular for complexes of $3d$-compounds with very localized d-orbital, see Section 4.3). Our isotropic a-values are slightly larger than the ZORA results, probably again reflecting the different degrees of saturation of the basis sets (Section 3.1.2). The spin-unrestricted ZORA SR data are also presented in Table 3.4 in comparison with the spin-restricted data, to demonstrate the importance of spin-polarization effects in this complex: the spin-polarized absolute a_{iso}-value of ^{47}Ti is notably smaller and agrees better with the experimental value: -259.2 MHz compared to -227.9 MHz, at the BP level, but it still overestimates the experiment, -184.8 MHz. Spin polarization effects are more prominent for ^{19}F atoms of TiF_3. The isotropic a-value (Table 3.4) even changes its sign when switching between RKS and UKS calculations, from 31.0 to -42.7 MHz [55, 56]; a similar observation holds for the t_{yy} component [55, 56]. The isotropic a-value of ^{19}F atom in unrestricted ZORA SR calculations is significantly reduced compared with restricted ZORA SR results. Note that the experimental a-values for ^{19}F were determined assuming an axial spin Hamiltonian, and thus cannot be directly compared with the calculated one.

Deviations from experimental values just mentioned may be partly explained by uncertainties in the geometry of TiF_3 molecule and high sensitivity of the calculated a-values to the geometric parameters. Indeed (Table 3.1), variation of the Ti-F bond length for as little as 0.02 Å ($\sim$1%) only causes the alteration of BP a_{iso}-value for F by 22% (4% for Ti).

3.3.4 Hyperfine Interactions in Test Molecules Containing Atoms of Heavy Elements

Finally, our novel DKH approach for calculating molecular hyperfine interactions was tested on a set of diatomic molecules containing heavy elements: ^{105}Pd^{1}H, ^{103}Rh^{13}C, ^{199}Hg^{1}H,

^{199}Hg^{19}F, and ^{199}Hg^{107}Ag. These all species all neutral and characterized by a doublet $^2\Sigma$ electronic state.

In Table 3.5 the calculated HFCCs are compared with ZORA SO results [62] and experiment [144, Appendix C]. The molecular systems under study were calculated here with BP *xc* functional, as done in the ZORA SO approach [62]. The present calculations were performed using the following uncontracted basis sets saturated with respect to HFCCs: Pd (22*s*,13*p*,9*d*,8*f*,8*g*), Rh (23*s*,15*p*,10*d*,9*f*,9*g*), Hg (21*s*,17*p*,12*d*,7*f*,4*g*), Ag (22*s*,13*p*,9*d*,9*f*), H (18*s*,5*p*,1*d*), C (17*s*,8*p*,7*d*), F (19*s*,8*p*,7*d*) (for details, see Appendix A). The initial orbital basis sets for 3*d*- and 4*d*-atoms [145, 132] were extended first with polarization functions to obtain the following sets of primitive basis functions: Ti (15*s*,11*p*,6*d*,5*f*); Rh, Pd (18*s*,13*p*,9*d*,8*f*,8*g*) as required for the DKee1 model Ref. [87] which will also be employed in **g**-tensor calculations, Section 4.3. The basis set for Hg was taken from Ref. [87]. The basis sets just mentioned were augmented with several tight *s*-type exponents, as described in Section 3.3.1, until the saturation of calculated *a*-values to within ∼1 MHz had been achieved. The basis sets used for Ag were the same as described in Section 3.3.2, and those for H, C and F atoms as listed in Section 3.3.3. We used experimental geometries for PdH (1.529 Å), RhC (1.613 Å), HgH (1.766 Å), taken from Ref. [146]. For HgF and HgAg, we employed distances optimized both with ZORA SR (2.077 Å and 2.801 Å, respectively [62]) with our DK SR method (1.978 Å and 2.825 Å, respectively).

Our DKH HFCC values for transition metal molecules ^{105}Pd^{1}H and ^{103}Rh^{13}C (Table 3.5) are in a good agreement with experiment. Also, for the heavy metal radicals one ZORA SO results [62] agree well with experiment. For these molecules spin-polarization effects are reported to be more important than SO effects [62]. For instance, the difference between restricted ZORA SO and restricted ZORA SR calculations for $a_\parallel(^{103}\mathrm{Rh})$ is less than 1 MHz, whereas the difference between restricted ZORA SR and unrestricted ZORA SR $a_\parallel(^{103}\mathrm{Rh})$ is 10 MHz [62]. The difference with experiment can be attributed to the lack of spin-polarization effects in the present method and the ZORA SO approach. For ^{199}HgX, the SO effects can not be neglected [62] and should be taken into account simultaneously with spin-polarization effects to obtain accurate results. In general, our DK_2 results for ^{199}Hg *a*-values in ^{199}HgX radicals overestimate the experiment similar to the overestimated *a*-value of ^{197}Au atom (Section 3.3.2) . The ligand $a_\perp$- and $a_\parallel$-values in ^{199}Hg^{1}H as well as the $a_\parallel$-value of ^{19}F in ^{199}Hg^{19}F molecule are underestimated. Because in the case of ^{199}Hg^{19}F only absolute values of $a_\parallel$ and $a_\perp$ are available from experiment [149], one can only calibrate the calculated *absolute* values against experiment, but one is not able to discuss the signs; such a restricted comparison furnishes reasonably good agreement. Similarly to *a*-value of ^{107}Ag atom (Section 3.3.2), both the $a_\parallel$- and $a_\perp$-values of ^{107}Ag in ^{199}Hg ^{107}Ag molecule are overestimated with respect to (the only available) absolute experimental values $a_\parallel$ and $a_\perp$ [151]. As already mentioned in the discussion of HFCCs results for the molecule TiF_3, deviations from experiment are probably related to the high sensitivity of the calculated *a*-values to the molecular bond length. As shown in Table 3.5, a very strong variation of

Table 3.5: Calculated hyperfine structures of MX systems compared with those of ZORA and experiment (MHz).

System	Method	$a_{\parallel}$ (M)	$a_{\perp}$ (M)	$a_{\parallel}$ (X)	$a_{\perp}$ (X)
^{105}Pd^{1}H	DK$_2^a$	−953	−931	109	88
	ZORA^b	−997	−996	130	107
	Exp.^{c}	−867	−801	103	106
^{103}Rh^{13}C	DK$_2^a$	−1087	−1081	90	60
	ZORA^b	−1077	−1069	91	63
	Exp.^{c}	−1113	−1089	89	55
^{199}Hg^{1}H	DK$_2^a$	15067	14278	527	526
	ZORA^b	10530	8262	533	532
	Exp.^{c}	7790	6608	707	711
^{199}Hg^{19}F	DK$_2^d$	31347	30853	1145	−261
	DK$_2^e$	29723	29107	1129	−143
	ZORA^b	20340	19558	1387	−687
	Exp.^{c}	22622	21800	1344	195
^{199}Hg^{107}Ag	DK$_2^f$	7190	6959	−1910	−1909
	DK$_2^g$	7062	6838	−1924	−1923
	ZORA^a	4827	4106	−1462	−1459
	Exp.^{c}	3130	2520	1562	1562

a) Present work, experimental geometries.
b) ZORA SO [62].
c) Ref. [147] (PdH), Ref. [148] (RhC), Ref. [149] (HgH), Ref. [150] (HgF), Ref. [151] (HgAg).
d) Present work, d(Hg-F)=2.077 Å taken from Ref. [62].
e) Present work, d(Hg-F)=1.978 Å optimized at the BP DK SR level.
f) Present work, d(Hg-Ag)=2.801 Å taken from Ref. [62].
g) Present work, d(Hg-Ag)=2.825 Å optimized at the BP DK SR level.

the Hg-F bond length by almost 0.1 Å as calculated in the present work and in ZORA SR study [62] leads to the alteration of $a_\perp$(Hg) by more than 1700 MHz. As a side remarks, we note that such a large difference in the distances is extremely puzzling but we have no rationalization yet, despite various attempts to augment basis set of F: the Hg-F does not change within 0.01 Å.

One reason for the discrepancies between our calculated and experimental values is the lack of spin-polarization effects. In the molecules under consideration, both relativistic and spin-polarization effects contribute to a-values and should be taken into account. However, the presented method for calculation of a-values has not been extended yet for the spin-unrestricted case and details of the possible ways how one can approach this problem (e.g. with noncollinear spin density functional theory [70, 152]) are not sufficiently clear at the moment. Another source of differences is due to the fact that experiments include environmental effects. For the systems under study, the HFCC values were measured at low temperature using trapping in Ar matrices for PdH, HgH, HgF, HgAg, and in Ne matrices for RhC [144, Appendix C]. Environment effects are expected to influence the values of hyperfine parameters, and agreement with experiment better than 10-15% cannot be expected [62].

3.4 Conclusions

A novel approach for calculating hyperfine coupling constants has been developed, based on the Douglas-Kroll-Hess scheme of treating the Dirac-Kohn-Sham equation that includes a magnetic field. The method is valid for paramagnetic molecules featuring a Kramers doublet ground state: systems with an effective spin $\frac{1}{2}$. The spin-orbit effects were included self-consistently in the two-component eigenfunctions of the Douglas-Kroll Hamiltonian. Therefore, hyperfine couplings are considered as a first-order property with respect to the perturbation by the nuclei magnetic moments. This approach should be especially advantageous for molecular systems of heavy atoms with strong spin-orbit interactions. The finite nucleus model based on the Gaussian distribution of magnetic moment was introduced to the hyperfine operator. It allowed us to reach basis set completeness in relativistic calculations of isotropic hyperfine coupling constants.

The presented results for a-values are in agreement with previous theoretical data for small test molecules of light elements and fit experimental results with an accuracy sufficient for interpreting experimental EPR spectra. At the same time the presented method is less accurate for molecular systems containing heavy atoms due to the fact that effects of spin-polarization and of a finite nucleus model on the wave functions are not taken into account. Thus, an important improvement of the current implementation is expected when the interactions of the electrons with finite nuclei as a part of the Douglas-Kroll Hamiltonian are treated self-consistently. Another notable gain in accuracy of calculated hyperfine coupling constant values is expected from taking spin-polarization effects into account

within the spin-orbit formalism; unfortunately, there is still no straightforward solution for the latter problem available in the literature, although a two-component relativistic Kohn-Sham solution can be obtained from unrestricted Douglas-Kroll-Hess calculations [70, 152].

3.5 Mathematical Supplement

3.5.1 Eigenvalues of a 2×2 Traceless Hermitian Matrix

Consider the eigenvalue problem of a 2×2 traceless Hermitian matrix:

$$\lambda_x \sigma_x + \lambda_y \sigma_y + \lambda_z \sigma_z \ . \tag{3.111}$$

Employing the explicit form of the Pauli matrices, Eq. (2.3), the resulting secular equation is

$$\det \begin{pmatrix} \lambda_z - E & \lambda_x - i\lambda_y \\ \lambda_x + i\lambda_y & -\lambda_z - E \end{pmatrix} = 0 \ , \tag{3.112}$$

or

$$-(\lambda_z - E)(\lambda_z + E) - (\lambda_x + i\lambda_y)(\lambda_x - i\lambda_y) = 0 \ . \tag{3.113}$$

The solutions of the preceding equation can be written as

$$E = \pm\sqrt{\lambda_x^2 + \lambda_y^2 + \lambda_z^2} \ . \tag{3.114}$$

3.5.2 Spin Rotation Operator

Consider a unitary transformation of the spin operator of an arbitrary spin j,

$$\vec{S}' = D^{(j)} \vec{S} D^{(j)-1} \ , \tag{3.115}$$

where the operator of the rotation group $D^{(j)}$ can be defined via the Euler angles α, β, γ as [3, Appendix C]:

$$D^{(j)} = e^{-i\alpha S_z} e^{-i\beta S_y} e^{-i\gamma S_z} \ . \tag{3.116}$$

Here S_x, S_y, and S_z are operators of spin j. To evaluate the right-hand side part of Eq. (3.115), one can employ the Baker-Hausdorff lemma [153, p. 60]:

$$\begin{aligned} e^{(iG\lambda)} A e^{(-iG\lambda)} = A + i\lambda [G, A] + \left(\frac{i^2\lambda^2}{2!}\right) [G, [G, A]] \\ ... + \left(\frac{i^n\lambda^n}{n!}\right) [G, [G, [G, ... [G, A]]]] + ... \ , \end{aligned} \tag{3.117}$$

where G is a Hermitian operator and λ a real parameter. Consider as an example the rotation of the spin component S_x around the axis z:

$$S_x' = e^{-i\alpha S_z} S_x e^{i\alpha S_z} \ . \tag{3.118}$$

Applying the Baker-Hausdorff lemma to the preceding equation we obtain

$$S'_x = S_x - i\alpha\,[S_z, S_x] + \frac{1}{2!}\,(i\alpha)^2 \;\; [S_z, [S_z, S_x]] + \;\; \ldots \;, \tag{3.119}$$

which, with the help of commutation relations, can be reduced to

$$\begin{aligned} S'_x &= S_x \left(1 - \frac{\alpha^2}{2!} + \ldots\right) + S_y \left(\alpha - \frac{\alpha^3}{3!} + \ldots\right) \\ &= S_x \cos\alpha + S_y \sin\alpha \;. \end{aligned} \tag{3.120}$$

Therefore, applying the same procedure for a rotation around the y-axis, we finally obtain that the spin operator behaves transforms like a vector (operator) under rotation:

$$S'_k = \sum_{q=1}^{3} Q_{kq} S_q \;. \tag{3.121}$$

Chapter 4

Calculation of Electronic g-Tensors Using the Relativistic Density Functional Douglas-Kroll-Hess Method

4.1 Zeeman Hamiltonian

The Zeeman Hamiltonian describes the interaction of an unpaired electron with an external magnetic field in a paramagnetic molecule. A homogeneous magnetic field $\vec{B}^0$ can be described by the vector potential [104, p. 180]

$$\vec{A} = \frac{1}{2}\left(\vec{B}^0 \times \vec{r}\right) \ . \tag{4.1}$$

Using this explicit form of the vector potential for the magnetic Hamiltonian Eq. (2.54) derived in Chapter 2, one can obtain the Hamiltonian for the Zeeman interaction which will be denoted in the following as $\hat{H}^Z$. Employing Eq. (3.10) one can write the terms which contribute to the Zeeman Hamiltonian as

$$h_Z = \left[\vec{p}\cdot\vec{A}\right] + \vec{A}\cdot\vec{p} + i\vec{\sigma}\cdot\left[\vec{p}\times\vec{A}\right] \ . \tag{4.2}$$

The square brackets show that the gradient does not act on the wave function. Assuming the vector potential of a homogeneous magnetic field, Eq. (4.1) , in Eq. (4.2) and employing the vector relation of Eq. (3.12) we obtain for the first term of Eq. (4.2)

$$\begin{aligned}\vec{p}\cdot\vec{A} &= \vec{p}\cdot\frac{1}{2}\left(\vec{B}^0\times\vec{r}\right) \\ &= \frac{1}{2}\vec{r}\cdot\left(\vec{p}\times\vec{B}^0\right) - \frac{1}{2}\vec{B}^0\cdot(\vec{p}\times\vec{r}) \ .\end{aligned} \tag{4.3}$$

The first term of Eq. (4.3) vanishes because vector $\vec{B}^0$ is a constant. The second term vanishes because $\nabla \times \vec{r} = 0$. Employing the definition for the orbital momentum $\vec{L} = \vec{r} \times \vec{p}$, the term $\vec{A} \cdot \vec{p}$ of Eq. (4.2) reads

$$\vec{A} \cdot \vec{p} = \frac{1}{2} \left(\vec{B}^0 \times \vec{r} \right) \cdot \vec{p} = \frac{1}{2} \vec{B}^0 \cdot (\vec{r} \times \vec{p}) = \frac{1}{2} \vec{L} \cdot \vec{B}^0 \ . \tag{4.4}$$

The third term of Eq. (4.2) can be obtained by using the vector relation Eq. (3.20)

$$i\vec{\sigma} \cdot \left[\vec{p} \times \vec{A} \right] = \frac{i\vec{\sigma}}{2} \cdot \left[\vec{p} \times \vec{B}^0 \times \vec{r} \right] \tag{4.5}$$

$$= \frac{i\vec{\sigma}}{2} \cdot \left[\vec{B}^0 (\vec{p} \cdot \vec{r}) - \left(\vec{B}^0 \cdot \vec{p} \right) \vec{r} + \vec{r} \left(\vec{p} \cdot \vec{B}^0 \right) - (\vec{r} \cdot \vec{p}) \, \vec{B}^0 \right] \ . \tag{4.6}$$

The last two terms in the preceding equation vanish because $\vec{B}^0$ is a constant. Combining the first two terms (note $\nabla \cdot \vec{r} = 3$) yields

$$i\vec{\sigma} \cdot \left[\vec{p} \times \vec{A} \right] = \vec{\sigma} \cdot \vec{B}^0 \ . \tag{4.7}$$

We collect all terms of Eq. (4.2) and obtain for $h \equiv h^Z$:

$$h_Z = \vec{\sigma} \cdot \vec{B}^0 + \frac{1}{2} \vec{L} \cdot \vec{B}^0 \ . \tag{4.8}$$

Here, the term $\vec{\sigma} \cdot \vec{B}^0$ accounts for the electron *spin Zeeman* interaction of the electron spin with an external magnetic field $\vec{B}^0$ [3, p. 56]. The second term $\frac{1}{2} \vec{L} \cdot \vec{B}^0$ describes the *orbital Zeeman* interaction due to the orbital motion of the electron in the magnetic field $\vec{B}^0$ [3, p. 57].

To finalize the expression for the Zeeman Hamiltonian, quantum electrodynamic corrections have to be introduced by multiplication of the electron spin Zeeman term by the factor $g_e/2$, where $g_e = 2.002319$ is the g-factor of the free electron; see Section 3.1. For the same reason, the orbital Zeeman term should be multiplied by $g'/2$, where $g' = 2.004638$ is the electronic SO g-factor [3, p. 72].

4.2 Spin Hamiltonian for Zeeman Interaction

This section describes the link between the Zeeman Hamiltonian with the results of EPR experiments. In general, all arguments presented in Section 3.2.3 for the case of hyperfine interaction are also valid for the Zeeman interaction if one substitutes the magnetic field created by a nucleus with the external homogeneous magnetic field.

A group of K degenerate levels of a paramagnetic molecule, split after application of a magnetic field, is represented by the concept of an "effective spin" $\vec{\tilde{S}}$, as described in detail in Chapter 3. This "effective spin" is a fictitious angular momentum such that the degeneracy of the group of levels involved is set equal to $K = 2\tilde{S} + 1$, the same as in an ordinary spin multiplet [2, p. 133].

According to Kramers theorem, in a molecular system containing an odd number of electrons at least twofold degeneracy of eigenstates must remain in the absence of an external magnetic field [2, p. 650]. To these states, a so-called Kramers doublet with just two levels, an effective spin $\tilde{S} = 1/2$ is assigned. The Kramers doublet states Φ and $\bar{\Phi}$, which are degenerate but can be split in an external magnetic field, are connected to each other by the time-reversal operator K, Eq. (3.55) . In Section 3.2.2, we demonstrated that for Kramers doublets the full Hamiltonian, which describes the perturbation of the molecular system by an external magnetic field, is equivalent to an effective spin Hamiltonian. The latter is a linear form of the operators $\tilde{S}_x$, $\tilde{S}_y$, $\tilde{S}_z$, Eq. (3.57), with real coefficients, Eq. (3.61), in the space $\left|\frac{1}{2}\right\rangle$ and $\left|-\frac{1}{2}\right\rangle$. For doublet states the effective spin Hamiltonian $\hat{H}^{eff}$ for the Zeeman interaction reads

$$\hat{H}^{eff} = \mu_B \vec{B}^0 \cdot \mathbf{g} \cdot \vec{\tilde{S}} \ . \tag{4.9}$$

Here, μ_B is the Bohr magneton, in atomic units $\mu_B = \alpha/2 = 1/2c$. Thus, the EPR **g**-"tensor" (which actually is not a tensor but merely a matrix [2, p. 652]) parametrizes the interaction between the external magnetic field $\vec{B}^0$ and the effective spin $\vec{\tilde{S}}$. The components of $\tilde{S}$ can be defined according to Eq. (3.57) . The matrix **g** can always be transformed to diagonal form (Section 3.2.3), yielding three principal g-values [2]. In terms of the spin Hamiltonian, the square of the ground state energy splitting ΔE between two eigenstates $\left|\frac{1}{2}\right\rangle$ and $\left|-\frac{1}{2}\right\rangle$ in the field $\vec{B}^0$ can be calculated using the standard properties of Pauli matrices (Appendix B):

$$\begin{aligned}
\Delta E^2 &= \mu_B^2[(B_x^0 g_{xx} + B_y^0 g_{yx} + B_z^0 g_{zx})^2 \\
&\quad + (B_x^0 g_{xy} + B_y^0 g_{yy} + B_z^0 g_{zy})^2 \\
&\quad + (B_x^0 g_{xz} + B_y^0 g_{yz} + B_z^0 g_{zz})^2] \\
&= \mu_B^2 \sum_{k,l} B_k^0 B_l^0 \sum_{\alpha} g_{k\alpha} g_{l\alpha} \ .
\end{aligned} \tag{4.10}$$

It is useful to introduce the quantity

$$G_{kl} = \sum_{\alpha} g_{k\alpha} g_{la} \ , \text{ or } \mathbf{G} = \mathbf{g}\mathbf{g}^T \ , \tag{4.11}$$

which form the components of *true* tensor **G** [2, p. 652][a]. The symmetric tensor **G** can be always transformed to diagonal form by a proper choice of coordinate system [2, p. 653]. The **G**-tensor possesses positive eigenvalues, the square roots of which give the principal values of the matrix **g** [2, p. 653]:

$$g_{xx} = \sqrt{G_{xx}}, \ g_{yy} = \sqrt{G_{yy}}, \ g_{zz} = \sqrt{G_{zz}} \ . \tag{4.12}$$

[a] One has to note that such a definition of the effective spin Hamiltonian is common in the literature, although another definition is possible, similar to used for HFCCs, Eq. (3.63), namely $\hat{H}^{eff} = \mu_B \vec{\tilde{S}} \cdot \mathbf{g} \cdot \vec{B}^0$. Consequently, **G**-tensor will be defined as $\mathbf{G} = \mathbf{g}^T\mathbf{g}$.

Therefore, the **g**-tensor components are related to the experimental energy splitting ΔE as follows:

$$G_{kl} = \sum_{\alpha} g_{k\alpha} g_{l\alpha} = \frac{1}{2\mu_B^2} \left. \frac{\partial^2 \left(\Delta E\right)^2}{\partial B_k^0 \partial B_l^0} \right|_{\vec{B}^0=0} . \tag{4.13}$$

Without a magnetic field, a two-component KS calculation with self-consistent treatment of the SO interaction in an open-shell system yields two degenerate solutions, represented by KS determinants, which can be chosen such that they are formally connected by time-reversal symmetry. Using the Zeeman Hamiltonian $\hat{H}^Z$, one can calculate the energy difference ΔE^Z between those KS determinants in terms of the standard first-order perturbation treatment. If those KS determinants are obtained from a ROKS calculation, the spinors of the paired electrons are also connected by time-reversal symmetry. Because all of them are occupied, they do not contribute to the matrix elements of the corresponding KS determinants of the magnetic Hamiltonian (Section 3.2.3). This also holds for the "half-electron method" approach used in the present work, see Section 3.2.3. Therefore, the only non-zero contributions emerge from the two degenerate spinors of the unpaired electron φ_0 and $\bar{\varphi}_0$ obtained at $\vec{B}^0 = 0$:

$$\det \begin{pmatrix} \langle \varphi_0 | \hat{H}^Z | \varphi_0 \rangle - E & \langle \varphi_0 | \hat{H}^Z | \bar{\varphi}_0 \rangle \\ \langle \bar{\varphi}_0 | \hat{H}^Z | \varphi_0 \rangle & \langle \bar{\varphi}_0 | \hat{H}^Z | \bar{\varphi}_0 \rangle - E \end{pmatrix} = 0 . \tag{4.14}$$

The difference between two solutions of this equation ΔE^Z can be written as

$$(\Delta E^Z)^2 = \left[\langle \varphi_0 | \hat{H}^Z | \varphi_0 \rangle - \langle \bar{\varphi}_0 | \hat{H}^Z | \bar{\varphi}_0 \rangle \right]^2 + 4 \langle \varphi_0 | \hat{H}^Z | \bar{\varphi}_0 \rangle \langle \bar{\varphi}_0 | \hat{H}^Z | \varphi_0 \rangle . \tag{4.15}$$

The latter energy difference can be substituted into Eq. (4.13), thus connecting theory and EPR experiment by $\Delta E^Z = \Delta E$. Then, according to Eq. (4.13), the **G**-tensor can be obtained by taking the second derivatives with respect to Cartesian components of the magnetic field:

$$\begin{aligned} G_{kl} &= \frac{1}{2\mu_B^2} \left. \frac{\partial^2 \left(\Delta E^Z\right)^2}{\partial B_k^0 \partial B_l^0} \right|_{\vec{B}^0=0} \\ &= \frac{1}{\mu_B^2} \left[\left(\Phi_{11}^k - \Phi_{22}^k\right) \left(\Phi_{11}^l - \Phi_{22}^l\right) + 2\Phi_{12}^k \Phi_{21}^l + 2\Phi_{12}^l \Phi_{21}^k \right] . \end{aligned} \tag{4.16}$$

To obtain Eq. (4.16) the Hellmann-Feynman theorem was used [109]:

$$\Phi_{11}^k \equiv \frac{\partial}{\partial B_k^0} \langle\varphi_0|\hat{H}^Z|\varphi_0\rangle\Big|_{\vec{B}^0=0} = \langle\varphi_0| \left.\frac{\partial \hat{H}^Z}{\partial B_k^0}\right|_{\vec{B}^0=0} |\varphi_0\rangle \ , \tag{4.17}$$

$$\Phi_{22}^k \equiv \frac{\partial}{\partial B_k^0} \langle\bar{\varphi}_0|\hat{H}^Z|\bar{\varphi}_0\rangle\Big|_{\vec{B}^0=0} = \langle\bar{\varphi}_0| \left.\frac{\partial \hat{H}^Z}{\partial B_k^0}\right|_{\vec{B}^0=0} |\bar{\varphi}_0\rangle \ ,$$

$$\Phi_{12}^k \equiv \frac{\partial}{\partial B_k^0} \langle\varphi_0|\hat{H}^Z|\bar{\varphi}_0\rangle\Big|_{\vec{B}^0=0} = \langle\varphi_0| \left.\frac{\partial \hat{H}^Z}{\partial B_k^0}\right|_{\vec{B}^0=0} |\bar{\varphi}_0\rangle \ ,$$

$$\Phi_{21}^k \equiv \frac{\partial}{\partial B_k^0} \langle\bar{\varphi}_0|\hat{H}^Z|\varphi_0\rangle\Big|_{\vec{B}^0=0} = \langle\bar{\varphi}_0| \left.\frac{\partial \hat{H}^Z}{\partial B_k^0}\right|_{\vec{B}^0=0} |\varphi_0\rangle \ .$$

The preceding relations are valid for φ_0 and $\bar{\varphi}_0$, which are independent of $\vec{B}^0$, as solutions of the DK Hamiltonian without magnetic field. The principal values of **g**-matrix can be obtained by calculation and diagonalization of **G**-tensor, Eq. (4.12).

4.3 Results and Discussion

4.3.1 Computational Details

The formalism described in Sections 4.1 and 4.2 was implemented into the parallel program ParaGauss [154, 69], a newly developed parallel implementation LCGTO-FF-DF method [88]. The details of the implementation can be found in Chapter 5. The two-component relativistic wave functions [86, 87] of a Kramers doublet representing an unpaired electron were employed to calculate **g**-tensors as explained in Section 4.2. The RKS approximation was used in the **g**-tensor calculations which were carried out with. the BP *xc* functional, both for the geometry optimization and the subsequent **g**-tensor calculations.

In **g**-tensor calculations, the following specially constructed orbital basis sets were used: (13*s*,8*p*,7*d*) for C, N, O, F; (8*s*,5*p*,1*d*) for H; (15*s*,11*p*,6*d*,5*f*) for Ti; (18*s*,13*p*,9*d*,8*f*,8*g*) for Rh and Pd (Appendix A). The considerable extension of basis sets mainly reflects an *indirect* sensitivity of *g*-values to basis completeness: the additional functions with l+1 or even l+2 (where l is the maximum angular momentum of the occupied atomic orbitals) are required only for the special transformations when calculating the relativistic contribution to the *ee* Hartree interactions [87, 71]; test calculations had shown that it is sufficient to use only the variant DKee1 of that work. In the computational procedure, these transformations precede the basis contraction step. Thus, one can considerably reduce the computational effort using very compact contractions for the most expensive exponents with l+1 and l+2. In the present work we utilized the following contractions: [5*s*,4*p*,1*d*] for H; [8*s*,7*p*,3*d*] for C, N, O, F; [10*s*,11*p*,6*d*,1*f*] for Ti; [10*s*,12*p*,9*d*,3*f*,1*g*] for Pd, Rh; they were shown to cause deviation of the calculated *g*-values by less than 1×10^{-5}. The auxiliary fitting basis sets used in the LCGTO-FF-DF method were constructed in a standard fashion by doubling

the s-type and p-type exponents of the orbital basis functions [88]; they were augmented by standard sets of 5 p-type and 5 d-type polarization functions [88].

To test the present method of **g**-tensor calculations and its implementation in ParaGauss, two benchmark sets of inorganic and organic radicals were considered: (i) CO^+, CN, NO_2, NF_2, HCO, C_3H_5, TiF_3, RhC, PdH; (ii) phenyl (Ph) C_6H_5, biphenyl radical anion (BPh^-) C_6H_5-$C_6H_5^-$, 1,4-benzoquinone radical anion (BQ^-) $C_6H_4O_2^-$, and tetramethyl-1,4-benzoquinone radical anion (duroquinone, DQ^-) $C_6(CH_3)_4O_2^-$. Set (i) allows a critical comparison with both experimental **g**-tensors [155, 156, 157, 158, 159, 143, 144] and results of other high-level calculations [28, 30, 58, 160, 48, 61, 62]. Experimental equilibrium geometries were used for molecules of this set, except those for TiF_3 [61] and C_3H_5 [160], which for consistency were taken from the cited calculations. The z-axis was always oriented along the main molecular symmetry axis; molecules belonging to point group C_{2v} (NO_2, NF_2) were located in the yz-plane. For set (ii) of organic radicals, first-principles calculated data are scarce [161]. However, these radicals with very small **g**-tensor anisotropy [162, 163, 164] are indispensable for evaluating the performance of the new **g**-tensor tool as prototypes of biologically important EPR-active organic species. We optimized the geometric parameters of these radicals at the GGA BP level. The planar organic radicals were oriented in the xy-plane with the substituting -C_6H_5 or O groups or the missing H atom pointing along the x-axis. A common gauge origin, at the center of mass, was employed in the **g**-tensor calculations (Section 3.1.3).

4.3.2 Critical Factors in g-Tensor Calculations

Before presenting the results of **g**-tensor calculations we discuss the relative importance of various parameters which might have an influence on the calculated g-values.

In Table 4.1 **g**-tensor values for a set of test molecules calculated with three different representations of the Zeeman operator, Eqs. (2.54, 2.78, 2.81, 4.8), are displayed. The notations DK_0, DK_1, and DK_2 denote the zero-order, first-order, and for the second-order DK transformations of the Zeeman operator, respectively; see Eq. (2.58, 2.57, 2.54) of Chapter 2. Because **g**-tensor shifts are known to be induced, at least to a very large extent, by SO interactions, one needs to describe this interaction adequately. The commonly used restriction of the DKH transformation to the nuclear potential only (i.e., neglecting the two-electron SO coupling terms) [65, 75, 67] systematically overestimates the **g**-tensor anisotropy for main-group molecules. This overestimation of SO interaction in the DK method is well known [165] and demonstrated in Table 4.1; see the results obtained with the DKnuc variant. An improved relativistic treatment of the Hartree part of the *ee* interaction, denoted in Table 4.1 as DKee1, has been implemented in the code ParaGauss [87]. The underlying transformation is partly carried out in a numeric fashion which requires a specially augmented orbital basis set [87] (see Section 4.3.1). The calculated results are compared with experiment and results obtained with data of the two-component ZORA

Table 4.1: EPR **g**-tensor shifts ($\times 10^5$) of small test molecules calculated with different DKH representations of the Zeeman operator and different methods to account for SO interactions. For comparison, results of the ZORA SO approach and experiment are also shown.

Species		Exp.[a]	DKee1[b]			DKnuc[b]	SNSO[b]	ZORA[c]
			DK_0	DK_1	DK_2	DK_1	DK_1	
NO_2	xx	390	501	472	441	609	446	500
	yy	−1130	−1484	−1513	−1527	−1976	−1463	−1600
	zz	−30	−42	−72	−5	0	−10	−60
HCO	xx	150	323	304	283	386	293	330
	yy	0	−1	−20	−18	−28	−23	−20
	zz	−750	−1056	−1076	−1085	−1432	−1045	−1230
TiF_3	$\perp$	−11130	−4494	−4526	−4564	−8253	−4311	−7970
	$\parallel$	−1110	5	−28	−181	−433	−179	−100
RhC	$\perp$	5178	4835	4815	4782	6271	4906	5028
	$\parallel$	158	−168	−188	−540	−891	−543	−202
PdH	$\perp$	29088	24781	24735	24682	30676	25047	29478
	$\parallel$	−3732	−1780	−1818	−1837	−2885	−1872	−2772

a) NO_2 [157] , HCO [158], RhC [144], TiF_3 [143], PdH [144].
b) Present work, BP level.
c) ZORA SO [61, 62].

Table 4.2: Calculated EPR **g**-tensor shifts Δg ($\times 10^5$) of small test molecules split in spin Zeeman $\Delta\sigma$ and orbital Zeeman ΔL contributions.

Species		Δg^a	$\Delta\sigma^a$	ΔL^a
CO^+	$\perp$	-350	-22	-328
	$\parallel$	-22	-24	2
NO_2	xx	472	-36	508
	yy	-1513	-31	-1481
	zz	-72	-38	-34
RhC	$\perp$	4815	-187	5003
	$\parallel$	-187	-355	168
PdH	$\perp$	24735	-1818	26553
	$\parallel$	-1818	-3598	1780

a) Present work, DK_1 BP level.

SO method which is rather close to the present computational approach [61, 62].

The g-shifts in Table 4.1 show that the differences of the calculated **g**-tensor components in the various representations of the Zeeman operator and do not depend significantly on Z; cf. the results for the light molecules NO_2, HCO and the molecules with heavy nucleus RhC, PdH. This finding is opposite to the "picture change" effect discussed in Chapter 3 for the isotropic component of HFCCs. Although the transformation of the Zeeman operator at the DK_2 level provides better agreement with experiment, the following calculations were carried out at the DK_1 level (Eqs. (2.57)), which was implemented earlier and is much less computational demanding than the DK_2 level (Eqs. (2.54)).

For molecules without very heavy atoms, this more precise treatment does not cause significant changes of common observable [87]. However, **g**-tensor values are much more sensitive to the relativistic *ee* interactions. With this methodological variant, the leading orbital Zeeman contribution ΔL of the g-shifts was reduced in absolute value by as much as 30% (or more) for all molecules under study when the Hartree potential was subjected to the relativistic transformation (Table 4.1). Thus, the accuracy of the calculated **g**-tensor components is improved *considerably* and *systematically* at the present level of approximation that uses wave functions obtained with Hartree part of the two-electron SO couplings taken into account [87]. Nevertheless, as follows from atomic calculations, even accounting for *ee* SO terms still causes a slight overestimation of the SO splitting for p-orbitals [165]. This is the rationalization for the overestimation of the **g**-tensor anisotropy in molecules of main-group elements.

A simplified scheme to account for SO effects was implemented in ParaGauss very recently [166]. This is an improved variant of Boettger's screened nuclear potential approximation for the SO interaction (SNSO) [165, 166]. In this approach, the electronic screening effects are approximated by employing effective nuclear charges during the calculation of the SO terms in the DK Hamiltonian. Similar to the DKee1 approximation, the SNSO strategy improves the calculated g-shifts by about 30% with respect to the DKnuc values and produces results in very good agreement with those of the DKee1 method. Deviations between SNSO and DKee1 results amount to a few percent, except for rather small values (Table 4.1). In fact, the SNSO results agree even slightly better with experiment then DKee1 values. In the following test calculations the earlier implemented DKee1 approximation was used, even though the SNSO method has a computational advantage over the DKee1 approximation by avoiding the extended basis set, required by DKee1 as described in Section 4.3.1.

The individual contributions – spin Zeeman shift $\Delta\sigma$ and orbital Zeeman shift ΔL (Eq. (4.8)) – are listed in Table 4.2. One notices that the orbital Zeeman contributions ΔL dominates the spin Zeeman shift $\Delta\sigma$ for all molecules under study. Thus, the overall shift values Δg are essentially determined by the orbital Zeeman contributions ΔL. Moreover, the anisotropy of the calculated **g**-tensor values is due to the ΔL contribution. However, $\Delta\sigma$ contribution ,in general, is not negligible and should be accounted in **g**-tensor calculations

4.3.3 Calculated g-Tensors for Selected Test Molecules

In Table 4.3 the calculated **g**-tensor values for a series of benchmark doublet-state radicals are presented and compared with results of other high-level calculations and experimental data. The computed g-components reproduce the experimental numbers for the main-group molecules in this touchstone set (i): the relative shifts Δg of the main g-components, their signs and the general trends traced from the EPR spectra. Transition metal radicals exhibit a somewhat less favorable situation which we address below in some detail. Let us begin with the main-group species.

For molecules of main-group elements (Table 4.3), the calculated deviations from experimental g-values are of similar size as in other computations [28, 30, 58, 160, 48, 61]. For the most thoroughly studied molecules, NO_2 in the gas-phase and HCO in matrix-isolation, the present Δg values are very close to those of the methodologically similar ZORA SO approach [61]. The remaining difference is probably a consequence of the fact that the present work neglects the two-electron xc contribution to the SO interaction. The latter two sets of g-shifts, obtained with a first-order perturbation DF-based method, are slightly larger in absolute values than those obtained with a second-order perturbation DF-based procedure [160], partly due to the inclusion of spin-polarization in the latter scheme. All three sets of DF g-shifts consistently overestimate the experimental values. The two-component GHF method [58] performs better for Δg, but it slightly underestimates the experimental shifts. Inspection of Table 4.3 shows that the data for the other main-group molecules confirm these trends as *systematic*: DF methods (except that by Malkina et al. [48]) [b] overestimate Δg-values and the GHF method tends to slightly underestimate them. This is encouraging message because the systematic deviations can be reduced step by step when improvements of the **g**-tensor calculations are possible in a rigorous fashion, like is the case in the present method.

As discussed in Refs. [58, 160, 167, 168, 48, 61, 62], transition metal radicals represent more critical cases for calculations of **g**-tensors than main-group systems. Our results for TiF_3, RhC, and PdH (Table 4.3) are in line with previously calculated data for d-metal molecules: agreement with experiment is qualitative and general features of EPR line splittings are reproduced. A key difference is the lack of the systematic overestimation of the **g**-tensor anisotropy. One can attempt to rationalize this finding, again by analyzing SO effects in atoms as described at the DK level with two-electron SO couplings. Indeed, for d (and f) atomic states, SO effects are shown to be slightly but systematically *underestimated* compared to those computed at the most accurate four-component Dirac-KS level [165]. When a transition metal atom is present in a radical, both p- and d- states of the

[b] Malkina et al. claimed that they accounted for spin-other-orbit terms in their study, which arise strictly only from relativistic contributions to the *ee* interactions. Rather than resorting to relativistic *ee* interactions, Malkina et al. incorporated SO coupling explicitly via suitably chosen perturbation operators. Because the present work does not include a relativistic treatment of the xc potential, some deviations from the results of Malkina et al. may arise.

Table 4.3: Calculated EPR **g**-tensor shifts ($\times 10^5$) of small test molecules compared with results of other methods and experiment

Molecule		Exp.[a]	MRCI[b]	ROHF[c]	GHF[d]	BP[e]	BP[f]	BP[g]	BP[h]	BP[i]
CO^+	$\perp$	−240	−238	−125	−280	−313	−246	−262		−350
	$\parallel$		−18	−18	−4	−14	−9	−16		−22
CN	$\perp$	−200			−198	−251		−203		−270
	$\parallel$				−6	−14		−14		−20
NO_2	xx	390	357	259	337	416	340	328	500	472
	yy	−1130	−1030	−708	−1101	−1372	−1123	−1127	−1600	−1513
	zz	−30	−54	−57	−62	−76	−69	−70	−60	−72
NF_2	xx	−10			−45	−74	−62	−64		−37
	yy	620			565	762	629	697		1027
	zz	280			289	468	393	426		603
HCO	xx	150			207	275	228	218	330	303
	yy	0			−18	−27	−22	−31	−20	−20
	zz	−750			−686	−947	−748	−789	−1230	−1076
C_3H_5	xx	0				−12	−7	−8		−13
	yy	80				77	60	63		96
	zz	40				66	50	73		76
TiF_3	$\perp$	−11130					−2658		−7970	−4526
	$\parallel$	−1110					−112		−100	−28
RhC	$\perp$	5178							5028	4680
	$\parallel$	158							−202	−173
PdH	$\perp$	29088							29478	24735
	$\parallel$	−3732							−2772	−1818

a) Exp. CO^+ [155], CN [156], NO_2 [157], NF_2 [160], HCO [158], C_3H_5 [159], RhC [144], TiF_3 [143], PdH [144]; b) Multi-reference CI [28]; c) Restricted open-shell Hartree-Fock [30]; d) GHF [58]; e) UKS [160]; f) UKS [48]; g) UKS [49]; h) ZORA SO [61, 62]; i) present work, DK_1 BP level

constituting atoms contribute to the g-shift.

Depending on the relative weights of both contributions, the overall effect may be either an overestimation or underestimation, with the latter being probably more common for a SOMO with notable d-character; see the results for TiF_3, PdH, and RhC in Table 4.3).

One can invoke further effects which may well cause differences for d-metal molecules, e.g. the influence of the xc potential on the precision of the computed g-values. Comparing results of LDA and GGA calculations, the latter resulted in a slight reduction of the **g**-tensor anisotropy (by 5–10%) for essentially all molecules listed in Table 4.3. This is an improvement for the main-group molecules, but not for the d-metal species. The **g**-tensor calculated for TiF_3 features the largest discrepancy with experiment, both for LDA or GGA. Obviously, this is an indication of a general situation that the commonly used xc potentials are still far from optimal for describing very delicate magnetic response properties (and thus electronic structure details) of transition metal systems. More specifically, complexes in the electron configuration $3d^1$, like TiF_3, are probably less accurately described by common xc potentials due to the known deficiency of these methods to reproduce proper electron localization, in particular in such compact states as $3d$. If this is indeed an important reason, one can hope to reach a significant improvement by employing DF approaches which are corrected for self-interaction [140].

Organic radicals (Table 4.4) also furnish a critical test for the precision and reliability of **g**-tensor calculations because the involved anisotropy of **g**-tensors is small. Thus, small uncertainties in the geometry would translate into variations of the **g**-tensor which are comparable to the anisotropy. Furthermore, environmental effects on **g**-tensors of organic radicals, which are commonly studied in matrices, often can be seen in measured g-shifts but are hard to model. Despite of the small g-shifts observed for hydrocarbon and benzoquinone anion radicals of medium size, the present method is able to reproduce not only the signs, but also the relative values of the measured **g**-tensor components. The whole variety of the conceivable improvements discussed above is also applicable to these biologically relevant organic radicals. Important for future applications is the finding that tiny changes of EPR line positions caused by the formation of intermolecular hydrogen bonds of organic molecules are almost quantitatively reproduced within the present DF method (Chapter 6, [73]).

As already mentioned, the gauge origin in this work has been chosen in the center of the nuclear charges (masses). A test displacement of the gauge origin for the CO^+ radical by 1 Å along the z axis, a typical uncertainty, resulted in a variation of $g_\perp$ by less than 10^{-5}. The effect for other radicals in Table 4.3 was of the same order. This change is even below the commonly achieved experimental accuracy. Therefore, the unphysical feature of the gauge dependence (Section 3.1.3) of calculated g-values is of minor importance when very good basis sets are employed as done in the present calculations. Further test studies have shown that gauge effects may also be neglected for organic radicals of moderate size (Table 4.4). However, measures to ensure gauge invariance may become relevant for large

Table 4.4: Calculated EPR **g**-tensor shifts ($\times 10^5$) of organic radicals in comparison with experiment

Species	Component	Calc[a].	Exp.[b]
C_6H_5	xx	-16	-2 ± 50
(Ph)	yy	-129	-92 ± 50
	zz	72	108 ± 50
C_6H_5-$C_6H_5^-$	xx	142	107 ± 2
(BPh^-)	yy	46	32 ± 2
	zz	-13	-5 ± 2
$C_6(CH_3)_4O_2^-$	xx	711	438 ± 5
(DQ^-)	yy	357	291 ± 5
	zz	-28	-14 ± 5
$C_6H_4O_2^-$	xx	907	473 ± 5
(BQ^-)	yy	362	306 ± 5
	zz	-30	-6 ± 5

a) Present work, DK_1 BP level.
b) Ph [162], BPh^- [163], DQ^- [164].

asymmetric molecules.

One more potential measure for improving the precision of calculated g-values in the present implementation is to go beyond the RKS approach, taking spin-polarization effects into account. Spin-polarization effects were estimated within a one-component DF method to *systematically decrease* the absolute Δg-values by as much as 20% (HCO, NO_2), making results already for light molecules notably more accurate [61]. In all **g**-tensor calculations with a self-consistent treatment of the SO interaction reported so far, spin-polarization effects have been neglected. This is a principal limitation because SO interactions eliminate spin as a "good" quantum number. Fortunately, there exists a way to partly overcome this limitation: a very recent implementation of the so-called noncollinear spin density functional (NCSDF) approach in the SO part of ParaGauss showed promising results for energies [152]. Spin-polarization effects on **g**-tensors calculated in a two-component NCSDF method employing properly constructed determinantal wave functions have yet to be quantified.

Another part of the *ee* interaction is the *xc* potential. Although it is smaller in magnitude than the Hartree contribution, it should also be subjected to the relativistic transformation to obtain further improved two-component wave functions when determining g-values. One can also profit from using special relativistic *xc* functionals modified due to relativistic kinematics of the electrons and, probably more important in the present context, due to the Breit contribution to the *ee* interaction. Such functionals are now available at both LDA and GGA levels [169]. However, very minor effect of these relativistic corrections on many molecular observables [113], a notable alteration of so sensitive indicator as **g**-tensor is anticipated.

4.4 Conclusions

We presented a novel scheme for calculating EPR **g**-tensor values of doublet-state systems within a relativistic DF method and its implementation as well as applications. We extended this approach of Neyman et al. [72] to the second-order DKH transformation of the Zeeman Hamiltonian method. The formalism is based on two-component solutions of the Kohn-Sham equations which include spin-orbit effects self-consistently. Therefore, the **g**-tensor can be considered as first-order property with respect to the perturbation by the external magnetic filed alone. The Zeeman energy splitting, an inherently relativistic effect, is naturally and transparently determined by the two-component ground-state wave function; one does not have to invoke virtual states. Because the widely adopted perturbative treatment of spin-orbit interaction is avoided, the method is also applicable to molecular systems with spin-orbit interaction of considerable strength.

Test calculations of **g**-tensors for small inorganic main-group and transition metal molecules as well as organic radicals demonstrated that the present method exhibits an accuracy sufficient for successful assigning and interpreting EPR spectra. This statement

holds even without further conceivable improvements proposed for the newly implemented scheme. The most important and straightforward future developments of ParaGauss for EPR calculations comprise an extension of the relativistic treatment of the exchange-correlation interaction and the inclusion of spin-polarization effects.

Chapter 5

Implementation

In this chapter we will describe details of the implementation of the formalism presented in Chapters 3 and 4. The method for calculating HFCCs and g-values using the DKH formalism was implemented in the code ParaGauss [154, 69], a newly developed parallel realization of the *linear combination of Gaussian-type orbitals fitting-functions density-functional* (LCGTO-FF-DF) method [88]. We focus mainly on the modifications of the integral part because the complete procedure of calculating HFCCs and **g**-tensors was coded and parallelized in line with the ParaGauss module for calculating dipole integrals [100, 154].

To calculate HFCCs, the code ParaGauss [69] has been extended by new types of integrals, Eqs. (3.27, 3.45, 3.104) :

$$\langle \chi_{\nu_a}^{l_a a\alpha} | \frac{\partial h_{point}}{\partial \mu_{\nu k}} | \chi_{\nu_b}^{l_b b\beta} \rangle = \langle \chi_{\nu_a}^{l_a a\alpha} | - \frac{8\pi}{3} \delta\left(\vec{r}_\nu\right) \sigma_k - \frac{\sigma_k}{r_\nu^3} + 3\frac{\left(\vec{\sigma}\cdot\vec{r}_\nu\right) r_{\nu k}}{r_\nu^5} + \frac{L_{\nu k}}{r_\nu^3} \; | \chi_{\nu_b}^{l_b b\beta} \rangle \tag{5.1}$$

and

$$\langle \chi_{\nu_a}^{l_a a\alpha} | \frac{\partial h_{finite}^{iso}}{\partial \mu_{\nu k}} | \chi_{\nu_b}^{l_b b\beta} \rangle = \langle \chi_{\nu_a}^{l_a a\alpha} | - \frac{8\pi}{3} \left(\frac{\eta_\nu}{\pi}\right)^{3/2} \sigma_k \exp\left(-\eta_\nu r_\nu^2\right) | \chi_{\nu_b}^{l_b b\beta} \rangle \tag{5.2}$$

over primitive Gaussian functions $\chi_{\nu_a}^{l_a a\alpha}$ (and $\chi_{\nu_b}^{l_b b\beta}$, respectively) of angular momentum l_a and exponent α located at center a. Similarly, to calculate g-values new integrals of the type, Eqs. (4.8, 4.17),

$$\langle \chi_{\nu_a}^{l_a a\alpha} | \frac{\partial h^Z}{\partial B_k^0} | \chi_{\nu_b}^{l_b b\beta} \rangle = \langle \chi_{\nu_a}^{l_a a\alpha} | \sigma_k + \frac{1}{2} L_k | \chi_{\nu_b}^{l_b b\beta} \rangle \tag{5.3}$$

have been added (see below Eq. (5.74)). The required overlap matrix elements for evaluation if σ_k term in Eq. (5.3) was implemented previously [100].

These primitive integrals required for the HFCCs and **g**-tensors are computed after completing the self-consistent field (SCF) part, in full analogy with the calculations of

dipole moments implemented earlier [100, 154]. Subsequently, the integrals were symmetry adapted according to the irreducible representation of the appropriate double group [70, 71], multiplied by contraction coefficients and combined into molecular integrals [101, 170] for calculation of HFCCs, Eqs. (3.104), and **g**-tensors, Eqs. (4.17).

5.1 General Remarks on Primitive Integrals

In the program ParaGauss, KS orbitals are constructed as linear combinations of so-called primitive basis functions which are given as simple analytical expressions, as just mentioned above. One can represent KS orbitals at any desired accuracy by increasing the number and quality of these primitive basis functions. The latter usually are centered on the nuclei of the atoms of a molecule and, in ParaGauss, are chosen as a product of a spherical harmonic and a radial part. The LCGTO-FF-DF method exploits the advantages of Gaussian-type radial functions $\exp(-\alpha r^2)$, namely matrix elements of GTOs can be analytically evaluated and efficiently implemented, even for complicated operators [100]. Cartesian Gaussian functions of the form $x^n y^l z^m \exp(-\alpha r^2)$ comprise another conceivable choice for basis functions [171]. Slater-type functions of the kind $\exp(-\zeta r)$ provide a more compact representation of atomic and molecular eigenfunctions, however the resulting matrix elements cannot be analytically evaluated for many important operators. A modification of the Slater-type functions, Dirac-type Slater orbitals of the form $r^{\eta-1}\exp(-\zeta r)$, are utilized for relativistic calculations [172, 173]. Finally, plane-waves basis sets are widely used in combination with periodic boundary conditions [109, 46].

A particular feature of the LCGTO-FF-DF method is that one expands the electron density in an auxiliary basis set of so-called "fitting functions" to evaluate the Hartree energy functional and the resulting contribution to the one-electron potential in the KS equation. To a large part, this auxiliary basis set of GTO functions is derived from the orbital basis functions, but additional functions are required to achieve sufficient accuracy [88].

As already mentioned in the beginning of this chapter, the primitive Gaussian basis functions employed in ParaGauss are products of radial and angular dependent parts. The primitive basis function with electron coordinates $\vec{r} = (r_x\ , r_y\ , r_z)$, centered at position $\vec{a} = (a_x,\ a_y,\ a_z)$, which belongs to an atom shell of angular momentum quantum number l, is given as

$$\chi_\nu^{la\alpha}(\vec{r}) = \left(\frac{2\alpha}{\pi}\right)^{3/4} \sqrt{\frac{(4\alpha)^l}{(2l-1)!!}} C_\nu^l(\vec{r}-\vec{a}) \exp\left(-\alpha(\vec{r}-\vec{a})^2\right) \ . \tag{5.4}$$

Here the Gaussian exponent α determines the radial extension of the basis function; the angular part $C_m^l(\vec{r}) = r^l C_m^l(\vec{r}/r)$ is a solid real spherical harmonic that can be expressed

with the help of the complex spherical harmonics $Y_{l,m}\left(\vec{r}/r\right)$ [174, 175]:

$$C_0^l\left(\vec{r}\right) = r^l Y_{0,0}\left(\vec{r}/r\right) \ , \tag{5.5}$$

$$C_{\nu=2m}^l\left(\vec{r}\right) = r^l \frac{1}{\sqrt{2}}\left[\left(-1\right)^m Y_{l,m}\left(\vec{r}/r\right) + Y_{l,-m}\left(\vec{r}/r\right)\right], \ m > 0 \ , \tag{5.6}$$

$$C_{\nu=2|m|+1}^l\left(\vec{r}\right) = r^l \frac{1}{\sqrt{2}i}\left[\left(-1\right)^m Y_{l,-m}\left(\vec{r}/r\right) - Y_{l,m}\left(\vec{r}/r\right)\right], \ m < 0 \ . \tag{5.7}$$

For complex spherical harmonics, the phase convention of Condon and Shortley is used [176, 177]. The magnetic quantum number $m = -l, ..., l$ of complex spherical harmonics is replaced by a shape quantum number $\nu = 1, ..., 2l+1$ of real solid harmonics; see the corresponding index in Eq. (5.4). Real basis functions offer the advantage that complex arithmetic can be avoided in non-relativistic calculations. The pre-factor in Eq. (5.4) normalizes the basis function.

One of the most convenient features of solid spherical harmonics is their simple generation via differentiation of the corresponding s-type Gaussian function [100, 170]

$$\chi_\nu^{la\alpha}\left(\vec{r}\right) = \left(\alpha^l \left(2l-1\right)!!\right)^{-1/2} C_\nu^l\left(\nabla_a\right) \chi_1^{0a\alpha}\left(\vec{r}\right) \ , \tag{5.8}$$

where in the differential operators $C_\nu^l\left(\nabla_a\right)$ the arguments x, y, z of the real solid harmonics $C_\nu^l\left(\vec{r}\right)$ are formally replaced by the differentiation operators (employing $\partial_{a_i} \equiv \frac{\partial}{\partial a_i}$) ∂_{a_x}, ∂_{a_y}, and ∂_{a_z} with respect to the corresponding Cartesian coordinates of the "anchor point" $\vec{a}$ of the GTO. For the first derivatives these relations read

$$\partial_{a_x} = C_2^1\left(\nabla_a\right), \ \partial_{a_y} = C_3^1\left(\nabla_a\right), \ \partial_{a_z} = C_1^1\left(\nabla_a\right) \ . \tag{5.9}$$

The action of a gradient spherical harmonic on a spherically symmetric function f depends only on the distance to the center $\vec{a}$ [100, 101]

$$C_\nu^l\left(\nabla\right) f((\vec{r}-\vec{a})^2) = C_\nu^l\left(\vec{r}-\vec{a}\right) 2^l f^{(l)}((\vec{r}-\vec{a})^2) \ , \tag{5.10}$$

where $f^{(l)}$ is the l-th derivative of f. The actual evaluation of primitive matrix elements is facilitated by employing two very useful differentiation rules, which describe the differentiation of a products of functions and of a real solid harmonic [100, 101]:

$$C_\nu^l\left(\nabla\right) f\left(\vec{r}\right) g\left(\vec{r}\right) = \sum_{l'=0}^{l} \sum_{\nu',\nu''} \varepsilon_{l'\nu'\nu''}^{l\nu} \left[C_{\nu'}^{l'}\left(\nabla\right) f\left(\vec{r}\right)\right] \left[C_{\nu''}^{l-l'}\left(\nabla\right) g\left(\vec{r}\right)\right] \ , \tag{5.11}$$

$$C_{\nu'}^{l'}\left(\nabla\right) C_\nu^l\left(\vec{r}\right) = \sum_{\nu''} \varepsilon_{l'\nu'\nu''}^{l\nu} \left(2l'-1\right)!! C_{\nu''}^{l-l'}\left(\vec{r}\right) \ . \tag{5.12}$$

These relations are based on the tensor properties of real solid harmonics. The coupling coefficients $\varepsilon_{l'\nu'\nu''}^{l\nu}$, the same in the both rules, can be derived from Glebsch-Gordon coefficients [100]; they usually are pre-computed and made available in tabulated form [178, 100].

Atom-centered basis functions f, such as the Gaussian functions used in the code ParaGauss, possess a very convenient feature that a partial derivative of f is the negative gradient with respect to the corresponding coordinate of the atomic center:

$$\nabla_b f((\vec{r}-\vec{b})^2) = -\nabla f((\vec{r}-\vec{b})^2) \ , \tag{5.13}$$

$$\nabla_b \left(C_\nu^l \left(\vec{r}-\vec{b}\right) \exp\left(-\beta\left(\vec{r}-\vec{b}\right)^2\right)\right) = -\nabla \left(C_\nu^l \left(\vec{r}-\vec{b}\right) \exp\left(-\beta\left(\vec{r}-\vec{b}\right)^2\right)\right) \ . \tag{5.14}$$

5.2 Evaluation of Primitive Integrals for Magnetic Interactions

For calculations of magnetic properties the existing ParaGauss code has been extended with new types of primitive integrals. The new three matrix elements that were introduced into ParaGauss for evaluating HFCCs are of three-center type: two centers $\vec{a}$ and $\vec{b}$ referring to the basis functions involved and one center $\vec{c} = (c_x, c_y, c_z)$ pertaining to the nucleus under study. For any vector $\vec{r}_c = (r_{c_x}, r_{c_y}, r_{c_z})$ starting at $\vec{c}$, we have

$$r_{c_x} = r_x - c_x, \ r_{c_y} = r_y - c_y, \ r_{c_z} = r_z - c_z \ , \tag{5.15}$$

$$r_c^2 = (r_x - c_x)^2 + (r_y - c_y)^2 + (r_z - c_z)^2 \ . \tag{5.16}$$

For calculating the dipolar hyperfine term, Eqs. (3.26, 5.1), the code ParaGauss was augmented by the following types of integrals:

$$HD1^{l_a l_b}_{\nu_a \nu_b i} \equiv \left\langle \chi^{l_a a\alpha}_{\nu_a} \left| \frac{3r_{c_i}^2 - r_c^2}{r_c^5} \right| \chi^{l_b b\beta}_{\nu_b} \right\rangle \ , \tag{5.17}$$

$$HD2^{l_a l_b}_{\nu_a \nu_b ij} \equiv \left\langle \chi^{l_a a\alpha}_{\nu_a} \left| \frac{3r_{c_i} r_{c_j}}{r_c^5} \right| \chi^{l_b b\beta}_{\nu_b} \right\rangle \ , \ i \neq j \ , \tag{5.18}$$

where the indices i, j stand for Cartesian components x, y, z of the vector $\vec{r}_c$. These integrals are known in the literature as the electric field gradient integrals [179].

The next integral required for evaluation of the orbital hyperfine term, Eqs. (3.19, 5.1), can be written as

$$HL^{l_a l_b}_{\nu_a \nu_b i} \equiv \left\langle \chi^{l_a a\alpha}_{\nu_a} \left| \left(\frac{\vec{r}_c \times \nabla}{r_c^3} \right)_i \right| \chi^{l_b b\beta}_{\nu_b} \right\rangle \ . \tag{5.19}$$

Here the index i denotes a Cartesian component of the vector quantity in parentheses. The integral of Eq. (5.19) is known as a matrix element of the one-electron SO operator [179].

A matrix element of the orbital momentum operator has to be evaluated for calculating of the orbital contribution to **g**-tensor, Eq. (4.4, 5.3),

$$L^{l_a l_b}_{\nu_a \nu_b i} \equiv \left\langle \chi^{l_a a\alpha}_{\nu_a} \left| (\vec{r} \times \nabla)_i \right| \chi^{l_b b\beta}_{\nu_b} \right\rangle \ . \tag{5.20}$$

Finally, evaluation of the isotropic contribution of HFCCs in the framework of the finite nucleus model requires the matrix element of the type, Eqs. (3.45, 5.2),

$$A^{l_a l_b}_{\nu_a \nu_b} \equiv \left\langle \chi^{l_a a \alpha}_{\nu_a} \left| \left(\frac{\eta}{\pi}\right)^{3/2} \exp\left(-\eta(\vec{r}-\vec{c})^2\right) \right| \chi^{l_b b \beta}_{\nu_b} \right\rangle \ . \tag{5.21}$$

The matrix elements $HD1^{l_a l_b}_{\nu_a \nu_b i}$ and $HD2^{l_a l_b}_{\nu_a \nu_b i}$, Eqs. (5.17, 5.18), can be calculated by the parameter differentiation of the nuclear attraction operator with respect to the nuclear coordinates $\vec{c}$ [179]

$$\partial_{c_x} \frac{1}{r_c} = -\frac{r_{c_x}}{r_c^3} \ . \tag{5.22}$$

Taking second derivatives with respect to the nuclear coordinates $\vec{c}$ we obtain

$$\partial_{c_x} \partial_{c_y} \frac{1}{r_c} = \frac{3 r_{c_x} r_{c_y}}{r_c^5} \tag{5.23}$$

and

$$\frac{1}{3}\left(2\partial^2_{c_z} - \partial^2_{c_x} - \partial^2_{c_y}\right) \frac{1}{r_c} = \frac{3r^2_{c_z} - r^2_c}{r_c^5} \ . \tag{5.24}$$

Eq. (5.24) is written so to avoid problems with the Dirac delta function which arises in $\nabla^2 r_c^{-1}$ according to Eq. (3.15).

Employing the notation for the nuclear attraction integral [100, 101]

$$N^{l_a l_b}_{\nu_a \nu_b} \equiv \left\langle \chi^{l_a a \alpha}_{\nu_a} \left| \frac{1}{r_c} \right| \chi^{l_b b \beta}_{\nu_b} \right\rangle \ , \tag{5.25}$$

one can rewrite Eqs. (5.17, 5.18) using Eqs. (5.23, 5.24) as

$$HD1^{l_a l_b}_{\nu_a \nu_b i} = \frac{1}{3}\left(2\partial^2_{c_z} - \partial^2_{c_x} - \partial^2_{c_y}\right) N^{l_a l_b}_{\nu_a \nu_b} \ , \tag{5.26}$$

$$HD2^{l_a l_b}_{\nu_a \nu_b i} = \partial_{c_x} \partial_{c_y} N^{l_a l_b}_{\nu_a \nu_b} \ . \tag{5.27}$$

The vector product of Eq. (5.19) can be written with a help of the unit antisymmetric tensor ϵ_{ijk} [57], where summation over Cartesian components i, j, $k = x$, y, z that occur twice is implied. For the i-th component we have

$$\left(\frac{\vec{r}_c \times \nabla}{r_c^3}\right)_i = \epsilon_{ijk} \frac{r_{c_j}}{r_c^3} \partial_k \ . \tag{5.28}$$

Using Eq. (5.14), one can exchange the gradients and rewrite Eq. (5.28) in a more convenient form as

$$\begin{aligned} HL^{l_a l_b}_{\nu_a \nu_b i} &= -\left\langle \chi^{l_a a \alpha}_{\nu_a} \left| \epsilon_{ijk} \frac{r_{c_j}}{r_c^3} \partial_{b_k} \right| \chi^{l_b b \beta}_{\nu_b} \right\rangle \\ &= -\epsilon_{ijk} \partial_{b_k} \left\langle \chi^{l_a a \alpha}_{\nu_a} \left| \frac{r_{c_j}}{r_c^3} \right| \chi^{l_b b \beta}_{\nu_b} \right\rangle \ . \end{aligned} \tag{5.29}$$

Employing Eq. (5.22), the latter equation can be written as

$$\begin{aligned} HL^{l_a l_b}_{\nu_a \nu_b i} &= \epsilon_{ijk} \partial_{b_k} \partial_{c_j} \left\langle \chi^{l_a a \alpha}_{\nu_a} \left| \frac{1}{r_c} \right| \chi^{l_b b \beta}_{\nu_b} \right\rangle \\ &= \epsilon_{ijk} \partial_{b_k} \partial_{c_j} N^{l_a l_b}_{\nu_a \nu_b} \ . \end{aligned} \tag{5.30}$$

Similarly, for Eq. (5.20) we obtain

$$\begin{aligned} L^{l_a l_b}_{\nu_a \nu_b i} &= - \left\langle \chi^{l_a a \alpha}_{\nu_a} \left| \epsilon_{ijk} r_j \partial_{b_k} \right| \chi^{l_b b \beta}_{\nu_b} \right\rangle \\ &= -\epsilon_{ijk} \partial_{b_k} \left\langle \chi^{l_a a \alpha}_{\nu_a} \left| r_j \right| \chi^{l_b b \beta}_{\nu_b} \right\rangle \ . \end{aligned} \tag{5.31}$$

Introducing the notation for a dipole matrix element [100]

$$D^{l_a l_b}_{\nu_a \nu_b j} \equiv \left\langle \chi^{l_a a \alpha}_{\nu_a} \right| r_j \left| \chi^{l_b b \beta}_{\nu_b} \right\rangle \ , \tag{5.32}$$

one obtains for Eq. (5.19)

$$L^{l_a l_b}_{\nu_a \nu_b i} = -\epsilon_{ijk} \partial_{b_k} D^{l_a l_b}_{\nu_a \nu_b j} \ . \tag{5.33}$$

The fundamental algorithmic idea for calculating primitive matrix elements is the same as used previously. [100, 170, 101]. First, matrix elements between s-type basis functions are calculated – usually a relatively simple task. Then, the expressions for the matrix elements for basis functions of higher angular momentum l are derived with the help of recursion relations that lead to tensor algebra manipulations.

Integrals of two *s*-type functions

The overlap matrix element between s-type basis functions can be easily obtained as [100]

$$S^{00}_{11} = \left\langle \chi^{0a\alpha}_1 | \chi^{0b\beta}_1 \right\rangle = \left(\frac{4\alpha\beta}{(\alpha+\beta)^2} \right)^{3/4} \exp\left(-\delta \left(\vec{b} - \vec{a} \right)^2 \right) \ , \tag{5.34}$$

where the factor δ is defined as

$$\delta = \frac{\alpha\beta}{\alpha+\beta} \ . \tag{5.35}$$

According to Eqs. (5.23, 5.24, 5.28), second derivatives of nuclear attraction integrals are required; the latter are given as [100]:

$$N^{00}_{11} = \left\langle \chi^{0a\alpha}_1 \left| \frac{1}{r_c} \right| \chi^{0b\beta}_1 \right\rangle = 2 \left(\frac{\alpha+\beta}{\pi} \right)^{1/2} I_0 \left((\alpha+\beta)\, d^2 \right) S^{00}_{11} \ . \tag{5.36}$$

The auxiliary functions $I_n(\tau)$ are related to the incomplete Γ function and, for convenience, will be referred to by this name in the following. The argument of the Γ function is abbreviated using

$$\vec{d} = \frac{\alpha\vec{a} + \beta\vec{b}}{\alpha+\beta} - \vec{c} \ . \tag{5.37}$$

The Γ function is defined by the expression [100]:

$$I_n(\lambda) = \int_0^1 t^{2n} e^{-\lambda t^2} dt \ . \tag{5.38}$$

The latter integrals cannot be calculated analytically; thus, they are numerically evaluated in ParaGauss with the algorithm of McMurchie and Davidson [179]. Derivatives of I_n can be obtained by parameter differentiation of the integral

$$\partial_\lambda^l I_n(\lambda) = I_n^{(l)}(\lambda) = (-1)^l I_{n+l}(\lambda) \ . \tag{5.39}$$

Thus the l-th derivative raises the order n of the incomplete Γ function to $n+l$. The first derivative of a nuclear attraction integral with respect to the i-th component of the nucleus position $\vec{c}$ is

$$\partial_{c_i} N_{11}^{00} = 4\frac{(\alpha+\beta)^{3/2}}{\pi^{1/2}} I_1\left((\alpha+\beta)\, d^2\right) S_{11}^{00} d_i \ . \tag{5.40}$$

The mixed second derivative used in Eq. (5.23) reads

$$\partial_{c_j}\partial_{c_i} N_{11}^{00} = 8\frac{(\alpha+\beta)^{5/2}}{\pi^{1/2}} I_2\left((\alpha+\beta)\, d^2\right) S_{11}^{00} d_i d_j \ . \tag{5.41}$$

The second derivative of the nuclear attraction integral, taken with respect to the same nuclear coordinate, Eq. (5.24), can be written as:

$$\partial_{c_i}^2 N_{11}^{00} = 4\frac{(\alpha+\beta)^{3/2}}{\pi^{1/2}} S_{11}^{00}\left\{2(\alpha+\beta) I_2\left((\alpha+\beta)\, d^2\right) d_i^2 - I_1\left((\alpha+\beta)\, d^2\right)\right\} \ . \tag{5.42}$$

The mixed derivative taken with respect to the nuclear position $\vec{c}$ and the center of the second primitive basis function $\vec{b}$ reads:

$$\begin{aligned}\partial_{b_j}\partial_{c_i} N_{11}^{00} = -8\frac{(\alpha+\beta)^{3/2}}{\pi^{1/2}} S_{11}^{00} d_i \cdot \\ \left\{\beta I_2\left((\alpha+\beta)\, d^2\right) d_j + \delta I_1\left((\alpha+\beta)\, d^2\right)(b_j - a_j)\right\} \ .\end{aligned} \tag{5.43}$$

Finally, substituting Eqs. (5.41, 5.42, 5.43) into Eqs. (5.26, 5.27, 5.30), one can sum up all terms and write

$$HD1_{11z}^{00} = \frac{8}{3}\frac{(\alpha+\beta)^{5/2}}{\pi^{1/2}} I_2\left((\alpha+\beta)\, d^2\right) S_{11}^{00}\left(2d_z^2 - d_x^2 - d_y^2\right) \ , \tag{5.44}$$

$$HD2_{11ij}^{00} = 8\frac{(\alpha+\beta)^{5/2}}{\pi^{1/2}} I_2\left((\alpha+\beta)\, d^2\right) S_{11}^{00} d_i d_j, \ i \neq j \ , \tag{5.45}$$

$$\begin{aligned}HL_{11k}^{00} = \epsilon_{kij} 8\frac{(\alpha+\beta)^{3/2}}{\pi^{1/2}} S_{11}^{00} d_i \cdot \\ \left\{\beta I_2\left((\alpha+\beta)\, d^2\right) d_j + \delta I_1\left((\alpha+\beta)\, d^2\right)(b_j - a_j)\right\} \ .\end{aligned} \tag{5.46}$$

In Eq. (5.46) the term $\beta I_2\left(\left(\alpha+\beta\right)d^2\right)d_j$ vanishes if one takes the summation convention of the antisymmetric tensor ϵ_{kij} into account. The δ factor in the second term of Eq. (5.46) derives from the differentiation of S_{11}^{00} according to Eq. (5.34). For the z component as example, we have:

$$HL_{11z}^{00} = 8\delta\frac{\left(\alpha+\beta\right)^{3/2}}{\pi^{1/2}}I_1\left(\left(\alpha+\beta\right)d^2\right)S_{11}^{00}\cdot \\ \left\{d_x\left(b_y-a_y\right)-d_y\left(b_x-a_x\right)\right\}\ . \tag{5.47}$$

s-type matrix element of the dipole moment can be obtained as a partial derivative of an s-type overlap integral S_{11}^{00}, Eq. (5.34), with respect to the center $\vec{b}$ [100]

$$\begin{aligned} D_{11j}^{00} &= \left\langle \chi_1^{0a\alpha}\left|r_j\right|\chi_1^{0b\beta}\right\rangle \\ &= \left\langle \chi_1^{0a\alpha}\left|b_j\right|\chi_1^{0b\beta}\right\rangle + \left\langle \chi_1^{0a\alpha}\left|\left(r_j-b_j\right)\right|\chi_1^{0b\beta}\right\rangle \\ &= b_j\left\langle \chi_1^{0a\alpha}|\chi_1^{0b\beta}\right\rangle + \frac{1}{2}\beta\frac{\partial}{\partial b_j}\left\langle \chi_1^{0a\alpha}|\chi_1^{0b\beta}\right\rangle \\ &= \frac{\alpha a_j+\beta b_j}{\alpha+\beta}S_{11}^{00} \\ &= C_j^1\left(\frac{\alpha\vec{a}+\beta\vec{b}}{\alpha+\beta}\right)S_{11}^{00}\ . \end{aligned} \tag{5.48}$$

Further differentiation of the dipole moment matrix element with respect to the vector component b_k yields

$$\begin{aligned} L_{11i}^{00} &= -\epsilon_{ijk}\partial_{b_k}C_j^1\left(\frac{\alpha\vec{a}+\beta\vec{b}}{\alpha+\beta}\right)S_{11}^{00} \\ &= \epsilon_{ijk}2\delta C_j^1\left(\frac{\alpha\vec{a}+\beta\vec{b}}{\alpha+\beta}\right)C_k^1\left(\frac{\alpha\vec{a}+\beta\vec{b}}{\alpha+\beta}\right)S_{11}^{00}\ , \end{aligned} \tag{5.49}$$

where the factor δ is defined by Eq. (5.35).

The calculation of the isotropic term in the case of a finite nucleus model requires a new type of primitive integrals, Eq. (5.2). For s-type basis functions, this integral can readily be written down for a Gaussian charge distribution as nucleus model:

$$\begin{aligned} A_{11}^{00} &= \left\langle \chi_1^{0a\alpha}\right|\left(\frac{\eta}{\pi}\right)^{3/2}\exp\left(-\eta(\vec{r}-\vec{c})^2\right)\left|\chi_1^{0b\beta}\right\rangle \\ &= \left(\frac{2\alpha}{\pi}\right)^{3/4}\left(\frac{2\beta}{\pi}\right)^{3/4}\left(\frac{\eta}{\pi}\right)^{3/2}\left(\frac{\pi}{\alpha+\beta+\eta}\right)^{3/2}\cdot \\ &\exp\left(-\frac{1}{\alpha+\beta+\eta}\left(\alpha\beta\left(\vec{b}-\vec{a}\right)^2+\beta\eta\left(\vec{b}-\vec{c}\right)^2+\alpha\eta\left(\vec{c}-\vec{a}\right)^2\right)\right)\ . \end{aligned} \tag{5.50}$$

The latter expression is in fact a generalization of two-center overlap integrals, Eq. (5.34), to three-center overlap integrals.

Integrals of two functions with $l > 0$

The usual way to calculate matrix elements between basis functions of higher angular momenta, for short referred to as *ll* integrals, requires the application of operators $C_\nu^l(\nabla_a)$ and $C_\mu^l(\nabla_b)$ to the corresponding *s*-type matrix elements according to Eq. (5.8) and subsequent usage of the "product rule" of Eq. (5.11) and the "differential rule" of Eq. (5.12) [180]. However, when applied to Eqs. (5.44, 5.45, 5.46), this strategy does not provide compact results because one has to apply the product rule three times to the expressions

$$C_\nu^l(\nabla_a)\, C_\mu^j(\nabla_b)\, I_2\left((\alpha+\beta)\, d^2\right) S_{11}^{00} d_i d_j \tag{5.51}$$

and

$$C_\nu^l(\nabla_a)\, C_\mu^j(\nabla_b)\, I_1\left((\alpha+\beta)\, d^2\right) S_{11}^{00} d_i\,(b_j - a_j)\ . \tag{5.52}$$

Alternatively, one can differentiate *ll* nuclear attraction integrals [101]:

$$N_{\nu_a\nu_b}^{l_a l_b} = P_N \sum_{L=0}^{l_a+l_b} I_L\left[(\alpha+\beta)\, d^2\right] X_{l_a\nu_a l_b\nu_b}^{L} \tag{5.53}$$

with the pre-factor

$$P_N = 2\left(\frac{\alpha+\beta}{\pi\alpha^{l_a}\,(2l_a-1)!!\beta^{l_b}\,(2l_b-1)!!}\right)^{1/2}. \tag{5.54}$$

The auxiliary quantity $X_{l_a\nu_a l_b\nu_b}^{L}$ comprises all angular dependences of $N_{\nu_a\nu_b}^{l_a l_b}$, where l_a and l_b are angular momenta of the primitive Gaussian functions; ν_a, ν_b are shape quantum numbers of the real solid harmonics, and L is a summation index. The quantity $X_{l_a\nu_a l_b\nu_b}^{L}$ is given by the expression

$$\begin{aligned} X_{l_a\nu_a l_b\nu_b}^{L} = & \sum_{L_1 M_1' M_1''}^{l_b} \varepsilon_{L_1 M_1' M_2''}^{l_b\nu_b}\,(-2\beta)^{L_1}\cdot \\ & \sum_{L_2 M_2' M_2''}^{l_a} \varepsilon_{L_2 M_2' M_2''}^{l_a\nu_a} S_{a[l_a-L_2,M_2'']b[l_b-L_1,M_1'']} \sum_{L_3 M_3' M_3''}^{l_a} \varepsilon_{L_3 M_3' M_3''}^{L_2 M_2'}\,(-2\alpha)^{L_3}\, C_{M_3'}^{L_3}\left(\vec{d}\right)\cdot \\ & \left[C_{M_3''}^{L_2-L_3}(\nabla_a)\, C_{M_1'}^{L_1}\left(\vec{d}\right)\right]\theta_{L_2-L_3}\delta_{L,L_1+L_3}\ , \end{aligned} \tag{5.55}$$

where $\theta_{L_2-L_3}$ is a step function, restricting this expression to $L_2 \geq L_3$. The Kronecker delta restricts possible values of L_1, L_3 in the summation. The quantity

$$S_{a[l_a-L_2,M_2'']b[l_b-L_1,M_1'']} = C_{M_2''}^{l_a-L_2}(\nabla_a)\, C_{M_1''}^{l_b-L_1}(\nabla_b)\, S_{11}^{00}\ , \tag{5.56}$$

which depends on the orbital momenta $l_a - L_2$ of center a and $l_b - L_1$ of center b as well as the shape quantum numbers M_2'' and M_1'', can be calculated by applying the "product" and

"differential" rules of Eqs. (5.11, 5.12) to the s-type overlap integral of Eq. (5.34). According to Eq. (5.8), Eq. (5.56) is an overlap matrix element between two l-type functions, except pre-factors. Because the term $S_{a[l_a-L_2,M_2'']b[l_b-L_1,M_1'']}$ does not depend on the position of the nuclear center $\vec{c}$, it can be precalculated for all centers $\vec{c}$.

For the first derivative of the nuclear attraction integral with respect to the i-th component of the nuclear center $\vec{c}$ we obtain

$$\begin{aligned}\partial_{c_i} N^{l_a l_b}_{\nu_a \nu_b} &= P_N \partial_{c_i} \sum_{L=0}^{l_a+l_b} I_L\left[(\alpha+\beta)\, d^2\right] X^L_{l_a \nu_a l_b \nu_b} \\ &= P_N \sum_{L=0}^{l_a+l_b} \left(\partial_{c_i} I_L\left[(\alpha+\beta)\, d^2\right]\right) X^L_{l_a \nu_a l_b \nu_b} \\ &+ I_L\left[(\alpha+\beta)\, d^2\right] \partial_{c_i} X^L_{l_a \nu_a l_b \nu_b}\ .\end{aligned} \tag{5.57}$$

The second derivative of the nuclear attraction integral with respect to the same coordinate of the nuclear position $\vec{c}$ yields:

$$\begin{aligned}\partial^2_{c_i} N^{l_a l_b}_{\nu_a \nu_b} &= P_N \partial_{c_i} \sum_{L=0}^{l_a+l_b} \partial_{c_i} I_L\left[(\alpha+\beta)\, d^2\right] X^L_{l_a \nu_a l_b \nu_b} \\ &= P_N \sum_{L=0}^{l_a+l_b} (\partial^2_{c_i} I_L\left[(\alpha+\beta)\, d^2\right]) X^L_{l_a \nu_a l_b \nu_b} \\ &+ 2(\partial_{c_i} I_L\left[(\alpha+\beta)\, d^2\right]) \partial_{c_i} X^L_{l_a \nu_a l_b \nu_b} \\ &+ I_L\left[(\alpha+\beta)\, d^2\right] \partial^2_{c_i} X^L_{l_a \nu_a l_b \nu_b}\ .\end{aligned} \tag{5.58}$$

The expression for the second mixed derivative of the nuclear attraction integral with respect to the different component of the nuclear position $\vec{c}$ can be obtained using the first derivative, Eq. (5.57), as

$$\begin{aligned}\partial_{c_j}\partial_{c_i} N^{l_a l_b}_{\nu_a \nu_b} &= P_N \partial_{c_i} \sum_{L=0}^{l_a+l_b} \partial_{c_j} I_L\left[(\alpha+\beta)\, d^2\right] X^L_{l_a \nu_a l_b \nu_b} \\ &= P_N \sum_{L=0}^{l_a+l_b} (\partial_{c_i}\partial_{c_j} I_L\left[(\alpha+\beta)\, d^2\right]) X^L_{l_a \nu_a l_b \nu_b} \\ &+ (\partial_{c_i} I_L\left[(\alpha+\beta)\, d^2\right]) \partial_{c_j} X^L_{l_a \nu_a l_b \nu_b} \\ &+ (\partial_{c_j} I_L\left[(\alpha+\beta)\, d^2\right]) \partial_{c_i} X^L_{l_a \nu_a l_b \nu_b} \\ &+ I_L\left[(\alpha+\beta)\, d^2\right] \partial_{c_i}\partial_{c_j} X^L_{l_a \nu_a l_b \nu_b}\ .\end{aligned} \tag{5.59}$$

Next, we expand all derivative terms in Eqs. (5.57, 5.58, 5.59). According to Eq. (5.39), the first derivative of the incomplete Γ function with respect to the i-th component of the nuclear center $\vec{c}$ is

$$\partial_{c_i} I_l\left[(\alpha+\beta)d^2\right] = 2\,(\alpha+\beta)\, I_{l+1}\left[(\alpha+\beta)d^2\right] d_i\ . \tag{5.60}$$

The second derivative of the incomplete Γ function with respect to a different, namely the j-th component of the nuclear center $\vec{c}$ yields

$$\partial_{c_j}\partial_{c_i} I_l\left[(\alpha+\beta)d^2\right] = \left(2\left(\alpha+\beta\right)\right)^2 I_{l+2}\left[(\alpha+\beta)d^2\right] d_j d_i \ . \tag{5.61}$$

Finally, the second derivative of the incomplete Γ function with respect to the same component of the nuclear center $\vec{c}$ can be written as

$$\begin{aligned}\partial_{c_i}^2 I_l\left[(\alpha+\beta)d^2\right] = &\left(2\left(\alpha+\beta\right)\right)^2 I_{l+2}\left[(\alpha+\beta)d^2\right] d_i^2 \\ &- 2\left(\alpha+\beta\right) I_{l+1}\left[(\alpha+\beta)d^2\right] \ .\end{aligned} \tag{5.62}$$

In the following, we will consider the derivatives of the auxiliary quantities $X^L_{l_a\nu_a l_b\nu_b}$. The first part of equation Eq. (5.55) does not depend on $\vec{c}$ and is proportional to the overlap integral $S^{l_a l_b}_{\nu_a\nu_b}$. Therefore, the derivative with respect to the i-th component of the nuclear position vector $\vec{c}$ reads:

$$\begin{aligned}\partial_{c_i} X^L_{l_a\nu_a l_b\nu_b} = &\sum_{L_1 M_1' M_1''}^{l_b} \varepsilon^{l_b\nu_b}_{L_1 M_1' M_2''} \left(-2\beta\right)^{L_1} \cdot \\ &\sum_{L_2 M_2' M_2''}^{l_a} \varepsilon^{l_a\nu_a}_{L_2 M_2' M_2''} S_{a[l_a-L_2,M_2'']b[l_b-L_1,M_1'']} \cdot \Big\{ \\ &\sum_{L_3 M_3' M_3''}^{l_a} \varepsilon^{L_2 M_2'}_{L_3 M_3' M_3''} \left(-2\alpha\right)^{L_3} \left\{ C_i^1\left(\nabla_c\right) C^{L_3}_{M_3'}\left(\vec{d}\right)\right\} \cdot \\ &\left[C^{L_2-L_3}_{M_3''}\left(\nabla_a\right) C^{L_1}_{M_1'}\left(\vec{d}\right)\right] \theta_{L_2-L_3}\delta_{L,L_1+L_3} + \\ &\sum_{L_3 M_3' M_3''}^{l_a} \varepsilon^{L_2 M_2'}_{L_3 M_3' M_3''} \left(-2\alpha\right)^{L_3} C^{L_3}_{M_3'}\left(\vec{d}\right) \cdot \\ &\left[C_i^1\left(\nabla_c\right) C^{L_2-L_3}_{M_3''}\left(\nabla_a\right) C^{L_1}_{M_1'}\left(\vec{d}\right)\right] \theta_{L_2-L_3}\delta_{L,L_1+L_3}\Big\} \ .\end{aligned} \tag{5.63}$$

To resolve the remaining deferential operators in Eq. (5.63) , the "product" rule of Eq. (5.11) and the "differential" rule of Eq. (5.12) have to be used again.

The second derivative with respect to another component of the nucleus position $\vec{c}$ can

be obtained from Eq. (5.63) as $\partial_{c_j}\partial_{c_i}X^L_{l_a\nu_a l_b\nu_b}$:

$$
\begin{aligned}
&\sum_{L_1 M_1^{'} M_1^{''}}^{l_b} \varepsilon^{l_b\nu_b}_{L_1 M_1^{'} M_2^{''}} \left(-2\beta\right)^{L_1} \cdot \\
&\sum_{L_2 M_2^{'} M_2^{''}}^{l_a} \varepsilon^{l_a\nu_a}_{L_2 M_2^{'} M_2^{''}} S_{a[l_a-L_2,M_2^{''}]b[l_b-L_1,M_1^{''}]} \cdot \{ \\
&\sum_{L_3 M_3^{'} M_3^{''}}^{l_a} \varepsilon^{L_2 M_2^{'}}_{L_3 M_3^{'} M_3^{''}} \left(-2\alpha\right)^{L_3} \left\{ C_j^1\left(\nabla_c\right) C_i^1\left(\nabla_c\right) C_{M_3^{'}}^{L_3}\left(\vec{d}\right)\right\} \cdot \\
&\left[C_{M_3^{''}}^{L_2-L_3}\left(\nabla_a\right) C_{M_1^{'}}^{L_1}\left(\vec{d}\right)\right] \theta_{L_2-L_3}\delta_{L,L_1+L_3} + \\
&\sum_{L_3 M_3^{'} M_3^{''}}^{l_a} \varepsilon^{L_2 M_2^{'}}_{L_3 M_3^{'} M_3^{''}} \left(-2\alpha\right)^{L_3} \left\{ C_i^1\left(\nabla_c\right) C_{M_3^{'}}^{L_3}\left(\vec{d}\right)\right\} \cdot \\
&\left[C_j^1\left(\nabla_c\right) C_{M_3^{''}}^{L_2-L_3}\left(\nabla_a\right) C_{M_1^{'}}^{L_1}\left(\vec{d}\right)\right] \theta_{L_2-L_3}\delta_{L,L_1+L_3} + \\
&\sum_{L_3 M_3^{'} M_3^{''}}^{l_a} \varepsilon^{L_2 M_2^{'}}_{L_3 M_3^{'} M_3^{''}} \left(-2\alpha\right)^{L_3} \{ C_j^1\left(\nabla_c\right) C_{M_3^{'}}^{L_3}\left(\vec{d}\right)\} \cdot \\
&\left[C_i^1\left(\nabla_c\right) C_{M_3^{''}}^{L_2-L_3}\left(\nabla_a\right) C_{M_1^{'}}^{L_1}\left(\vec{d}\right)\right] \theta_{L_2-L_3}\delta_{L,L_1+L_3} + \\
&\sum_{L_3 M_3^{'} M_3^{''}}^{l_a} \varepsilon^{L_2 M_2^{'}}_{L_3 M_3^{'} M_3^{''}} \left(-2\alpha\right)^{L_3} C_{M_3^{'}}^{L_3}\left(\vec{d}\right) \cdot \\
&[C_j^1\left(\nabla_c\right) C_i^1\left(\nabla_c\right) C_{M_3^{''}}^{L_2-L_3}\left(\nabla_a\right) C_{M_1^{'}}^{L_1}\left(\vec{d}\right)] \theta_{L_2-L_3}\delta_{L,L_1+L_3}\} \ .
\end{aligned}
\tag{5.64}
$$

To write down the primitive integral $HL^{l_a l_b}_{\nu_a\nu_b k}$, Eq. (5.19), one combines the second mixed derivatives with respect to the nuclear position $\vec{c}$ and the basis function center $\vec{b}$ of an ll nuclear potential integral $N^{l_a l_b}_{\nu_a\nu_b}$:

$$
\begin{aligned}
HL^{l_a l_b}_{\nu_a\nu_b k} = \epsilon_{kij}\partial_{c_i}\partial_{b_j} N^{l_a,l_b}_{\nu_a,\nu_b} = \epsilon_{kij}\{ & \\
P_N \sum_{L=0}^{l_a+l_b} & (\partial_{c_i}\partial_{b_j} I_L\left[\left(\alpha+\beta\right)d^2\right]) X^L_{l_a\nu_a l_b\nu_b} \\
& + (\partial_{c_i} I_L\left[\left(\alpha+\beta\right)d^2\right])\partial_{b_j} X^L_{l_a\nu_a l_b\nu_b} \\
& + (\partial_{b_j} I_L\left[\left(\alpha+\beta\right)d^2\right])\partial_{c_i} X^L_{l_a\nu_a l_b\nu_b} \\
& + I_L\left[\left(\alpha+\beta\right)d^2\right]\partial_{c_i}\partial_{b_j} X^L_{l_a\nu_a l_b\nu_b}\} \ .
\end{aligned}
\tag{5.65}
$$

The derivative with respect to the i-th coordinate component of the center $\vec{b}$ can be obtained using the derivative with respect to center $\vec{c}$, Eq. (5.60),

$$
\partial_{b_j} I_l\left[(\alpha+\beta)d^2\right] = \left(-\frac{\beta}{\alpha+\beta}\right)\partial_{c_j} I_l\left[(\alpha+\beta)d^2\right] \ . \tag{5.66}
$$

Then, the first term of Eq. (5.65) turns to

$$\partial_{b_j}\partial_{c_i} I_l\left[(\alpha+\beta)d^2\right] = \left(-\frac{\beta}{\alpha+\beta}\right)\partial_{c_i}\partial_{c_j} I_l\left[(\alpha+\beta)d^2\right] \ . \tag{5.67}$$

The right-hand side of this equation can be calculated with the help of Eq. (5.61). Because Eq. (5.61) contains an antisymmetric combination $d_i d_j - d_j d_i$, it vanishes after summation, Eq. (5.65). The remaining terms of Eq. (5.65) read

$$\begin{aligned} HL^{l_a l_b}_{\nu_a \nu_b k} = P_N \sum_{L=0}^{l_a+l_b} &(\partial_{c_i} I_L\left[(\alpha+\beta)\,d^2\right])\partial_{b_j} X^L_{l_a\nu_a l_b\nu_b} \\ &- (\partial_{c_j} I_L\left[(\alpha+\beta)\,d^2\right])\partial_{b_i} X^L_{l_a\nu_a l_b\nu_b} \\ &+ (\partial_{b_j} I_L\left[(\alpha+\beta)\,d^2\right])\partial_{c_i} X^L_{l_a\nu_a l_b\nu_b} \\ &- (\partial_{b_i} I_L\left[(\alpha+\beta)\,d^2\right])\partial_{c_j} X^L_{l_a\nu_a l_b\nu_b} \\ &+ I_L\left[(\alpha+\beta)\,d^2\right]\left(\partial_{c_i}\partial_{b_j} - \partial_{c_j}\partial_{b_i}\right) X^L_{l_a\nu_a l_b\nu_b} \ . \end{aligned} \tag{5.68}$$

The derivative of the auxiliary quantity X is lengthy, but straightforward:

$$\begin{aligned} \partial_{b_i} X^L_{l_a\nu_a l_b\nu_b} = \sum_{L_1 M_1' M_1''}^{l_b} &\varepsilon^{l_b\nu_b}_{L_1 M_1' M_2''} (-2\beta)^{L_1} \cdot \{ \\ &\sum_{L_2 M_2' M_2''}^{l_a} \varepsilon^{l_a\nu_a}_{L_2 M_2' M_2''} \partial_{b_i} S_{a[l_a-L_2,M_2'']b[l_b-L_1,M_1'']} \cdot \\ &\sum_{L_3 M_3' M_3''}^{l_a} \varepsilon^{L_2 M_2'}_{L_3 M_3' M_3''} (-2\alpha)^{L_3} C^{L_3}_{M_3'}\left(\vec{d}\right) \cdot \\ &\left[C^{L_2-L_3}_{M_3''}(\nabla_a)\, C^{L_1}_{M_1'}\left(\vec{d}\right)\right]\theta_{L_2-L_3}\delta_{L,L_1+L_3} + \\ &\sum_{L_2 M_2' M_2''}^{l_a} \varepsilon^{l_a\nu_a}_{L_2 M_2' M_2''} S_{a[l_a-L_2,M_2'']b[l_b-L_1,M_1'']} \cdot \\ &\sum_{L_3 M_3' M_3''}^{l_a} \varepsilon^{L_2 M_2'}_{L_3 M_3' M_3''} (-2\alpha)^{L_3}\left[C^1_{m_i}(\nabla_b)\, C^{L_3}_{M_3'}\left(\vec{d}\right)\right] \cdot \\ &\left[C^{L_2-L_3}_{M_3''}(\nabla_a)\, C^{L_1}_{M_1'}\left(\vec{d}\right)\right]\theta_{L_2-L_3}\delta_{L,L_1+L_3} + \\ &\sum_{L_2 M_2' M_2''}^{l_a} \varepsilon^{l_a\nu_a}_{L_2 M_2' M_2''} S_{a[l_a-L_2,M_2'']b[l_b-L_1,M_1'']} \cdot \\ &\sum_{L_3 M_3' M_3''}^{l_a} \varepsilon^{L_2 M_2'}_{L_3 M_3' M_3''} (-2\alpha)^{L_3} C^{L_3}_{M_3'}\left(\vec{d}\right) \cdot \\ &\left[C^1_i(\nabla_b)\, C^{L_2-L_3}_{M_3''}(\nabla_a)\, C^{L_1}_{M_1'}\left(\vec{d}\right)\right]\theta_{L_2-L_3}\delta_{L,L_1+L_3}\} \ . \end{aligned} \tag{5.69}$$

Similarly, the second derivative $\partial_{c_j}\partial_{b_i}X^L_{l_a\nu_a l_b\nu_b}$ reads:

$$
\begin{aligned}
&\sum_{L_1 M_1' M_1''}^{l_b} \varepsilon^{l_b\nu_b}_{L_1 M_1' M_2''} (-2\beta)^{L_1} \cdot \{ \\
&\sum_{L_2 M_2' M_2''}^{l_a} \varepsilon^{l_a\nu_a}_{L_2 M_2' M_2''} \partial_{a_i} S_{a[l_a-L_2,M_2'']b[l_b-L_1,M_1'']} \cdot \{ \\
&\sum_{L_3 M_3' M_3''}^{l_a} \varepsilon^{L_2 M_2'}_{L_3 M_3' M_3''} (-2\alpha)^{L_3} \{ C^1_{m_j} (\nabla_c) C^{L_3}_{M_3'} \left(\vec{d}\right) \} \cdot \\
&\left[C^{L_2-L_3}_{M_3''} (\nabla_a) C^{L_1}_{M_1'} \left(\vec{d}\right) \right] \theta_{L_2-L_3} \delta_{L,L_1+L_3} + \\
&\sum_{L_3 M_3' M_3''}^{l_a} \varepsilon^{L_2 M_2'}_{L_3 M_3' M_3''} (-2\alpha)^{L_3} C^{L_3}_{M_3'} \left(\vec{d}\right) \cdot \\
&\left[C^1_j (\nabla_c) C^{L_2-L_3}_{M_3''} (\nabla_a) C^{L_1}_{M_1'} \left(\vec{d}\right) \right] \theta_{L_2-L_3} \delta_{L,L_1+L_3} \} + \\
&\sum_{L_2 M_2' M_2''}^{l_a} \varepsilon^{l_a\nu_a}_{L_2 M_2' M_2''} S_{a[l_a-L_2,M_2'']b[l_b-L_1,M_1'']} \cdot \{ \\
&\sum_{L_3 M_3' M_3''}^{l_a} \varepsilon^{L_2 M_2'}_{L_3 M_3' M_3''} (-2\alpha)^{L_3} \left[C^1_j (\nabla_c) C^1_i (\nabla_a) C^{L_3}_{M_3'} \left(\vec{d}\right) \right] \cdot \\
&\left[C^{L_2-L_3}_{M_3''} (\nabla_a) C^{L_1}_{M_1'} \left(\vec{d}\right) \right] \theta_{L_2-L_3} \delta_{L,L_1+L_3} + \\
&\sum_{L_3 M_3' M_3''}^{l_a} \varepsilon^{L_2 M_2'}_{L_3 M_3' M_3''} (-2\alpha)^{L_3} \left[C^1_i (\nabla_a) C^{L_3}_{M_3'} \left(\vec{d}\right) \right] \cdot \\
&\left[C^1_j (\nabla_c) C^{L_2-L_3}_{M_3''} (\nabla_a) C^{L_1}_{M_1'} \left(\vec{d}\right) \right] \theta_{L_2-L_3} \delta_{L,L_1+L_3} \} + \\
&\sum_{L_2 M_2' M_2''}^{l_a} \varepsilon^{l_a\nu_a}_{L_2 M_2' M_2''} S_{a[l_a-L_2,M_2'']b[l_b-L_1,M_1'']} \cdot \{ \\
&\sum_{L_3 M_3' M_3''}^{l_a} \varepsilon^{L_2 M_2'}_{L_3 M_3' M_3''} (-2\alpha)^{L_3} \{ C^1_j (\nabla_c) C^{L_3}_{M_3'} \left(\vec{d}\right) \} \cdot \\
&\left[C^1_i (\nabla_b) C^{L_2-L_3}_{M_3''} (\nabla_a) C^{L_1}_{M_1'} \left(\vec{d}\right) \right] \theta_{L_2-L_3} \delta_{L,L_1+L_3} \\
&\sum_{L_3 M_3' M_3''}^{l_a} \varepsilon^{L_2 M_2'}_{L_3 M_3' M_3''} (-2\alpha)^{L_3} C^{L_3}_{M_3'} \left(\vec{d}\right) \cdot \\
&\left[C^1_j (\nabla_c) C^1_i (\nabla_b) C^{L_2-L_3}_{M_3''} (\nabla_a) C^{L_1}_{M_1'} \left(\vec{d}\right) \right] \theta_{L_2-L_3} \delta_{L,L_1+L_3} \} \} .
\end{aligned}
\tag{5.70}
$$

To calculate the matrix element of the orbital momentum operator, Eq. (5.20, 5.33), one has to derive the matrix element of a dipole moment component. Having derived it for

s-type basis functions, one can generalize the expression for the case of two l-type functions by the application of the deferential relations of Eq. (5.8) to Eq. (5.48)

$$D^{l_a l_b}_{\nu_a \nu_b j} = \left(\alpha^l (2l-1)!!\right)^{-1/2} \left(\alpha^l (2l-1)!!\right)^{-1/2} C^{l_a}_{\nu_a}(\nabla_a)\, C^{l_b}_{\nu_b}(\nabla_b) \cdot C^1_j\left(\frac{\alpha\vec{a}+\beta\vec{b}}{\alpha+\beta}\right) S^{00}_{11} \ . \tag{5.71}$$

Employing the "product rule" of Eq. (5.11) with respect to $C^{l_a}_{\nu_a}(\nabla_a)$ we obtain

$$D^{l_a l_b}_{\nu_a \nu_b j} = \left(\alpha^l (2l-1)!!\right)^{-1/2} \left(\alpha^l (2l-1)!!\right)^{-1/2} \cdot C^{l_b}_{\nu_b}(\nabla_b) \sum_{l'_a=0}^{l_a} \sum_{\nu'_a,\nu''_a} \varepsilon^{l_a \nu_a}_{l'_a \nu'_a \nu''_a} \left[C^{l'_a}_{\nu'_a}(\nabla_a)\, C^1_i\left(\frac{\alpha\vec{a}+\beta\vec{b}}{\alpha+\beta}\right)\right] \left[C^{l_a-l'_a}_{\nu''_a}(\nabla_a)\, S^{00}_{11}\right] \ . \tag{5.72}$$

Application of the "product rule" once again with respect to $C^{l_b}_{\nu_b}(\nabla_b)$ yields

$$D^{l_a l_b}_{\nu_a \nu_b j} = \left(\alpha^l (2l-1)!!\right)^{-1/2} \left(\alpha^l (2l-1)!!\right)^{-1/2} \cdot \sum_{l'_a=0}^{l_a} \sum_{\nu'_a,\nu''_a} \varepsilon^{l_a \nu_a}_{l'_a \nu'_a \nu''_a} \sum_{l'_b=0}^{l_b} \sum_{\nu'_b,\nu''_b} \varepsilon^{l_b \nu_b}_{l'_b \nu'_b \nu''_b} \left[C^{l'_b}_{\nu'_b}(\nabla_b)\, C^{l'_a}_{\nu'_a}(\nabla_a)\, C^1_i\left(\frac{\alpha\vec{a}+\beta\vec{b}}{\alpha+\beta}\right)\right] \cdot \left[C^{l_b}_{\nu_b}(\nabla_b)\, C^{l_a-l'_a}_{\nu''_a}(\nabla_a)\, S^{00}_{11}\right] \ . \tag{5.73}$$

Then, the expression for the matrix element of the i-th component angular momentum operator can be obtained by substituting the Eq. (5.73) into Eq. (5.33)

$$\begin{aligned} L^{l_a l_b}_{\nu_a \nu_b i} = -\epsilon_{ijk} &\left(\alpha^l (2l-1)!!\right)^{-1/2} \left(\alpha^l (2l-1)!!\right)^{-1/2} \cdot \\ &\sum_{l'_a=0}^{l_a} \sum_{\nu'_a,\nu''_a} \varepsilon^{l_a \nu_a}_{l'_a \nu'_a \nu''_a} \sum_{l'_b=0}^{l_b} \sum_{\nu'_b,\nu''_b} \varepsilon^{l_b \nu_b}_{l'_b \nu'_b \nu''_b} \cdot \{ \\ &\left[C^{l'_b}_{\nu'_b}(\nabla_b)\, C^{l'_a}_{\nu'_a}(\nabla_a)\, \partial_{b_k} C^1_i\left(\frac{\alpha\vec{a}+\beta\vec{b}}{\alpha+\beta}\right)\right] \cdot \\ &\left[C^{l_b}_{\nu_b}(\nabla_b)\, C^{l_a-l'_a}_{\nu''_a}(\nabla_a)\, S^{00}_{11}\right] + \\ &\left[C^{l'_b}_{\nu'_b}(\nabla_b)\, C^{l'_a}_{\nu'_a}(\nabla_a)\, C^1_i\left(\frac{\alpha\vec{a}+\beta\vec{b}}{\alpha+\beta}\right)\right] \cdot \\ &\left[\partial_{b_k} C^{l_b}_{\nu_b}(\nabla_b)\, C^{l_a-l'_a}_{\nu''_a}(\nabla_a)\, S^{00}_{11}\right] \} \ . \end{aligned} \tag{5.74}$$

Here the term $\partial_{b_k} C^1_i\left(\frac{\alpha\vec{a}+\beta\vec{b}}{\alpha+\beta}\right)$ vanishes because the quantity $\partial_{b_k} b_i$ equals to zero. Then, Eq.

(5.74) turns to

$$L^{l_a l_b}_{\nu_a \nu_b i} = -\epsilon_{ijk} \left(\alpha^l (2l-1)!!\right)^{-1/2} \left(\alpha^l (2l-1)!!\right)^{-1/2} \cdot \sum_{l'_a=0}^{l_a} \sum_{\nu'_a,\nu''_a} \varepsilon^{l_a \nu_a}_{l'_a \nu'_a \nu''_a} \sum_{l'_b=0}^{l_b} \sum_{\nu'_b,\nu''_b} \varepsilon^{l_b \nu_b}_{l'_b \nu'_b \nu''_b} \cdot \left[C^{l'_b}_{\nu'_b} (\nabla_b) C^{l'_a}_{\nu'_a} (\nabla_a) C^1_i \left(\frac{\alpha \vec{a} + \beta \vec{b}}{\alpha + \beta} \right) \right] \cdot \left[\partial_{b_k} C^{l_b}_{\nu_b} (\nabla_b) C^{l_a - l'_a}_{\nu''_a} (\nabla_a) S^{00}_{11} \right] \ . \tag{5.75}$$

Here the first term can be calculated using the nested differentiation rule of Eq. (5.12). The remaining term $C^{l_b}_{\nu_b} (\nabla_b) C^{l_a - l'_a}_{\nu''_a} (\nabla_a) S^{00}_{11}$ is obtained using the "product" rule of Eq. (5.11).

The derivation of the ll integrals of Eq. (5.50) can follow the technique described above. Applying the usual extension rules, Eq. (5.8), and designating for convenience

$$C_N = \left(\frac{2\alpha}{\pi} \right)^{3/4} \left(\frac{2\beta}{\pi} \right)^{3/4} \left(\frac{\eta}{\pi} \right)^{3/2} \left(\frac{\pi}{\alpha + \beta + \eta} \right)^{3/2}, \tag{5.76}$$

and

$$\theta = -\frac{1}{\alpha + \beta + \eta} \left(\alpha\beta \left(\vec{b} - \vec{a} \right)^2 + \beta\eta \left(\vec{b} - \vec{c} \right)^2 + \alpha\eta \left(\vec{c} - \vec{a} \right)^2 \right) \ , \tag{5.77}$$

one has

$$A^{l_a l_b}_{\nu_a \nu_b} = C_N \left(\alpha^{l_a} (2l_a - 1)!!\right)^{-1/2} \left(\beta^{l_b} (2l_b - 1)!!\right)^{-1/2} \cdot C^{l_a}_{\nu_a} (\nabla_a) C^{l_b}_{\nu_b} (\nabla_b) \exp(\theta) \ . \tag{5.78}$$

Employing the following relation

$$\begin{aligned} & C^l_\nu (\nabla) \exp\left(-\alpha (\vec{r} - \vec{a})^2 - \beta (\vec{r} - \vec{b})^2 \right) \\ & = C^l_\nu (\nabla) \exp\left(-(\alpha + \beta) \left(\vec{r} - \frac{\alpha \vec{a} + \beta \vec{b}}{\alpha + \beta} \right)^2 - (\alpha + \beta) \left(\frac{\alpha a^2 + \beta b^2}{\alpha + \beta} - \left(\frac{\alpha \vec{a} + \beta \vec{b}}{\alpha + \beta} \right)^2 \right) \right) \\ & = C^l_\nu \left(\alpha (\vec{r} - \vec{a}) + \beta (\vec{r} - \vec{b}) \right) (-2)^l \exp\left(-\alpha (\vec{r} - \vec{a})^2 - \beta (\vec{r} - \vec{b})^2 \right) \ , \end{aligned} \tag{5.79}$$

we finally obtain for the ll primitive integrals

$$
\begin{aligned}
A^{l_a l_b}_{\nu_a \nu_b} &= C_N \left(\alpha^{l_a} (2l_a-1)!!\right)^{-1/2} \left(\beta^{l_b} (2l_b-1)!!\right)^{-1/2} \cdot \qquad (5.80)\\
& C^{l_a}_{\nu_a}(\nabla_a)\, C^{l_b}_{\nu_b}(\nabla_b) \exp(\theta) \\
&= C_N \cdot C^{l_a}_{\nu_a}(\nabla_a) \left(2\frac{\alpha\beta}{\alpha+\beta+\eta}\right)^{l_b} C^{l_b}_{\nu_b}\left(\vec{a} - \frac{(\alpha+\eta)\,\vec{b} - \eta\vec{c}}{\alpha}\right) \exp(\theta) \\
&= C_N \cdot \left(2\frac{\alpha\beta}{\alpha+\beta+\eta}\right)^{l_b} \sum_{l'_a=0}^{l_a} \sum_{\nu',\nu''} \varepsilon^{l_a\nu_a}_{l'\nu'\nu''} \left[C^{l'_a}_{\nu'}(\nabla_a)\, C^{l_b}_{\nu_b}\left(\vec{a} - \frac{(\alpha+\eta)\,\vec{b} - \eta\vec{c}}{\alpha}\right)\right] \cdot \\
& \left[C^{l_a - l'_a}_{\nu''}(\nabla_a) \exp(\theta)\right] \\
&= C_N \cdot \left(2\frac{\alpha\beta}{\alpha+\beta+\eta}\right)^{l_b} \sum_{l'_a=0}^{l_a} \sum_{\nu',\nu''} \varepsilon^{l_a\nu_a}_{l'\nu'\nu''} \left[C^{l'_a}_{\nu'}(\nabla_a)\, C^{l_b}_{\nu_b}\left(\vec{a} - \frac{(\alpha+\eta)\,\vec{b} - \eta\vec{c}}{\alpha}\right)\right] \cdot \\
& C^{l_a - l'_a}_{\nu''}\left(\vec{b} - \frac{(\beta+\eta)\,\vec{a} - \eta\vec{c}}{\beta}\right) \left(2\frac{\alpha\beta}{\alpha+\beta+\eta}\right)^{l_a - l'_a} \exp(\theta)\ .
\end{aligned}
$$

The remaining unresolved term in square brackets can be calculated using the "differential" rule of Eq. (5.12).

In the point nucleus model, calculation of the isotropic term requires one to evaluate the matrix element of a delta-function, Eq. (3.25). This term can be calculated merely by taking the value of the basis functions at the location of the nucleus. Alternatively, one can calculate the isotropic term as sum of second derivatives of the nuclear attraction integral with respect to the components of nuclear positions $\vec{c}$, Eq. (3.24). With the notation

$$\nabla^2_c = \partial^2_{c_x} + \partial^2_{c_y} + \partial^2_{c_z}\ , \qquad (5.81)$$

we obtain

$$
\begin{aligned}
\left\langle \chi^{l_a a\alpha}_{\nu_a} | \delta(\vec{r} - \vec{c}) \, | \chi^{l_b b\beta}_{\nu_b} \right\rangle &= -\frac{1}{4\pi} \left\langle \chi^{l_a a\alpha}_{\nu_a} | \nabla^2_r \frac{1}{|\vec{r} - \vec{c}|} | \chi^{l_b b\beta}_{\nu_b} \right\rangle \qquad (5.82)\\
&= \frac{1}{4\pi} \left\langle \chi^{l_a a\alpha}_{\nu_a} | \nabla^2_c \frac{1}{|\vec{r} - \vec{c}|} | \chi^{l_b b\beta}_{\nu_b} \right\rangle \\
&= \frac{1}{4\pi} \nabla^2_c \left\langle \chi^{l_a a\alpha}_{\nu_a} | \frac{1}{|\vec{r} - \vec{c}|} | \chi^{l_b b\beta}_{\nu_b} \right\rangle \\
&= \frac{1}{4\pi} \left(\partial^2_{c_x} + \partial^2_{c_y} + \partial^2_{c_z}\right) N^{l_a l_b}_{\nu_a \nu_b}\ .
\end{aligned}
$$

This approach has an advantage that the isotropic term can be calculated in one routine, simultaneously with other contributions.

We close this section with some general remarks. To avoid unnecessary recalculations during the assembly of the second derivatives of nuclear attraction primitive matrix elements, the structures which have been used to calculate the matrix elements are stored in memory and re-used. In fact, some intermediate terms are computed already in the

integral part, before the SCF part. However, since storage of these quantities would cause a significant overhead, they are calculated again in the HFCC and **g**-tensor integral parts. The other possibility, namely calculation of second derivatives of nuclear attraction matrix elements in the normal integral part, is not practical because in this case a large number of terms would have to be stored during the whole SCF part. Finally, after relativistic transformations, the orbital contraction and the symmetry adaptation with respect to the orbital basis is performed for all remaining matrix elements of HFCCs and **g**-tensors.

5.3 Conclusions

In this chapter the modifications of the integral part of the ParaGauss code required for HFCCs and **g**-tensors calculations were presented. These modifications comprise the implementations of the new type primitive integrals over Gaussian primitive basis functions, namely the second derivatives of the nuclear attraction integral, the matrix element of the orbital momentum operator, and the matrix element of a Gaussian function. Both s-type and l-type derived primitive integrals are explicitly written down.

Part II

Applications

Chapter 6

Hydrogen-Bonding Effects on Electronic g-Tensors of Semiquinone Anion Radicals

6.1 Introduction

The advent of high-field/high-frequency EPR spectroscopy (e.g., W-band, 95 GHz; F-band, 150 GHz) opened the opportunity to resolve **g**-tensor components of much smaller anisotropy than with conventional spectrometers (e.g., X-band, 9 GHz) [181, 11, 182]. This modern technique is of particular importance for organic radicals where at common lower fields only slightly split **g**-tensor components usually overlap with the hyperfine structure. Resolved **g**-tensor components were demonstrated to furnish very delicate (often unique) details of the structure of radical species, their environment, and dynamics of motion as well as of the local behavior of their wave functions [181, 11].

Semiquinones, derivatives of the 1,4-benzoquinone anion radical (BQ), play a crucial role in such ubiquitous processes as photosynthesis and respiration. They are formed, for instance, in the primary electron-transfer step of photosynthesis. In a protein environment, like the photosystem [183, 184], semiquinones undergo various rather weak interactions which, however, may cause dramatic changes in their biological action. Hydrogen bonding with specific amino acid residues of the environment is one of the most important interactions of semiquinones *in vivo*.

Monitoring alterations in the hydrogen-bonding environment of semiquinones by means of high-field EPR spectroscopy is becoming a well-established experimental practice [11]. **g**-tensor values, in particular, the g_{xx}-component oriented along the carbonyl bonds of a quinone, were shown to be very sensitive indicators for probing the presence and properties of the hydrogen bonds [185]. For instance, the duroquinone (tetramethyl-1,4-benzoquinone) anion radical, DQ, in a frozen solution of isopropyl alcohol, *i*PrOH, where hydrogen bonds with the solvent molecules are formed, features g_{xx}-value of 2.00610 which is notably lower

than the value of 2.00670 measured in an absolutely water-free 2-methyltetrahydrofuran solvent [164]. This Δg_{xx}-shift of -60×10^{-5} has been attributed to the presence of hydrogen bonds. Thus, g-values close to 2.0061 registered in photosystems were also considered as indication of hydrogen bonding. Clearly, the unequivocal separation of various phenomena taking place under real experimental conditions, such as electrostatic interactions, H-bonding or π-stacking, is usually hardly possible by experimental means alone. Here, high-level electronic structure calculations of EPR parameters can provide very important complementary information on model systems that allows to better understand and interpret experimental results.

Thus far, computational studies of magnetic properties of hydrogen-bonded complexes of semiquinone anion radicals have essentially been restricted to the description of hyperfine couplings [186, 187, 188, 189]. Only very recently a DF method with the SO operator computed in the atomic mean-field approximation has been applied to calculate H-bonding effects on **g**-tensor values of semiquinones [190]. In this context one should also mention a study of hydrogen-bond effects on **g**-tensors of the tyrosyl radical carried out with a multiconfigurational self-consistent field linear response theory [191].

Clearly, there is a general need and potential for deepening our understanding of the relations between the electronic and geometric structure of paramagnetic systems and their **g**-tensor values with the help of "first-principles" quantum chemical methods. A universal theoretical description of EPR parameters, applicable to both organic radicals of biological relevance and systems of heavy atoms, requires employment of a relativistic computational method that treats SO interaction self-consistently. Such a universally applicable tool for relativistic DF calculations of electronic **g**-tensors, described in Chapters 4, was used for this purpose.

In this work, Ref. [73], we have carried out a series of **g**-tensor calculations of hydrogen-bonded complexes of two benchmark semiquinone anion radicals, BQ and DQ. A goal of this study was (i) to examine the applicability of our new computational scheme to describe delicate effects of the hydrogen bonding on g-values and, more importantly, (ii) to explore general trends in the **g**-tensor dependency on the structure and stoichiometry of the hydrogen-bonded complexes of the biologically-relevant semiquinones.

6.2 Computational Details

All-electron calculations have been carried out using the program ParaGauss [154, 69], a parallel implementation of the LCGTO-FF-DF method [88]. The two-component relativistic KS functions [86, 87] of a Kramers doublet representing an unpaired electron were employed to calculate **g**-tensors as outlined above. These KS functions were generated in the spin-restricted half-electron fashion. GGA BP were used in the **g**-tensor calculations. Another modern GGA *xc* potential RPBE [192] was employed for the geometry optimization and the calculation of hydrogen-bond energies. GGA *xc* functionals have been shown

to provide a reasonably accurate description of rather weak interactions, like those of the hydrogen bonding [193, 194, 195].

In **g**-tensor calculations, the following specially constructed orbital basis sets mentioned above were used (Appendix A): (13s,8p,7d) for C and O; (8s,5p,1d) for H. For the former atoms, a (13s,8p) basis set [196] was extended by 7 d-type exponents, identical to the p-type exponents (except for the smallest one). For H, the analogous procedure was applied to derive 5 p-type exponents from the s-type exponents [196], except for the three most diffuse ones; the polarization d-type exponent of H was set to 1.0. This basis set extension mainly reflects an *indirect* sensitivity of g-values to basis completeness: the extra functions with l+1 (where l is the maximum angular momentum of the occupied atomic orbitals) are required only for the special DKH transformations when calculating the relativistic contribution to the *ee* Hartree interactions [87]. A sufficiently accurate for the present purposes DKee1 scheme of the Hartree term transformations was employed [87]. In the code, these transformations precede the basis contraction step. Thus, one can considerably reduce the computational effort by using very compact contractions for the most expensive l+1 exponents. In this work we use the following contractions: [5s,4p,1d] for H; [8s,7p,3d] for C and O; these contractions (of general type for s- and p-type functions) were shown to cause deviations of the calculated g-values by less than 10^{-5}. The auxiliary fitting basis sets were constructed in a standard fashion by doubling the s- and p-type exponents of the orbital basis functions [88]; they were augmented by standard sets of 5 p- and 5 d-type polarization functions [88], Appendix A.

The planar semiquinone anion radicals (free and in hydrogen-bonded complexes) were oriented in the xy-plane with the CO groups pointing along the x-axis. The geometries were optimized automatically imposing symmetry constraints (see Section 6.3) using analytical energy gradients [197]. The RPBE binding energies were corrected for the basis set superposition error by applying the counterpoise method [198]. In **g**-tensor calculations, a common gauge origin at the center of mass has been employed throughout. Gauge corrections have been shown in test calculations to be very small [72] and thus were neglected in this work.

6.3 Models

Anion radicals BQ and DQ have been chosen as the simplest, yet adequate, models of semiquinone species that participate in the primary electron transfer step of photosynthesis. Water (H_2O, W) and methanol (MeOH, M) molecules have been chosen to represent typical cases of hydrogen-bonding interactions with a protein environment (and a solvent). Complexes of the semiquinones with one, two, and four hydrogen-bonded W or M molecules in various orientations and configurations have been investigated (Figure 6.1).

Figure 6.1: Hydrogen-bonded model complexes of BQ and DQ anion radicals with one to four water (H_2O, W) or methanol (MeOH, M) molecules bound in different orientations. The semiquinone rings are located in the xy-plane with the CO groups aligned along the x-axis; top view (along the z-axis). Left column: BQ1Wv – BQ+1W vertical (C_s); BQ2Wv – BQ+2W vertical (C_{2v}); BQ2Wp – BQ+2W planar (C_{2h}); BQ2Wl – like BQ2Wp but with linear C_a-O_a-H_1 moiety (C_{2h}); BQ4Wc – BQ+4W *cis* (D_{2h}); BQ4Wt – BQ+4W *trans* (D_{2h}); BQ4Mc – BQ+4M cis (D_{2h}); BQ4Mt – BQ+4M trans (D_{2h}). Right column: DQ2Wv – DQ+2W vertical (C_{2v}); DQ2Wp – DQ+2W planar (C_{2h}); DQ2Wl – like DQ2Wp but with linear C_a-O_a-H_1 moiety (C_{2h}); DQ4Wc – DQ+4W *cis* (D_{2h}); DQ4Wt – DQ+4W *trans* (D_{2h}); DQ4Mc – DQ+4M *cis* (D_{2h}); DQ4Mt – DQ+4M *trans* (D_{2h}).

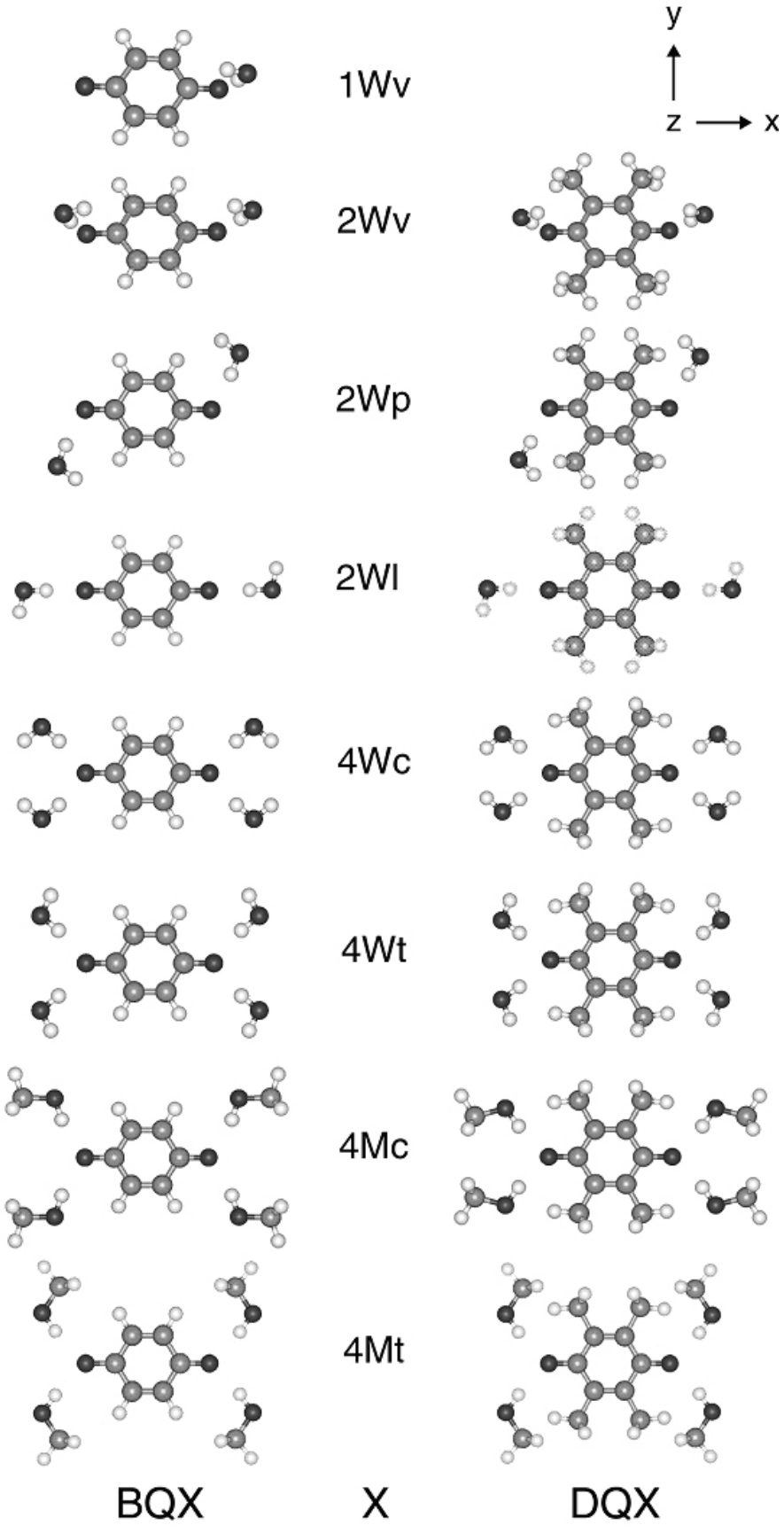
y
z
x
1Wv
2Wv
2Wp
2Wl
4Wc
4Wt
4Mc
4Mt
BQX
X
DQX

Keeping in mind the model character of the present study, we refrained from a geometry optimization of *all* complexes under consideration. Rather, we carefully designed groups of models that share some of the structural features, but differ in selected geometric or electronic properties. In this way, one is able to differentiate better between structural (conformational) and "chemical" effects. Therefore, besides the parent BQ and DQ, the structure of the following complexes were optimized: BQ2W (C_i), BQ4Wc (C_{2h}), DQ4Wc (C_{2h}). For **g**-tensor calculation, the geometries of the remaining complexes under study were derived by displacing solvent molecules such that the lengths of the hydrogen bonds and/or pertinent angles were kept equal to those in the optimized structures. For the adopted structural parameters, see Tables 6.1 and 6.2.

In some of the models built as just outlined, the calculated hydrogen-bond energies may be close to zero or even negative (Tales 6.1, 6.2) as a result of unfavorable intermolecular contacts. No attempt has been made to repair this situation because (i) under experimental conditions the structures represented by the models may become favorable, and (ii) no clear correlation was found between the strength of the hydrogen bonds and **g**-tensor values (Section 6.4.2).

6.4 Results and Discussion

Organic radicals are known to exhibit very small **g**-tensor anisotropies. Thus, they require particularly precise and reliable **g**-tensor calculations. There are two important aspects of this issue that we would like to comment on before we will discuss the present results.

The first question is how adequate are the calculated molecular models with respect to the systems dealt with under experimental conditions. On the one hand, even small deviations of the optimized geometry from the appropriate structure could translate into variations of the principal values of the **g**-tensor, comparable to its anisotropy. Since we rely on high-level DF calculations, we assume such uncertainties to be usually minor and will not discuss them here. On the other hand, environmental effects on organic radicals, which are commonly studied in matrices, can be noticed in measured **g**-tensors but are hard to model. This study is focuses *exclusively* on one particular contribution to environmental effects experienced by radicals in solvents, namely, on the *specific* effect of hydrogen bonding with individual molecules of the solvent. Investigation of another effect of water or alcohol solvents due to their dielectric nature is feasible [199] but goes beyond the scope of the present study. We adhere to the present restricted model, despite the fact that the trend of the gas-phase acidity of the molecules, *t*BuOH > *i*PrOH > EtOH > MeOH > H_2O, is reversed when long-range electrostatic interactions in a solvent are taken into account [200].

Table 6.1: Calculated parameters of the benzoquinone anion radical (BQ) and its complexes with water (W) or methanol (M) molecules.

Parameter	BQ	BQ1Wv	BQ2Wv	BQ2Wp	BQ2Wl	BQ4Wc	BQ4Wt	BQ4Mc	BQ4Mt
$r(C_a\text{-}O_a)$	1.281	1.287	1.287	1.287	1.287	1.293	1.293	1.298	1.298
$r(C_a\text{-}C_b)$	1.465	1.465	1.465	1.465	1.465	1.456	1.456	1.447	1.447
$r(C_b\text{-}C_b)$	1.384	1.384	1.384	1.384	1.384	1.382	1.382	1.377	1.377
$r(C_b\text{-}H_b)$	1.101	1.101	1.101	1.101	1.101	1.098	1.098	1.095	1.095
$r(O_a\text{-}H_1)$	–	1.783	1.783	1.783	1.783	1.843	1.843	1.843	1.843
$r(H_1\text{-}O)$	–	1.002	1.002	1.002	1.002	0.994	0.994	1.003	1.003
r(O-R)	–	0.973	0.973	0.973	0.973	0.973	0.973	1.411	1.411
$\angle C_a\text{-}C_b\text{-}C_b$	122.7	122.7	122.7	122.7	122.7	121.9	121.9	121.6	121.6
$\angle C_a\text{-}C_b\text{-}H_b$	116.3	116.3	116.3	116.3	116.3	117.3	117.3	117.6	117.6
$\angle C_a\text{-}O_a\text{-}H_1$	–	118.8	118.8	118.8	180.0	130.0	130.0	114.9	114.9
$\angle O_a\text{-}H_1\text{-}O$	–	173.7	173.7	173.7	173.7	169.2	169.2	173.4	173.4
$\angle H_1\text{-O-R}$	–	101.7	101.7	101.7	101.7	102.4	102.4	109.1	109.1
E	–	37.5	32.2	38.0	30.0	38.9	36.1	43.6	0.2
$\Delta g_{xx}\times10^5$	0^a	-1	-47	-149	-63	-237	-202	-268	-281
$\Delta g_{yy}\times10^5$	0^a	2	1	-7	-21	-19	-14	-8	-7
$\Delta g_{zz}\times10^5$	0^a	4	10	2	2	4	3	4	2

Distances (r, Å), bond angles (degree), energy of hydrogen bonds (E, kJ/mol per bond), and Δg-shifts with respect to BQ. Atoms in the semiquinone fragment are indicated by letter subscripts, H_1 is the atom of W or M molecules involved in the hydrogen bond; R labels H_2 (W) or C (M) atoms (see Figure 6.1). a) Calculated reference values: g_{xx}=2.01139, g_{yy}=2.00594, g_{zz}=2.00202.

Table 6.2: Calculated parameters of the duroquinone anion radical (DQ) and its complexes with water (W) or methanol (M) molecules.

Parameter	DQ	DQ2Wv	DQ2Wp	DQ2Wl	DQ4Wc	DQ4Wt	DQ4Mc	DQ4Mt
$r(C_a\text{-}O_a)$	1.284	1.289	1.289	1.289	1.296	1.296	1.300	1.300
$r(C_a\text{-}C_b)$	1.472	1.472	1.472	1.472	1.466	1.466	1.459	1.459
$r(C_b\text{-}C_b)$	1.393	1.393	1.393	1.393	1.396	1.396	1.393	1.393
$r(C_b\text{-}C_c)$	1.521	1.521	1.521	1.521	1.520	1.520	1.511	1.511
$r(O_a\text{-}H_1)$	–	1.806	1.806	1.806	1.867	1.867	1.867	1.867
$r(H_1\text{-}O)$	–	1.002	1.002	1.002	0.993	0.993	1.000	1.000
r(O-R)	–	0.973	0.973	0.973	0.971	0.971	1.411	1.411
$\angle C_a\text{-}C_b\text{-}C_b$	120.7	120.7	120.7	120.7	121.2	121.2	121.5	121.5
$\angle C_a\text{-}C_b\text{-}C_c$	114.2	114.2	114.2	114.2	119.2	119.2	120.2	120.2
$\angle C_a\text{-}O_a\text{-}H_1$	–	118.8	118.8	180.0	139.1	139.1	133.8	133.8
$\angle O_a\text{-}H_1\text{-}O$	–	175.9	175.9	175.9	174.6	174.6	172.4	172.4
$\angle H_1\text{-}O\text{-}R$	–	101.7	101.7	101.7	103.4	103.4	111.5	111.5
E	–	36.1	−33.4	28.4	33.5	29.7	29.8	−110.5
$\Delta g_{xx}\times 10^5$	0^a	−50	−149	−53	−377	−359	−186	−141
$\Delta g_{yy}\times 10^5$	0^a	−7	−5	−21	−197	−193	−24	−21
$\Delta g_{zz}\times 10^5$	0^a	−2	−1	2	4	4	4	3

Distances (r, Å), bond angles (degree), energy of hydrogen bonds (E, kJ/mol per bond), and Δg-shifts with respect to DQ. Notations as in Table 6.1. a) Reference calculated values: g_{xx}=2.00943, g_{yy}=2.00589, g_{zz}=2.00204.

The second question deals with the genuine accuracy of our relativistic method to calculate **g**-tensors; it has been discussed in detail in Chapter 4 for a series of benchmark inorganic and organic radicals. There, we noted a *systematic* overestimation of the **g**-tensor anisotropy for radicals formed by main-group elements. For instance, g-shifts (in 10^{-5} units) computed for biphenyl anion radical, C_6H_5-$C_6H_5^-$, and for DQ [72] compare with experimental values [164, 201] (in parentheses) as follows: C_6H_5-$C_6H_5^-$ $\Delta g_{xx} = 142$ (107±2), $\Delta g_{yy} = 46$ (32±2), $\Delta g_{zz} = -13$ (-5±2); DQ $\Delta g_{xx} = 711$ (438±5), $\Delta g_{yy} = 357$ (291±5), $\Delta g_{zz} = -28$ (−14±5). Clearly, despite the small g-shifts for quinone (and other organic) radicals, the present method is able to reproduce not only the signs, but also the relative values of measured **g**-tensor components.

6.4.1 Structure and Stoichiometry of the H-bonded Model Complexes

Decisive information on the stoichiometry of hydrogen-bonded complexes of quinones in (liquid or frozen) alcohol solutions is still lacking. Obviously, the number of hydrogen-bonded solvent molecules can vary for different solvents. The solvents studied experimentally show a strong dependence of hyperfine structures on the dielectric constant of the medium [189]. Results of EPR investigations of BQ in frozen methanol solutions are consistent with the presence of *one hydrogen bond per oxygen atom of quinone molecules* with the bond angle C_a-O_a-H_1 close to 180° [185]. The latter value deviates notably from the bond angles 110-140° optimized in this work (see Tables 6.1 and 6.2) and in other high-level computational studies of hydrogen-bonded complexes of quinones [186, 189]. This finding is indicative of considerable collective solvent effects on the direction of the hydrogen bonds and thus implies a limited applicability of structures that have been fully optimized in the gas phase. Rather, studies of model complexes that map various conceivable structures (see below) are more relevant to derive general trends of **g**-tensor values depending on the shape of the hydrogen-bonded complexes.

Models with one to four hydrogen-bonded water or alcohol molecules per quinone anion radical have been employed in previous calculations [186, 187, 188, 189, 190]. We also followed this line and considered this series of models for BQ and DQ derivatives. The geometric parameters of the key systems studied here are displayed in Tables 6.1 and 6.2. The formation of hydrogen bonds of BQ and DQ only slightly affects the structure of the parent species. In line with other calculations [186, 187, 188, 189, 190], we only note an elongation of the C_a-O_a bonds by 0.01 Å (water environment) or 0.02 Å (methanol environment); also, the C_a-C_b bonds shrink slightly.

Optimized hydrogen-bond lengths in the present study (Tables 6.1, 6.2), $r(O_a$-$H_1)$, cover a rather narrow range of distances 1.78-1.87 Å depending on the number and orientation of the solvent molecules coordinated to a semiquinone. This range agrees with other DF results [186, 187, 188, 189, 190] and the values are notably smaller than the sum of the van

der Waals radii of the H and O atoms, 2.40 Å (1.00 Å + 1.40 Å). As already mentioned, a significant alteration of the hydrogen-bond length and direction with respect to the values optimized in the gas-phase approximation can be expected from the interactions between the solvent molecules (or from a spatial hindrance of the nearby hydrogen-bonded amino acid residues in a protein environment). Elongation of the hydrogen bonds seems to be more probable than shrinking. To test the sensitivity of the calculated **g**-tensors to hydrogen-bond distance, we studied the system BQ4Wc also at $r(O_a\text{-}H_1)$ set to 1.943 and 2.043 Å, keeping all other geometric parameters fixed at the values given in Table 6.1.

We found an essentially linear dependence for both xx- and yy-components of the **g**-tensor with slopes (per 0.1 Å) of $\sim 27\times10^{-5}$ (g_{xx}) and $\sim 4\times10^{-5}$ (g_{yy}). Thus, more than 10% of the shifts Δg_{xx} and Δg_{yy} induced by hydrogen bonds would disappear in a case of the bond elongation by only 0.1 Å. This high sensitivity becomes even more clear if one takes into account that the overall calculated energy loss accompanying this stretch of four hydrogen bonds in BQ4Wc by 0.1 Å is 2.4 kJ/mol; for a further stretch increment by 0.1 Å it is 5.7 kJ/mol (or only 1.4 kJ/mol per H-bond). *Nonspecific* environmental effects on radicals of such small energy variations are usually unavoidable under experimental conditions; they are manifested in the measured **g**-tensor values [181].

6.4.2 Effect of the Hydrogen Bonding on g-Tensors

First we would like to address the question concerning the accuracy of our newly developed tool for **g**-tensor calculations. In particular, we want to explore whether this tool is capable of describing the subtle effects of hydrogen bonding on g-values. To answer this question, one needs a touchstone set of pertinent experimental results to be reproduced by quantum chemical models. We consider the following assumptions appropriate for examining the accuracy of computed g-values: (i) the experimental conditions for BQ in a frozen methanol solution, under which the EPR spectra were measured, correspond to a situation where *one* hydrogen bond occurs at each oxygen atom of the semiquinone with a bond angle $C_a\text{-}O_a\text{-}H_1$ near 180° [185]; (ii) structure and stoichiometry of the paramagnetic species in the system DQ/*i*PrOH as well as the g-shifts induced by the hydrogen-bonds formation ($\times10^{-5}$), $\Delta g_{xx}= -60$, $\Delta g_{yy}= -12$, $\Delta g_{zz}= 3$ [164] are similar to those of BQ/MeOH. The first assumption on the number and orientation of the hydrogen bonds might not look very convincing, but it has been concluded that only this molecular arrangement (of several conceivable ones) is consistent with the EPR data [185].

Inspection of Tables 6.1 and 6.2 makes evident that the calculated results agree in excellent fashion with this "experimental" touchstone set of data (see BQ2Wl and DQ2Wl). Indeed, the computed Δg_{xx}-value of paramagnetic complexes of BQ is by a factor 3–6 overestimated when one assumes semiquinone complexes with four hydrogen bonds (two at each O atom). A single (vertically oriented) hydrogen bond with one of the two phenolate oxygen atoms (BQ1Wv) is computed to affect all three principal g-values to negligible

extent. Thus, only BQ and DQ complexes with one hydrogen bond per oxygen atom form adequate models. For the planar species BQ2Wp and DQ2Wp with the angle C_a-O_a-H_1 at ∼119° (as optimized for the moiety BQ2W in C_i symmetry), calculated Δg shifts are essentially indistinguishable and qualitatively fit the measured values [164]. Nevertheless, Δg_{xx} is overestimated in absolute value by more than a factor of 2. Switching from the planar arrangement to that of hydrogen-bonded water molecules oriented perpendicularly to the quinone ring in the models BQ2Wv and DQ2Wv leads to Δg_{xx} of -47×10^{-5} or -50×10^{-5}, respectively. These numbers are considerably closer to the measured value of -60×10^{-5}; however, agreement with experiment of the calculated values Δg_{yy} and Δg_{zz} for BQ2Wv (both in magnitude and sign) is not satisfactory. On the other hand, for the models BQ2Wl and DQ2Wl with an *assumed* linear arrangement of the H-bond moiety C_aO_a-H_1 (as suggested in Ref. [185]), all three Δg-components agree quantitatively with experiment. Note that the energy cost per H-bond to form the linear complex BQ2Wl from the more stable BQ2Wp one is 8 kJ/mol only (Table 6.1).

Having advanced arguments that support the high precision of calculated H-bonding effects on **g**-tensors, we now discuss general trends noticeable among the series of models under investigation. We also will comment on conceivable experimental structures and pertinent results of previous calculations.

The observed trends and magnitudes of g-components in semiquinone systems are qualitatively reproduced in most of our models. The g_{xx}-component is the most sensitive indicator of hydrogen bonding, in line with experiment [164], followed by the g_{yy}-component; both components exhibit negative shifts. On the other hand, the g_{zz}-component directed normal to the quinone plane is essentially insensitive to details of the models. For planar model systems with two and four solvent molecules and angles C_a-O_a-H_1 far from 180° (as determined in the geometry optimization of isolated solvation complexes), the Δg_{xx}-shifts per hydrogen bond are calculated at $50–70\times10^{-5}$ (BQ derivatives) and $40–90\times10^{-5}$ (DQ complexes). The g_{yy}-component of the latter moieties is notably more influenced by hydrogen bonding than of the corresponding complexes with BQ.

While H-bonds in the molecular plane of the semiquinones have been found to exert strong effects on the g-shifts, a water molecule located in the plane perpendicular to the ring (BQ1Wv) leaves the principal values of the semiquinone **g**-tensor essentially unchanged. This finding can be generalized as a property of the hydrogen bonds formed in a plane normal to the ring: they exert minimal effects on the g_{xx}-component as can be seen by comparison of the g_{xx}-shifts calculated for BQ2Wv and BQ2Wp (Table 6.1) and DQ2Wv and DQ2Wp (Table 6.2). This seems to be a purely conformational feature because the O_a-H_1 bond lengths were kept unchanged and the difference in the bond strength is small (Tables 6.1, 6.2). As expected, a larger number of hydrogen bonds causes a stronger shift Δg_{xx}, although the dependence is not linear. The H-bonding shifts for the DQ complexes with four water molecules are computed larger than for the corresponding BQ systems.

No clear difference between the effect of hydrogen-bonded water vs. methanol molecules

on **g**-tensors could be found: for BQ derivatives, slightly stronger bonding with four methanol molecules (than with water, as rationalized in Ref. [200]) is somewhat more reflected in g-values, while for the DQ complexes the opposite is found in our model systems. Also, we were not able to identify a distinct dependence of the **g**-tensor on the strength of the hydrogen bonds; rather, the conformational factor seems to prevail. However, this lack of correlation of Δg_{xx}-shifts with the strength of the hydrogen bonds can be partly due to the usage of non-optimized structures adopted to take (although indirectly) some possible collective effects of the environment into account.

The formation of hydrogen bonds can cause slight deviations of the principal **g**-tensor axes. For instance, in BQ2Wp the xx-direction forms an angle of 4.0° (or 2.0° per H-bond) with the Cartesian vector x. In the DQ2Wp congener, the angle is more than twice as large, 9.3°, probably partly due to a stronger repulsion between the H atoms of water and DQ molecules. In the systems BQ2Wl and DQ2Wl, favored in the present study, the xx direction departs from the vector x by 0.4°. Even in BQ1Wv a deviation of the axis by 0.6° has been calculated (now in the vertical plane).

Finally, we would like to comment on how the present results agree with those of the previous computational studies of hydrogen bonding effects on the electronic structure and EPR parameters of semiquinones. First, the influence of hydrogen bonds on magnetic properties of quinone anion radicals rationalized in terms of a slightly enhanced spin-density near the C_a nucleus at the expense of its decrease on O_a (mainly) and C_b atoms [186], is in line with our data. Second, a linear complex of a tyrosyl radical with one water molecule exhibits essentially the same set of the calculated **g**-tensor values, namely, $\Delta g_{xx}= -60\times10^{-5}$, $\Delta g_{yy}= -10\times10^{-5}$, $\Delta g_{zz}= 0$ [191], as calculated here for the species BQ2Wl (Table 6.1). Hydrogen bonding was shown to increase the electron affinity of semiquinones by ca. 0.6 eV and thus notably affect their functionality in photochemical processes [189]. Our data support this finding, but we calculate this effect somewhat larger: the electron affinity of BQ2Wl and DQ2Wl are by 0.86 eV and 0.75 eV, respectively, larger than the electron affinities of the corresponding reference systems BQ and DQ.

Third, the results of the recent DF study of **g**-tensor values as reflected by hydrogen bonding in the BQ/H_2O complexes [190] show satisfactory agreement with the present data. For instance, for the moiety BQ4Wt the g-shifts due to hydrogen bonding, $\Delta g_{xx}= -180\times10^{-5}$, $\Delta g_{yy}= -13\times10^{-5}$ [190], nicely fit the present values (Table 6.1); for BQ2Wp [190], however the value $\Delta g_{xx}=-83\times10^{-5}$ is almost half as large as the shift of -149×10^{-5} calculated here, despite the fact that the Δg_{yy}values are the same, -7×10^{-5}. These differences can be partly attributed to neglected spin-polarization effects in the present calculations, as it was explained in Chapter 4, and/or to deficiencies of the more approximate perturbational treatment of SO interaction in Ref. [190]. As for the models, the previous study [190] completely relied on optimized structures of the hydrogen-bonded complexes, favoring as many as up to six H_2O molecules coordinated to a semiquinone anion radical, but models with "linear" moieties like BQ2Wl were not taken into account [190]. Such

linear structures have been suggested on the basis of experimental EPR data [185] and have been classified as probable moieties in our investigation. Given the small energy differences between solvated complexes of differently structured first coordination shells, a more comprehensive computational investigation of such environment effects on the radical may be helpful.

To summarize, the present results are reliable enough to encourage further studies of more sophisticated models and other environmental interactions of semiquinone anion radicals devoted to rationalizing dependence of EPR parameters, both hyperfine- and **g**-tensors.

6.5 Conclusion

This study has been devoted to the first application of the developed and implemented relativistic density functional Douglas-Kroll approach (Chapters 2 and 4) to calculate electronic **g**-tensors. Here, we had chosen a very critical but challenging subject, namely modeling the influence of delicate hydrogen-bonding effects on EPR g-components of semiquinone anion radicals as experienced by them in water and alcohol solutions as well as in protein environments. We were able to demonstrate quantitative agreement of the calculated **g**-tensors for complexes containing one water molecule per each oxygen atom and *linear* hydrogen-bonded fragments C_a-O_a-H_1 with measured EPR parameters for semiquinone anion radicals in alcohol solvents. We have identified and rationalized general trends in the dependence of calculated **g**-tensor values on the electronic and spatial structure of hydrogen-bonded complexes. We also showed that the **g**-tensor features are more sensitive to the conformation than to the strength of hydrogen bonds. The set of model systems considered here and the predictions concerning the principal values and directions of **g**-tensors should be of help when extracting more information from EPR spectra on structure and electronic properties of paramagnetic systems of biological relevance.

Chapter 7

Electronic g-Values of Na^+-NO and Cu^+-NO Complexes in Zeolites: Analysis Using a Relativistic Density Functional Method

7.1 Introduction

High-field EPR spectroscopy recently opened an opportunity for resolving components of **g**-tensors of much smaller anisotropy than was possible with conventional spectrometers [181, 11]. This modern technique is of particular importance for radicals of main group elements where at common lower fields only slightly split peaks of g-components often overlap with the hyperfine structure. Resolved **g**-tensors are known to contain very delicate information on the structure of radical species, their environment and as well as on the local behavior of their wave functions [181, 11]. A significant limiting factor, however, is the difficulty to interpret EPR g-values in terms of conventional quantities characterizing the electronic structure.

Fortunately, nowadays not only the need for clarifying the relations between the electronic and geometric structure of paramagnetic systems and their g-values became evident. Also, means to achieve this target are potentially provided by modern "first-principles" electronic structure methods. A theoretical description of EPR parameters, applicable to both light and heavy atom systems, requires employment of a relativistic computational method that treats SO interaction self-consistently. There, the Zeeman energy splitting is transparently determined solely by two-component *ground-state* orbital wave functions without invoking virtual states. This allows one to analyze shifts of the principal g-values from the free-electron one g_e, $\Delta g = g - g_e$, in terms of particular atomic orbital contributions, as we will demonstrate in the following.

Such a quantum chemical analysis of g-shifts may provide key information about the

geometrical and electronic structure of paramagnetic adsorption complexes on oxides. As an example, we will consider adsorption complexes of nitric oxide with monovalent cations in zeolite materials, such as Cu^+-NO and Na^+-NO species, for which the determination of the structure relies almost solely on a proper interpretation of their EPR parameters [202]. These NO complexes are of special interest because the Cu^+-NO species is an intermediate in the catalytic decomposition of nitric oxide into nitrogen and oxygen over CuZSM-5 zeolites [203, 204]. Specific features in the g-values were found for Cu^+-NO complexes in Cu-ZSM-5 [205] in comparison with Na^+-NO species in catalytically inactive NaA and NaZSM-5 zeolites [206]. Whereas for the principal values of the **g**-tensor of the Na^+-NO complexes the relation $g_1 < g_2 < g_3 < g_e$ was obtained in line with a simple electrostatic interaction model, the Cu^+-NO complexes gave $g_1 < g_e < g_2 \sim g_3$ implying a substantial admixture of Cu $3d$ atomic orbitals to the ground state orbital of the unpaired electron due to covalent bonding contributions. However, sophisticated quantum chemical approaches have to be applied to corroborate and rationalize the contribution of the $3d$ orbitals of the Cu^+ cation to the g-values of the Cu^+-NO species. Such a more detailed interpretation of the **g**-tensor parameters is necessary for designing a reliable structural and electronic model of Cu^+-NO adsorption complex. This model, in turn, is expected to contribute to a deeper understanding of the direct catalytic NO decomposition mediated by the system CuZSM-5.

In this work, Ref. [74], we explore the advantage of including SO interaction in the ground-state wave function to rationalize the notable difference in parameters of the **g**-tensor measured for complexes of NO molecules with charge compensating Na^+ and Cu^+ cations in zeolites. We will show (i) that these characteristic g-value features of the two kinds of paramagnetic systems are already inherent to their simplest models, $[Na\text{-}NO]^+$ and $[Cu\text{-}NO]^+$ and (ii) that the difference is essentially due to the covalent contribution to the adsorption bond mediated by Cu $3d$ orbitals.

7.2 Computational Details

All calculations were performed with the code ParaGauss [154, 69], a parallel implementation of the LCGTO-FF-DF method [88]. The two-component relativistic KS functions [86, 87] of the Kramers doublet representing an unpaired electron were employed to calculate g-values. These KS functions were obtained from the spin-restricted half-electron fashion as outlined in Chapter 4. The gradient-corrected xc functional BP86 was used throughout [124, 125].

For calculations of g-factors, the following special orbital basis sets were constructed: $(13s,8p,7d)$ for N and O; $(13s,8p,7d)$ for Na and $(15s,11p,6d,6f)$ for Cu. For the atoms N and O, the original $(13s,8p)$ basis set [196] was extended by 7 d-type exponents, identical to the p-type exponents (except for the smallest one). The analogous procedure was applied to derive 6 f-type exponents from the d-type exponents for Cu [131, 207] as well as 7

d-type exponents from the p-type exponents of the basis (12s,6p) for Na [208]; the latter set was extended by one s-type exponent, 0.18983, and by two p-type exponents, 0.143647 and 0.047833. The extra functions with l+1 (l being the maximum angular momentum of the occupied atomic orbitals) are required only for the DKH transformations to compute the relativistic contribution to the *ee* Hartree interaction on the sufficient DKee1 level of accuracy (Chapter 4, [87]). These transformations precede the basis contraction step; thus, one can reduce the extra computational costs by using very compact contractions for the most expensive l+1 exponents. The following contractions were employed: [9s,7p,3d] for Na, [10s,11p,6d,1f] for Cu and [8s,7p,3d] for N and O. The accuracy of these so-called generalized contractions (based on atomic eigenvectors) in terms of the calculated g-values is $\sim 10^{-5}$. The auxiliary fitting basis set was constructed by scaling the s- and p-type exponents of the orbital basis following our usual technique [88]. This basis set was augmented by standard sets of 5 p- and 5 d-type polarization functions on each atom [88]. All basis sets employed in the present study are listed in Appendix A.

7.3 Models

Already at a conventional nonrelativistic level, it is rather difficult to construct and study very accurate models for such complicated adsorption systems as those considered here. These models have to explicitly take into account not only fragments of a sufficiently extended part of the zeolite host, but also its electrostatic field and probably other accompanying species present. Leaving aside the problem how to design such a precise model, it does not seem justified to spend this computational effort at the present fully relativistic level to calculate g-values for the aim of this study, namely to rationalize the difference in "g -signatures" of the Na^+-NO and Cu^+-NO complexes, which is manifested irrespective of the zeolite substrate. This goal can (and will have to) be achieved already by analyzing simpler generalized models, applicable (at least in the first approximation) to the whole range of conceivable adsorption situations.

Thus, we consciously restricted ourselves to the minimal models $[Na\text{-}NO]^+$ and $[Cu\text{-}NO]^+$, that completely neglect any zeolite environment. This strategy implies that one does not necessarily rely on the structure of such models optimized quantum mechanically, because even subtle ignored interactions with the zeolite frameworks are able to alter the structure of the M^+-N-O species sufficiently to notably affect very sensitive g parameters. Rather, we proceed here along the line recently proposed to study weakly bound hydrogen-bonded complexes of benzoquinone radical-anions (Chapter 6), where for calculating g-values a series of structures was mapped on the basis of experimental considerations.

The structural parameters of our models $[M\text{-}NO]^+$ are listed in Tables 7.1 and 7.2. The structure of the rather strongly bound complex of Cu^+ ion with NO, with a calculated Cu-NO bond energy of $\sim$180 kJ/mol, is expected to be only slightly changed when the zeolite environment is included. Thus, the bond lengths Cu-N and N-O were taken as optimized;

only for the angle Cu-N-O (a variable exhibiting a very shallow potential curve), two different values were adopted for comparison. In the other complex, the species Na^+ and NO species interacting significantly weaker, with a binding energy of 34 kJ/mol only. The optimized distance r(Na-N) = 2.5 Å is notably longer than the bond length r(Na-N) = 2.1 Å estimated based on the experimental EPR parameters for NO adsorbed in NaA zeolites [209], which also predicted the angle Na-N-O to be ∼142°. Both the r(Na-N) and ∠Na-N-O variables are subject to relatively large uncertainties in the minimum energy values due to the particularly shallow potential energy surface. Thus, we choose to consider model complexes $[Na\text{-}NO]^+$ with geometries covering the range of possible uncertainties (see Table 7.1). Due to a very weak structural perturbation of NO by Na^+, we adopted the experimental distance of free NO molecule, r(N-O) = 1.151 Å, in the $[Na\text{-}NO]^+$ models [210]. To mimic the purely electrostatic effect on the calculated g-values, we substituted a point charge $q = +1\ e$ for the metal cation of the models $[Na\text{-}NO]^+$ and $[Cu\text{-}NO]^+$ models at one of their representative geometries. All models were calculated in the symmetry point group C_s.

7.4 Results and Discussion

In Tables 7.1 and 7.2, we compare g-values calculated for the models $[Na\text{-}NO]^+$ and $[Cu\text{-}NO]^+$, respectively, with experimental data. There, the main axes of **g**-tensor with respect to the positions of atoms in the complexes are oriented in such a way that the g_2-component is perpendicular to the M-N-O plane and the g_1 component is directed almost along the N-O bond, with a deviation defined by the perturbation caused by the presence of the metal cation M^+ (see Figure 7.1).

$[Na\text{-}NO]^+$ species at all geometries considered (Table 7.1) feature g-values in qualitative agreement with experiment [206], namely, $g_1 < g_2 \sim g_3 < g_e$, despite the simplicity of the model. The alteration of the g components due to a variation of the Na-N-O angle by the reasonable value of 15° is comparable in magnitude to that observed for the adsorption complexes with NaA and NaZSM-5 zeolites, where the g_1-component changes even more. Note that, beyond the simplicity of the model, an additional factor has be taken into account when comparing computed and measured g-values: the present DKH KS approach somewhat overestimates SO effects for radicals of main group atoms. For instance, for a free NO molecule, the calculated SO energy splitting $\Delta\varepsilon$ between the highest occupied orbital and the lowest unoccupied orbital (HOMO-LUMO) $2\pi_x$* and $2\pi_y$* levels, 0.019 eV, is almost 30% larger than the experimental value of 0.015 eV [211]. The parameter $\Delta\varepsilon$ may serve as a measure for the perturbation (polarization) experienced by a NO molecule in the presence of a metal cation. For the complex $[Na\text{-}NO]^+$ (structures **1**, **2** and **3**, see Table 7.1), the energy splitting increases with a shortening of the distance between the NO moiety and the cation, from 0.13 eV (structure **1**) to 0.22 eV (structure **3**), or by ∼0.2 eV/Å. A further splitting, by 0.04 eV, is induced when the Na-N-O angle increases from 130° (**3**) to 145° (**2**).

Figure 7.1: Direction of the main axes of **g**-tensors with respect to orientation of the models (g_2 axis is directed perpendicular to the M-N-O plane): (a) [Na-NO]$^+$ (**3**), the calculated angle between the g_1 and N-O directions is 2.2°; (b) [Cu-NO]$^+$ (**2**), the calculated angle between the g_1 and N-O directions is 27.6°.

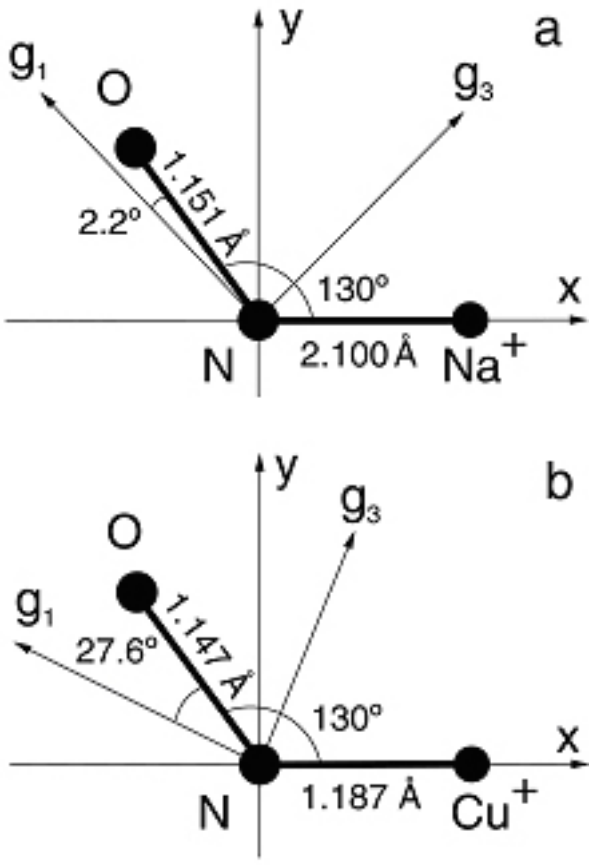

The Na-NO interaction in the $[Na\text{-}NO]^+$ complexes is essentially of electrostatic origin, as follows from the calculated large positive charge of the Na center, based on an analysis of the electrostatic field generated around the representative $[Na\text{-}NO]^+$ complex (**3**), $q(Na) = 0.91\ e$, or on the Mulliken population analysis, $q(Na) = 0.90\ e$. These large charge values imply that one can try to mimic the electronic structure of a $[Na\text{-}NO]^+$ system by an even simpler, purely electrostatic model q^+-NO (structure **4**). Indeed, both calculated g-components and the splitting $\Delta\varepsilon$ for $[Na\text{-}NO]^+$ (**3**) and q^+-NO (structure **4**) models are in qualitative agreement with each other (Table 7.1), corroborating the electrostatic origin of the shifts Δg. This finding for an interacting NO radical is in line with the widely-used scheme to describe **g**-tensor components in related O_2^- species perturbed by electrostatic field [212]; this scheme seems also applicable to $[Na\text{-}NO]^+$. According to the O_2^- approach, the shifts Δg decrease when the splitting $\Delta\varepsilon$ increases, in agreement with the calculated results for our $[Na\text{-}NO]^+$ models (Table 7.1).

Two types of Cu^+-NO complexes were detected by EPR spectroscopy in CuZSM-5 zeolite (Table 7.2) [205]. Based on the results of DF calculations, employing embedded cluster models [213], their structural arrangement was tentatively assigned as follows [205]. One of the adsorption species is formed by Cu^+ ions coordinated to two oxygen atoms of a single AlO_4 tetrahedron located at the channel intersection. In another type of complexes, Cu^+ ions are coordinated to three or four oxygen atoms of the alumosilicate six- (or five-) rings that build the channel walls. Our studies of simplified models $[Cu\text{-}NO]^+$ (structures **1** and **2**; Table 7.2) at geometries consistent with those computed for more realistic embedded cluster models of NO adsorption in Cu-exchanged zeolites [214, 215, 216] furnish g-values that nicely match the experimental pattern [205], $g_1 < g_e < g_2 \sim g_3$ (in the present notation). Quantitatively, the measured g_1 component, 1.891–1.917, is particularly sensitive to the formation of the adsorption bond M-NO; these experimental values falls between the calculated g_1-values, 1.867 (**1**) and 1.950 (**2**). The calculated g_2 and g_3 values ($> g_e$) are rather close to each other, although they are not so close to remain unresolved in the experimental spectrum (Table 7.2). The overestimation of the computed g_2 and g_3 parameters by 0.002–0.014 compared to the measured values may be partly ascribed to the above mentioned overestimation of SO effects at the present computational level. However, the major reason of the difference is probably the neglected influence of the zeolite environment.

Of primary importance for this study is the finding that our $[Cu\text{-}NO]^+$ models correctly reproduce the fashion of **g**-tensor splitting for CuZSM-5/NO complexes, $g_1 < g_e < g_2 \sim g_3$ (Table 7.2). This pattern is qualitatively different from the pattern $g_1 < g_2 \sim g_3 < g_e$ of Na^+-NO complexes (Table 7.1). In particular, the result g_2, $g_3 > g_e$ obtained for Cu^+-NO complexes cannot be explained in the framework of O_2^- radical scheme [211], applicable to the Na^+-NO moieties, as has been already mentioned. Indeed, the electrostatic model q^+-NO (**3**) of the representative $[Cu\text{-}NO]^+$ (**2**) system yields, as expected, the pattern g_2, $g_3 < g_e$(Table 7.1) instead of g_2, $g_3 > g_e$.

Table 7.1: Calculated g-components, shifts Δg and HOMO-LUMO energy splitting $\Delta\varepsilon$/eV for various models[a] of Na^+-NO complexes in zeolites compared with experimental data

	[Na-NO]$^+$ **1**[b]	[Na-NO]$^+$ **2**[c]	[Na-NO]$^+$ **3**[d]	q^+-NO **4**[d]	NaA/ NO[e]	NaZSM-5/ NO[e]
g_1	1.7264	1.8580	1.8337	1.7921	1.8842	1.8460
Δg_1	−0.2759	−0.1443	−0.1686	−0.2102	−0.1181	−0.1563
g_2	1.9824	1.9966	1.9946	1.9903	1.9936	1.9914
Δg_2	−0.0199	−0.0057	−0.0077	−0.0120	−0.0087	−0.0109
g_3	1.9880	2.0018	1.9999	1.9955	1.9993	1.9939
Δg_3	−0.0143	−0.0005	−0.0024	−0.0068	−0.0030	−0.0084
$\Delta\varepsilon$	0.134	0.261	0.221	0.172		

a) r(N-O) is set to the experimental value of a free molecule, 1.151 Å, Ref. [210]
b) Structure **1** – r(Na-N) = 2.5 Å, ∠Na-N-O = 130°
c) Structure **2** – r(Na-N) = 2.1 Å, ∠Na-N-O = 145°
d) Structures **3** and **4** – r(X-N) = 2.1 Å, ∠X-N-O = 130°, where X is Na or q, respectively
e) Experimental data from Ref. [206]

Table 7.2: Calculated g-components, shifts Δg and HOMO-LUMO energy splitting $\Delta\varepsilon$/eV for various models[a] of Cu^+-NO complexes in zeolites compared with experimental data.

	$[Cu\text{-}NO]^+$	$[Cu\text{-}NO]^+$	q^+-NO	$[Cu\text{-}NO]^+$	CuZSM-5/NO	
	1[b]	**2**[c]	**3**[c]	**2**[d]	Exp.[e]	
g_1	1.8668	1.9502	1.8791	1.9498	1.891	1.917
Δg_1	−0.1355	−0.0521	−0.1232	−0.0525	−0.111	−0.085
g_2	2.0123	2.0191	2.0029	2.0100	2.005	2.005
Δg_2	0.0100	0.0168	0.0006	0.0077	0.003	0.003
g_3	2.0074	2.0157	1.9980	2.0016	2.005	2.005
Δg_3	0.0051	0.0134	−0.0043	−0.0007	0.003	0.003
$\Delta\varepsilon$	0.296	0.518	0.293			

a) Optimized structure of $[Cu\text{-}NO]^+$ species: r(N-O) = 1.147 Å, r(Cu-N) = 1.87 Å, ∠Cu-N-O = 132°

b) Structure **1** – ∠Cu-N-O = 145°, the bond lengths as optimized for $[Cu\text{-}NO]^+$ species

c) Structures **2** and **3** – ∠X-N-O = 130°, where X is Cu or q, respectively; the bond lengths as in the structure **1**

d) Contribution of Cu $3d$ orbitals to the diagonal matrix elements , that define Δg values, are set to zero

e) Experimental data for two kinds of adsorption complexes detected in CuZSM-5, Ref. [205]

Clearly, the covalent character of the Cu^+-NO bond contributes significantly to the **g**-tensor anisotropy of $[Cu\text{-}NO]^+$ moieties, at variance with the essentially ionic (electrostatic) Na^+-NO bonding. A number of calculated parameters manifest notable covalence effects and concomitantly reduced electrostatic effects in the interactions of NO molecules with Cu^+ cations, as compared to Na^+ ions. For instance, comparing $[Cu\text{-}NO]^+$ (**2**) with $[Na\text{-}NO]^+$ (**3**), one notices for the Cu congener a considerably enhanced energy of the adsorption bond, by almost 150 kJ/mol; also, the splitting $\Delta\varepsilon$ is more than doubled and the positive charge of the metal atom, 0.63 e in the Mulliken scheme and 0.83 e as derived from the electrostatic potential, is notably reduced. Furthermore, the g_1 axis, calculated for the Cu complex, deviates from the N-O direction by as much as 27.6°, compared to 2.2° only for the Na congener (see Figure 7.1); this clearly implies a much stronger interaction in the Cu system. The question is whether a specific channel of covalent contributions in the Cu^+-NO adsorption is responsible for the characteristic EPR signature g_2, $g_3 > g_e$.

Recall that, in the two-component relativistic method employed here, the ground-state wave function *completely* defines the calculated g-values. Moreover, in the approximation adopted here, the integrals determining the **g**-tensor are calculated *solely* on the two Kramers components of the SOMO. Thus, the structure of the SOMO alone defines pattern and magnitude of the **g** anisotropy. Therefore, one is able to relate details of the spatial distribution of SOMO to the magnitude of g-values if one decomposes the matrix elements, which form the **G**-tensor (Chapter 4), into individual contributions of atoms or even particular angular momentum components l of the radical under study. In general, the results of such an analysis will depend also on the assignment of non-diagonal contributions.

We implemented in our DF code ParaGauss an option to switch off contributions of the basis functions of a specified atom and angular momentum to the matrix elements and to compute g-values on such a "reduced" SOMO. In this analysis, we benefit from the advantage of using orbital basis functions contracted in generalized fashion, i.e. in the form of atomic orbital (AO). To simplify our analysis, we relied on the finding that for radicals built of not particularly heavy atoms, the major contributions to the shifts Δg from g_e come from the orbital Zeeman term (Chapter 4, Eq. (4.8)), whereas the effect of the spin Zeeman term is usually an order of magnitude smaller and often essentially isotropic (Chapter 4, Table 4.2). The same also holds for the model complexes $[Na\text{-}NO]^+$ and $[Cu\text{-}NO]^+$; thus, we neglected the spin Zeeman term in the analyses of these models.

We validated this new analytic scheme by rationalizing the most significantly shifted g-values of the touchstone radical NO_2, calculated at $\Delta g_{xx} = 0.0047$ and $\Delta g_{yy} = -0.0151$ (Δg_{zz} is very small, -0.0007). The positive shift Δg_{xx} is by 88% due to the contribution of O $2p$ AO and by 12% of N $2p$ AO. The negative Δg_{yy} value results from O $2p$ (∼60%) and N 2p (∼40%) channels, which are partly counteracted by a positive off-diagonal effect (O $2p$, N $2p$), that comprises ∼60% of the O $2p$ contribution. These data are in line with the expectation of a stronger SO contribution of $2p$ AOs of the heavier O atom as compared to the N atom. Further justification of our analysis derives from the dominance of *diagonal*

AO contributions to the calculated shifts Δg.

Let us now return to the central issue of the *qualitatively* different **g**-tensor anisotropy calculated for the [Cu-NO]$^+$ and [Na-NO]$^+$ models. Probably, already the first attempt to find an explanation for the difference in the g-values in the structure of SOMO would focus on the examination of a d-orbital contribution in the case of [Cu-NO]$^+$ species, an aspect that is completely absent in the [Na-NO]$^+$ system. However, the Cu d Mulliken population of the SOMO of [Cu-NO]$^+$ (**2**) is 0.05 e only. This value does not seem large enough to rationalize the alteration of the g-patterns from g_2, $g_3 < g_e$ for Na$^+$-NO complexes to g_2, $g_3 > g_e$ for Cu$^+$-NO species. To examine the influence of Cu $3d$ orbitals on the g-values of model [Cu-NO]$^+$ (**2**) in a more reliable fashion, we applied the analysis outlined in the preceding two paragraphs.

When the diagonal Cu $3d$ contributions to the matrix elements are set to zero for the model [Cu-NO]$^+$ (**2**) (Table 7.2), the value g_3 becomes smaller than g_e and the component g_2 is notably reduced although it remains slightly larger than g_e. Actually, the **g**-tensor pattern of the model [Cu-NO]$^+$ without a diagonal Cu $3d$ component (the corresponding off-diagonal terms are significantly smaller) is now similar to that observed and calculated for the Na$^+$-NO systems. Therefore, not unexpectedly, even a rather small admixture of atomic orbitals of the high angular momentum $l = 2$ is able to noticeably affect g-values. Keeping in mind the approximate character of our analysis scheme, the present results strongly support the interpretation of the observed qualitatively different **g**-tensor signatures of Na$^+$-NO and Cu$^+$-NO complexes in zeolites as a manifestation of a significantly stronger covalent effects in the Cu congeners, where a small contribution of Cu $3d$ orbitals to the SOMO affects the g-values in a significant fashion.

7.5 Conclusions

We presented relativistic DF calculations of the electronic g-values of simple isolated M$^+$-NO model complexes to rationalize the experimentally observed differences in the g parameters of Na$^+$-NO ($g_1 < g_2 < g_3 < g_e$) and Cu$^+$-NO ($g_1 < g_e < g_2 \sim g_3$) adsorption complexes formed upon nitric oxide adsorption in ZSM-5 and A zeolites. The **g**-tensor parameters of the Na$^+$-NO species are primarily determined by electrostatic interactions between the alkali metal cation and the adsorbed NO molecule where the bond angle Na-N-O and the bond length Na-N have a noticeable influence on the magnitude of the g-shifts. In turn, the geometry of the Na$^+$-NO complexes significantly affects the HOMO-LUMO energy splitting $\Delta\varepsilon$ between the $2\pi_x^*$ and $2\pi_y^*$ orbitals of the NO molecule. Therefore, this energy splitting, which can be determined by the g-shifts of the NO probe, can only be considered as a reliable measure for the electric field at the alkali metal cation if the geometry of the M$^+$-NO adsorption complex is explicitly known. The calculated orientations of the principal axes of the **g**-tensor are determined by the N-O molecule in accordance with the experimental results.

In the case of the Cu^+-NO species, covalent bonding contributions have a noticeable impact on both the sign of the g-value shift from g_e and the orientation of the g_1 axis in the adsorption complex. Our calculations and the results of the new atomic orbital analysis tool strongly support the model that the positive g-shifts of the parameters g_2 and g_3, in accordance with the experimentally found relation $g_1 < g_e < g_2 \sim g_3$, are caused by an admixture of Cu $3d$ AOs to the SOMO. Furthermore, in such NO adsorption complexes with transition metal ions, the orientation the g_1 axis may deviate by almost 30° from the NO bond direction. The significant misalignment of the principal axes of the **g**-tensor with respect to the NO molecular frame has to be taken into account in any analysis of the Cu hyperfine interaction in powder EPR spectra of Cu^+-NO complexes where the **g**-tensor frame serves as reference for the orientation of the principal axes of the Cu hyperfine coupling tensor.

Part III

Summary

Chapter 8

Summary

This thesis is devoted to the development and realization of the Douglas-Kroll-Hess (DKH) approach [75, 99, 77] for calculation of magnetic properties such as hyperfine coupling constants (HFCCs) and electronic **g**-tensors. The method employs first-order perturbation theory for describing magnetic interactions. It operates by two-component Kohn-Sham (KS) eigenfunctions obtained after the Douglas-Kroll (DK) decoupling of the four-component Dirac-Kohn-Sham equation. Since this scheme takes into account the spin-orbit effect self-consistently, it is applicable to molecular systems with spin-orbit interaction of considerable strength. The splitting of the energy levels due to magnetic interactions is naturally and transparently determined by the two-component ground-state KS function without invoking virtual states, which allows one to avoid the second-order perturbative sum-over-states formalism, that is widely used for calculating magnetic properties. The method was implemented in the parallel density functional code ParaGauss [75, 86], which is based on the linear combination of Gaussian-type orbitals approach, namely, in its relativistic variant. The DKH approach developed and implemented for calculating HFCCs and electronic **g**-tensors was validated for selected test sets of molecules by comparing with experiment and other theoretical results (Part I of the thesis, Chapters 2–5). In Part II of the thesis, two groups of applications, to hydrogen-bonding effects in semiquinone anion radicals (Chapter 6) and to adsorption nitrosyl complexes formed with main-group and transition-metal cations in zeolites (Chapter 7), exemplify the accuracy and interpretation power of the novel scheme for calculating electronic **g**-tensors.

Electronic **g**-tensors and HFCCs describe the response of the system under investigation to an external magnetic field and the field, created by magnetic nuclei, respectively. Thus, one has to include these types of magnetic interactions in the DK Hamiltonian. To this end, in Chapter 2 a vector potential of a magnetic field was introduced into the Dirac-Kohn-Sham Hamiltonian via the common minimal substitution to a gauge-invariant momentum [57]. After a DK transformation accurate to second order, the resulting terms which depend on the vector potential form the magnetic Hamiltonian, which can be employed for calculations of magnetic parameters such as HFCCs, **g**-tensors, and nuclear shielding

by means of the first-order perturbation theory. Three different approximations of the magnetic DK Hamiltonian were derived and tested, as described in Chapters 3 and 4; they demonstrate the so-called "picture change" effect. Finally, the technique of Hess [66, 98] for evaluating the relativistic matrix elements in the DK approach was discussed in Chapter 2.

In Chapter 3, the magnetic DK Hamiltonian derived in Chapter 2 was specified for a field induced by magnetic nuclei. The resulting hyperfine Hamiltonian yields three well-known terms, namely the Fermi-contact term, dipole hyperfine term, and orbital hyperfine term [3, 17]. In the framework of the point nucleus approach, solutions of the relativistic equations exhibit a weak singularity at the origin [79]; therefore, as we illustrated, the Fermi-contact term of HFCCs, calculated using the point nucleus model, exhibits a strong dependence on the basis set and, in general, no basis set saturation (convergence) with respect to this magnetic parameter can be reached. Thus, reliable calculations of HFCCs (in particular, for heavier nuclei) require introduction of a more accurate finite nucleus model [17, 94]. The latter was implemented by adopting the simplified scheme based on the classical finite macroscopic distribution of the magnetic moment [104, 94]. Small radiative corrections arising from quantum electrodynamics along with the dependence of the calculated results on the choice of gauge origin were discussed. Next, the concepts widely used in the experimental determination of HFCCs, namely, those of the effective spin and the effective spin Hamiltonian, were introduced to connect the quantities obtained using the hyperfine Hamiltonian and the hyperfine coupling tensor. The derived formalism was examined for calculations of HFCCs of Cu, Ag, and Au atoms with different basis sets and different DK approximations on the hyperfine Hamiltonian. The implemented simplified finite nucleus model was found to provide isotropic HFCCs featuring very rapid convergence with respect to extension of the basis set. The picture change effect was demonstrated to play a crucial role for the precision of the isotropic part of HFCCs. Application of the present new method to a series of radicals and molecules containing heavy elements resulted in a very satisfactory accuracy of the computed HFCC values.

In Chapter 4, the Zeeman Hamiltonian was derived from the DK magnetic Hamiltonian by employing the vector potential of a homogeneous magnetic field. The resulting Zeeman Hamiltonian contains the standard two terms: spin Zeeman and orbital Zeeman contributions [3, 61]. The link between the Zeeman Hamiltonian and the effective spin Hamiltonian was traced and expressions for **g**-tensors were derived. The influence of different approximations for accounting of the Coulomb (Hartree) "screening" by the electron density repulsion on the quality of calculated **g**-tensors was analyzed. Sufficiently accurate g-values were obtained employing the first-order DKH transformation (DKee1) of the Hartree term [71, 87]. The computationally less intensive screened nuclear potential approximation for the spin-orbit interaction [165, 166], improved over Boettger's original suggestion, can also be utilized for calculations of **g**-tensors; its results are very close to those of the DKee1 model. Our calculations of **g**-tensors for small inorganic main-group and transition metal

molecules as well as organic radicals demonstrated that the present method exhibits an accuracy sufficient for successfully assigning and interpreting EPR spectra.

Common details of the implementation of HFCCs and **g**-tensors within the parallel program ParaGauss were provided in Chapter 5. The implementation had to deal mainly with augmenting the integral part by new types of integrals for the primitive basis functions employed in the ParaGauss code. These primitive basis functions consist of a Gaussian radial part and an angular part based on real spherical harmonics. All required primitive integrals, namely the second derivatives of the nuclear attraction integral, the orbital momentum integral, and the matrix element of a Gaussian function were written explicitly.

Chapter 6, the first one in Part II describing applications of our newly implemented method, is devoted to the study of hydrogen-bonding effects on electronic **g**-tensors of semiquinone anion radicals, 1,4-benzoquinone and tetramethyl-1,4-benzoquinone (duroquinone) with water and methanol molecules. This study demonstrated that the novel computational scheme is able to quantitatively represent very delicate effects on g-values. Furthermore, general trends of how **g**-tensors depend on the structure and stoichiometry of hydrogen-bonded semiquinone complexes were explored.

Finally, in Chapter 7 the present DKH scheme for calculations of **g**-tensors was applied to interpret the electronic g-values of surface complexes formed by probe NO molecules with Na^+ and Cu^+ cations in zeolites. A new tool for the analysis of g-values in terms of contributions of particular atomic orbitals was presented. This tool allowed us to explain, based on such simple models as molecular Na^+–NO and Cu^+–NO, that the difference in the observable **g**-tensors of Na^+–NO ($g_1 < g_2 < g_3 < g_e$) and Cu^+–NO ($g_1 < g_e < g_2 \sim g_3$) adsorption complexes in zeolites is due to a substantial effect of the (rather small) admixture of Cu $3d$ atomic orbitals to the ground state of the unpaired electron due to the covalent bonding contributions.

In summary, in this work, we developed a new two-component DKH method for calculating the magnetic properties of molecular systems, HFCCs and **g**-tensors; we implemented corresponding modules in the parallel density functional program ParaGauss and carried out some applications. The first such results showed reasonably good agreement with experiment and, where available, with reliable data of other theoretical calculations. These method development contributions added more flexibility and notably extended the scope of application opportunities of the code ParaGauss in the rather timely field of predicting magnetic parameters by quantum chemistry calculations.

Beyond the currently accomplished implementation, this work suggests further directions for development. One of the most important future improvements of ParaGauss for EPR calculations should aim at including spin-polarization effects, e.g. using the already implemented non-collinear spin density functional approach [70, 152]. The latter formalism does not provide a straightforward account for magnetic resonance parameters; it has not been yet justified in the literature for this purpose. The implementation for the isotropic part of HFCCs can be done at low cost. Moreover, an option to compute

HFCCs on the one-component SR level should be implemented to enable the evaluation of the spin-polarization effects on these parameters in an economic albeit sufficiently reliable fashion. The implementation of the finite nuclear model into the DK Hamiltonian, that will affect also the KS eigenfunction in a self-consistent fashion (not only the magnetic operator like it is presently realized), is expected to significantly improve the quality of the isotropic HFCCs for systems containing heavy atoms. Further improvements due to a relativistic treatment of the exchange-correlation interactions for calculations of EPR parameters are also anticipated. The basis sets employed so far for calculating EPR parameters can be definitely reduced, thus rendering treatment of even more complex models. For instance, polarization functions in the orbital basis sets needed for accurate numerical transformations of the Hartree term for **g**-tensor calculations can be removed when it will be possible to perform this transformation in an analytical fashion. Finally, one has to note that the presented DKH method can be relatively easily extended for calculations of nuclear shielding parameters [94], as measured by NMR spectroscopy.

Appendix A

Basis Sets

The exponents in parentheses have been employed only in HFCCs calculations.

Table A.1: Orbital basis of H derived from a (8s) basis set of Ref. [196]

	s	p	d
1	0.07279100	0.07279100	1.00000000
2	0.18112000	0.18112000	
3	0.46554400	0.46554400	
4	1.28270900	1.28270900	
5	3.90450500	3.90450500	
6	13.73217300		
7	60.24195900		
8	402.00995000		
9	(2682.71488148)		
10	(17902.44031350)		
11	(119467.54811365)		
12	(797237.40464174)		
13	(5320168.44235590)		
14	(35502840.29605807)		
15	(236919504.09924337)		
16	(1581024249.17433143)		
17	(10550577868.12766266)		
18	(70406695792.02081299)		

Table A.2: Fitting basis of H

	s	r^2	p	d
1	0.14558200	0.14558200	0.10000000	0.20000000
2	0.36224000	0.36224000	0.25000000	0.50000000
3	0.93108800	0.93108800	0.62500000	1.25000000
4	2.56541800	2.56541800	1.56250000	3.12500000
5	7.80901000	7.80901000	3.90625000	7.81250000
6	27.46434600			
7	120.48391800			
8	804.01990000			

Table A.3: Orbital basis of C derived from a (13s,8p) basis set of Ref. [196]

	s	p	d
1	0.09908700	0.06542900	0.15474000
2	0.24606800	0.15474000	0.36194400
3	0.61301300	0.36194400	0.86515000
4	1.54711800	0.86515000	2.17931700
5	3.57701500	2.17931700	6.08036500
6	8.38397600	6.08036500	19.55761100
7	20.65931100	19.55761100	83.33315500
8	53.91874600	83.33315500	
9	151.71075000		
10	472.82279000		
11	1694.32760000		
12	7524.78560000		
13	50557.50100000		
14	(339685.54630500)		
15	(2282277.96244000)		
16	(15334160.53317252)		
17	(103027099.73403923)		

Table A.4: Fitting basis of C

	s	r^2	p	d
1	0.19817400	0.13085800	0.10000000	0.20000000
2	0.49213600	0.30948000	0.25000000	0.50000000
3	1.22602600	0.72388800	0.62500000	1.25000000
4	3.09423600	1.73030000	1.56250000	3.12500000
5	7.15403000	4.35863400	3.90625000	7.81250000
6	16.76795200	12.16073000		
7	41.31862200	39.11522200		
8	107.83749200	166.66631000		
9	303.42150000			
10	945.64558000			
11	3388.65520000			
12	15049.57120000			
13	101115.00200000			

Table A.5: Orbital basis of N derived from a (13s,8p) basis set of Ref. [196]

	s	p	d
1	0.14109300	0.09426400	0.23244900
2	0.35833600	0.23244900	0.55769600
3	0.90185600	0.55769600	1.35000000
4	2.33347100	1.35000000	3.40510400
5	5.26508600	3.40510400	9.39403800
6	12.26362200	9.39403800	29.83738900
7	30.23728300	29.83738900	126.66657000
8	79.61581000	126.66657000	
9	225.47879000		
10	703.77729000		
11	2512.68570000		
12	11123.65400000		
13	74761.71500000		
14	(502471.04321400)		
15	(3377091.46010000)		
16	(22697321.33603393)		
17	(152547954.92447996)		

Table A.6: Fitting basis of N

	s	r^2	p	d
1	0.28218600	0.18852800	0.10000000	0.20000000
2	0.71667200	0.46489800	0.25000000	0.50000000
3	1.80371200	1.11539200	0.62500000	1.25000000
4	4.66694200	2.70000000	1.56250000	3.12500000
5	10.53017200	6.81020800	3.90625000	7.81250000
6	24.52724400	18.78807600		
7	60.47456600	59.67477800		
8	159.23162000	253.33314000		
9	450.95758000			
10	1407.55458000			
11	5025.37140000			
12	22247.30800000			
13	149523.43000000			

Table A.7: Orbital basis of O derived from a (13s,8p) basis set of Ref. [196]

	s	p	d
1	0.19166500	0.12889200	0.33759700
2	0.49515500	0.33759700	0.85022300
3	1.25387700	0.85022300	2.10252500
4	3.22286200	2.10252500	5.31306400
5	7.43830900	5.31306400	14.62180900
6	17.39559600	14.62180900	46.53336700
7	42.69945100	46.53336700	200.00000000
8	111.65428000	200.00000000	
9	315.97875000		
10	987.36516000		
11	3534.54470000		
12	15679.24000000		
13	105374.95000000		
14	(708189.94335800)		
15	(4759508.74352000)		
16	(31987073.08978540)		
17	(214974464.80044979)		

Table A.8: Fitting basis of O

	s	r^2	p	d
1	0.38333000	0.25778400	0.10000000	0.20000000
2	0.99031000	0.67519400	0.25000000	0.50000000
3	2.50775400	1.70044600	0.62500000	1.25000000
4	6.44572400	4.20505000	1.56250000	3.12500000
5	14.87661800	10.62612800	3.90625000	7.81250000
6	34.79119200	29.24361800		
7	85.39890200	93.06673400		
8	223.30856000	400.00000000		
9	631.95750000			
10	1974.73032000			
11	7069.08940000			
12	31358.48000000			
13	210749.90000000			

Table A.9: Orbital basis of F derived from a (13s,8p) basis set of Ref. [196]

	s	p	d
1	0.24086100	0.15481000	0.40397300
2	0.62390000	0.40397300	0.99506000
3	1.56815700	0.99506000	2.44703000
4	3.91940100	2.44703000	6.27499500
5	8.53274300	6.27499500	17.60456800
6	18.94287400	17.60456800	56.91900500
7	44.64472700	56.91900500	245.33029000
8	113.44230000	245.33029000	
9	314.03534000		
10	967.09483000		
11	3441.53920000		
12	15281.00700000		
13	103109.46000000		
14	(695736.91979145)		
15	(4694524.26150710)		
16	(31676568.27595825)		
17	(213739438.08724040)		
18	(1442218961.21628594)		
19	(9731454104.61314583)		

Table A.10: Fitting basis of F

	s	r^2	p	d
1	0.48172200	0.30962000	0.10000000	0.20000000
2	1.24780000	0.80794600	0.25000000	0.50000000
3	3.13631400	1.99012000	0.62500000	1.25000000
4	7.83880200	4.89406000	1.56250000	3.12500000
5	17.06548600	12.54999000	3.90625000	7.81250000
6	37.88574800	35.20913600		
7	89.28945400	113.83801000		
8	226.88460000	490.66058000		
9	628.07068000			
10	1934.18966000			
11	6883.07840000			
12	30562.01400000			
13	206218.92000000			

Table A.11: Orbital basis of Na derived from a (12s,6p) basis set of Ref. [208]

	s	p	d
1	0.02461700	0.04788233	0.14364700
2	0.05806500	0.14364700	0.43094100
3	0.18982000	0.43094100	1.28490000
4	0.62053500	1.28490000	3.67106000
5	1.82902000	3.67106000	10.60450000
6	5.27901000	10.60450000	34.51490000
7	14.57900000	34.51490000	148.92800000
8	38.78340000	148.92800000	
9	109.56300000		
10	339.52900000		
11	1216.20000000		
12	5385.07000000		
13	36631.10000000		

Table A.12: Fitting basis of Na

	s	r^2	p	d
1	0.04923400	0.09576467	0.10000000	0.20000000
2	0.11613000	0.28729400	0.25000000	0.50000000
3	1.24107000	0.86188200	0.62500000	1.25000000
4	3.65804000	2.56980000	1.56250000	3.12500000
5	10.55802000	7.34212000	3.90625000	7.81250000
6	29.15800000	21.20900000		
7	77.56680000	69.02980000		
8	219.12600000	297.85600000		
9	679.05800000			
10	2432.40000000			
11	10770.14000000			
12	73262.20000000			

Table A.13: Orbital basis of Ti derived from a (14s,9p,5d) basis set of Ref. [145]

	s	p	d	f
1	0.03330200	0.06110000	0.07200000	0.26204900
2	0.08557600	0.15600000	0.26204900	0.80019800
3	0.20500000	0.39816200	0.80019800	2.34871000
4	0.51280600	1.01618000	2.34871000	7.08634000
5	1.28569000	2.47878000	7.08634000	25.99240000
6	5.00882000	6.27465000	25.99240000	
7	12.22050000	14.78140000		
8	39.81010000	36.37270000		
9	95.92500000	96.97770000		
10	243.65000000	301.23000000		
11	670.79000000	1264.70000000		
12	2048.75000000			
13	7199.32000000			
14	31226.80000000			
15	206082.00000000			
16	(1360042.99909052)			
17	(8975635.71478901)			
18	(59234918.70365036)			
19	(390922237.19003147)			
20	(2579900485.62760401)			
21	(17026113847.05150604)			

Table A.14: Fitting basis of Ti

	s	r^2	p	d
1	0.06660400	0.31200000	0.10000000	0.20000000
2	0.17115200	2.03236000	0.25000000	0.50000000
3	0.41000000	12.54930000	0.62500000	1.25000000
4	1.02561200	72.74540000	1.56250000	3.12500000
5	2.57138000	602.46000000	3.90625000	7.81250000
6	10.01764000			
7	24.44100000			
8	79.62020000			
9	191.85000000			
10	487.30000000			
11	1341.58000000			
12	4097.50000000			
13	14398.64000000			
14	62453.60000000			
15	412164.00000000			

Table A.15: Orbital basis of Cu derived from a (14s,9p,5d) basis set of Ref. [131]

	s	p	d	f
1	0.04079100	0.09910000	0.14910000	0.14910000
2	0.11330300	0.26500000	0.41487500	0.41487500
3	0.33050000	0.71144500	1.47329000	1.47329000
4	0.96408000	1.90667000	4.51628000	4.51628000
5	2.57848000	4.69382000	13.54900000	13.54900000
6	9.39357000	11.74350000	48.54390000	48.54390000
7	22.29830000	27.05510000		
8	67.35910000	65.32390000		
9	158.39900000	172.19500000		
10	395.09900000	532.10600000		
11	1071.97000000	2245.29000000		
12	3239.82000000			
13	11373.40000000			
14	50072.90000000			
15	337200.00000000			
16	(875044.17202917)			
17	(2270766.02313826)			
18	(5892706.33033512)			
19	(15291750.68754202)			
20	(39682554.32757045)			
21	(102977425.55033098)			
22	(267229525.73661119)			
23	(693468680.57515359)			

Table A.16: Fitting basis of Cu

	s	r^2	p	d
1	0.08158200	0.53000000	0.10000000	0.20000000
2	0.22660600	3.81334000	0.25000000	0.50000000
3	0.66100000	23.48700000	0.62500000	1.25000000
4	1.92816000	130.64780000	1.56250000	3.12500000
5	5.15696000	1064.21200000	3.90625000	7.81250000
6	18.78714000			
7	44.59660000			
8	134.71820000			
9	316.79800000			
10	790.19800000			
11	2143.94000000			
12	6479.64000000			
13	22746.80000000			
14	100145.80000000			
15	674400.00000000			

Table A.17: Orbital basis of Rh derived from a (17s,11p,8d) basis set of Ref. [132]

	s	p	d	f	g
1	0.01302676	0.03666106	0.04588040	0.11470100	0.11470100
2	0.03256689	0.09165264	0.11470100	0.28675251	0.28675251
3	0.08666224	0.22913160	0.28675251	0.98418167	0.98418167
4	0.22528131	0.57282901	0.98418167	2.80165710	2.80165710
5	0.58562612	1.61212010	2.80165710	7.32756180	7.32756180
6	1.37915560	4.98026990	7.32756180	18.14429700	18.14429700
7	4.27669890	11.45249600	18.14429700	45.58960000	45.58960000
8	8.76811950	28.33969100	45.58960000	125.21726000	125.21726000
9	24.10646100	63.38924500	125.21726000	427.76314000	427.76314000
10	52.77752400	145.05149000	427.76314000		
11	119.97225000	295.61964000			
12	287.03175000	449.35425000			
13	707.98545000	3421.38900000			
14	1877.65690000	1094.68120000			
15	5454.03610000	14624.40800000			
16	17663.47800000				
17	65520.72100000				
18	297407.01000000				
19	2019224.50000000				
20	(13709386.27640367)				
21	(93078938.01587954)				
22	(631953066.86162293)				
23	(4290602011.89315271)				

Table A.18: Fitting basis of Rh

	s	r^2	p	d
1	0.06513378	0.07332211	0.10000000	0.20000000
2	0.17332447	0.45826321	0.25000000	0.50000000
3	0.45056263	3.22424030	0.62500000	1.25000000
4	1.17125225	22.90499306	1.56250000	3.12500000
5	2.75831127	126.77850342	3.90625000	7.81250000
6	8.55339813	591.23931885		
7	17.53623772	6842.77929688		
8	48.21292496	29248.83398438		
9	105.55505371			
10	239.94453430			
11	574.06353760			
12	1415.97106934			
13	3755.31445312			
14	10908.07421875			
15	35326.97656250			
16	131041.52343750			
17	594814.12500000			
18	4038448.00000000			

Table A.19: Orbital basis of Pd derived from a (17s,11p,8d) basis set of Ref. [132]

	s	p	d	f	g
1	0.01350000	0.09040000	0.09700000	0.26602317	0.26602317
2	0.04006742	0.21430000	0.26602317	0.77945515	0.90000000
3	0.11247078	0.50827979	0.77945515	1.99012450	1.99012450
4	0.48448268	1.31341920	1.99012450	4.78979460	4.78979460
5	1.11647520	3.03040990	4.78979460	11.16811900	11.16811900
6	2.24996060	6.80629510	11.16811900	27.05091300	27.05091300
7	5.41188880	14.68536800	27.05091300	71.70931700	71.70931700
8	10.57934800	32.27830200	71.70931700	242.47077000	242.47077000
9	28.71975700	71.08694300	242.47077000		
10	64.11928400	167.49952000			
11	165.14908000	439.60614000			
12	374.64803000	1369.83110000			
13	905.94369000	5841.59920000			
14	2398.15000000				
15	7155.55590000				
16	25013.15100000				
17	109352.60000000				
18	722049.07000000				
19	(4767649.41563223)				
20	(31480521.05430775)				
21	(207864110.68761352)				
22	(1372515036.75603843)				

Table A.20: Fitting basis of Pd

	s	r^2	p	d
1	0.02700000	0.18080000	0.10000000	0.20000000
2	0.08013483	0.42860000	0.25000000	0.50000000
3	0.22494156	1.01655958	0.62500000	1.25000000
4	0.96896536	2.62683840	1.56250000	3.12500000
5	2.23295040	6.06081980	3.90625000	7.81250000
6	4.49992120	13.61259020		
7	10.82377760	29.37073600		
8	21.15869600	64.55660400		
9	57.43951400	142.17388600		
10	128.23856800	334.99904000		
11	330.29816000	879.21228000		
12	749.29606000	2739.66220000		
13	1811.88738000	11683.19840000		
14	4796.30000000			
15	14311.11180000			
16	50026.30200000			
17	218705.20000000			
18	1444098.14000000			

Table A.21: Orbital basis of Ag derived from a (17s,11p,8d) basis set of Ref. [132]

	s	p	d	f
1	0.04187616	0.08450000	0.11079500	0.11079500
2	0.11787222	0.21870000	0.28806987	0.28806987
3	0.23790000	0.56583919	0.83680243	0.83680243
4	0.48011424	1.46406860	2.13327020	2.13327020
5	1.09452650	3.39422830	5.10188890	5.10188890
6	2.13744300	7.41932520	11.89264200	11.89264200
7	5.64123010	15.80857100	28.98667800	28.98667800
8	11.10299600	34.25554400	77.12569900	77.12569900
9	30.19493500	74.96490400	260.66912000	260.66912000
10	67.29248000	175.50623000		
11	173.46788000	458.34731000		
12	393.96647000	1426.66420000		
13	954.42758000	6116.67420000		
14	2531.37430000			
15	7559.23930000			
16	26465.70500000			
17	116697.35000000			
18	782615.55000000			
19	(2026712.80822201)			
20	(5248509.06298903)			
21	(13591884.98366683)			
22	(35198441.15578582)			
23	(91152203.04513477)			
24	(236053752.58545253)			
25	(611300355.31980658)			
26	(1583063689.18598294)			

Table A.22: Fitting basis of Ag

	s	r^2	p	d
1	0.08375233	0.16900000	0.10000000	0.20000000
2	0.23574444	0.43740000	0.25000000	0.50000000
3	0.47580000	1.13167840	0.62500000	1.25000000
4	0.96022848	2.92813720	1.56250000	3.12500000
5	2.18905300	6.78845660	3.90625000	7.81250000
6	4.27488600	14.83865000		
7	11.28246000	31.61714200		
8	22.20599200	68.51108800		
9	60.38987000	149.92981000		
10	134.58496000	351.01246000		
11	346.93576000	916.69462000		
12	787.93294000	2853.32840000		
13	1908.85520000	12233.34800000		
14	5062.74860000			
15	15118.47900000			
16	52931.41000000			
17	233394.70000000			
18	1565231.10000000			

Table A.23: Orbital basis of Au derived from a (19s,15p,10d,6f) basis set of Ref. [70]

	s	p	d	f	g
1	0.05600000	0.10000000	0.14000000	0.42000000	0.42000000
2	0.14000000	0.21000000	0.35000000	1.10000000	1.10000000
3	0.34000000	0.45500000	0.88000000	3.33817196	3.33817196
4	0.84000000	1.00000000	2.20000000	9.91205025	9.91205025
5	2.10000000	2.25000000	5.54659700	27.75035858	27.75035858
6	5.15347004	4.95650673	14.00382996	86.82437134	86.82437134
7	13.35270023	10.79928970	36.86191177		
8	26.24551010	26.13319016	90.53779602		
9	58.48051071	55.26807022	243.20320130		
10	113.61409760	127.80000310	816.72155760		
11	233.43910220	285.45651250			
12	621.27697750	677.79077150			
13	1429.49792500	1773.84399400			
14	3491.37988300	5459.12402300			
15	9358.39257800	23072.80078000			
16	28274.94141000				
17	99928.78906000				
18	446529.50000000				
19	3095417.00000000				
20	(8149926.03264395)				
21	(21457947.13202375)				
22	(56496647.12004165)				
23	(148750069.90034828)				
24	(391644184.62470669)				
25	(1031160304.34881985)				
26	(2714942835.88980293)				
27	(7148175284.73821068)				

Table A.24: Fitting basis of Au

	s	r^2	p	d
1	0.11200000	0.42000000	0.10000000	0.20000000
2	0.28000000	2.00000000	0.25000000	0.50000000
3	0.68000000	9.91301346	0.62500000	1.25000000
4	1.68000000	52.26638032	1.56250000	3.12500000
5	4.20000000	255.60000620	3.90625000	7.81250000
6	10.30694008	1355.58154300		
7	26.70540046	10918.24804600		
8	52.49102020			
9	116.96102142			
10	227.22819520			
11	466.87820440			
12	1242.55395500			
13	2858.99585000			
14	6982.75976600			
15	18716.78515600			
16	56549.88282000			
17	199857.57812000			
18	893059.00000000			
19	6190834.00000000			

Table A.25: Orbital basis of Hg, Ref. [217]

	s	p	d	f	g
1	0.03540000	0.03565117	0.09470000	0.32107000	6.99053855
2	0.11502142	0.12098559	0.31770870	0.89655000	17.96913593
3	0.36966000	0.43329749	0.58190000	2.50347372	46.50682347
4	1.19101465	1.13615849	1.06592791	6.99053855	141.67003300
5	3.97128138	2.57814855	2.98372742	17.96913593	
6	7.88463714	6.54562308	7.24521429	46.50682347	
7	24.96225844	14.22083751	16.74128691	141.67003300	
8	47.20885021	31.84123149	38.41383919		
9	129.37122750	67.49641762	87.15954757		
10	295.86069360	152.73995610	209.48926320		
11	815.30690120	342.12164350	569.59392440		
12	2018.85221100	808.31023300	2026.60092700		
13	5227.86558100	2067.83929400			
14	14283.90305000	5936.04412400			
15	41558.04818000	20136.27904000			
16	130511.79550000	87530.35277000			
17	450884.57570000	580663.66810000			
18	1762480.83200000				
19	8154966.32100000				
20	48353729.07000000				
21	457744654.80000001				

Table A.26: Fitting basis of Hg

	s	r^2	p	d
1	0.07080000	0.07130234	0.10000000	0.20000000
2	0.23004284	0.24197118	0.25000000	0.50000000
3	0.73932000	0.86659498	0.62500000	1.25000000
4	2.38202930	2.27231698	1.56250000	3.12500000
5	7.94256276	5.15629710	3.90625000	7.81250000
6	15.76927428	13.09124616		
7	49.92451688	28.44167502		
8	94.41770042	63.68246298		
9	258.74245500	134.99283524		
10	591.72138720	305.47991220		
11	1630.61380240	684.24328700		
12	4037.70442200	1616.62046600		
13	10455.73116200	4135.67858800		
14	28567.80610000	11872.08824800		
15	83116.09636000	40272.55808000		
16	261023.59100000	175060.70554000		
17	901769.15140000	1161327.33620000		
18	3524961.66400000			
19	16309932.64200000			
20	96707458.14000000			
21	915489309.60000002			

Appendix B

Nuclear Parameters

Table B.1: Nuclear parameters used in HFCCs calculations (taken from Ref. [128])

Isotope	Spin	Magnetic moment[a]
^{1}H	$\frac{1}{2}$	2.7928
^{13}C	$\frac{1}{2}$	0.7024
^{14}N	1	0.4036
^{17}O	$\frac{5}{2}$	−1.8937
^{19}F	$\frac{1}{2}$	2.6288
^{47}Ti	$\frac{5}{2}$	−0.7883
^{63}Cu	$\frac{3}{2}$	2.2260
^{103}Rh	$\frac{1}{2}$	−0.0883
^{105}Pd	$\frac{5}{2}$	−0.6420
^{107}Ag	$\frac{1}{2}$	−0.1135
^{197}Au	$\frac{3}{2}$	0.1449
^{199}Hg	$\frac{1}{2}$	0.5027

a) In nuclear magnetons.

Bibliography

[1] N. M. Atherton, *Electron Spin Resonance. Theory and Applications* (Wiley, Chichester, 1973).

[2] A. Abragam and B. Bleaney, *Electron Paramagnetic Resonance of Transition Ions* (Clarendon, Oxford, 1970).

[3] J. E. Harriman, *Theoretical Foundations of Electron Spin Resonance* (Academic Press, New York, 1978).

[4] B. H. Bielski and J. M. Gebicki, *Atlas of Electron Spin Resonance Spectra* (Academic Press, New York, 1967).

[5] C. P. Poole, Jr and H. A. Farach, *Handbook of Electron Spin Resonance* (American Inst. of Physics, New York, 1994).

[6] F. Gerson and W. Huber, *Electron Spin Resonance Spectroscopy of Organic Radicals* (Wiley-VCH, Weinheim, 2003).

[7] F. E. Mabbs and D. Collison, *Electron Paramagnetic Resonance of d-Transition Metal Compounds* (Elsevier, Amsterdam, 1992).

[8] J. R. Pilbrow, *Transition Ion Electron Paramagnetic Resonance* (Clarendon Press, Oxford, 1990).

[9] K. Möbius, Biol. Magn. Reson. **13**, 253 (1993).

[10] Y. S. Lebedev, Appl. Magn. Reson. **7**, 339 (1994).

[11] D. Stehlik and K. Möbius, Ann. Rev. Phys. Chem. **48**, 745 (1997).

[12] J. H. Freed, Ann. Rev. Phys. Chem. **51**, 655 (2000).

[13] B. Engels, L. A. Eriksson, and S. Lunell, Adv. Quantum Chem. **27**, 297 (1996).

[14] F. Neese and E. I. Solomon, in *Magnetoscience–From Molecules to Materials, Vol. 4*, edited by M. Drillon and J. S. Miller (Wiley, New York, 2002).

[15] M. Kaupp, in *EPR Spectroscopy of Free Radicals in Solids. Trends in Methods and Applications*, edited by A. Lund and M. Shiotani (Kluwer, Dordrecht, 2003).

[16] *Calculation of NMR and EPR Parameters: Theory and Applications*, edited by M. Kaupp, M. Bühl, and V. G. Malkin (Wiley-VCH, Weinheim, 2004).

[17] E. van Lenthe, A. van der Avoird, and P. E. S. Wormer, J. Chem. Phys. **108**, 4783 (1998).

[18] F. Neese, J. Chem. Phys. **118**, 3939 (2003).

[19] A. Arbuznikov, J. Vaara, and M. Kaupp, J. Chem. Phys. **120**, 2127 (2004).

[20] M. Munzarová and M. Kaupp, J. Phys. Chem. A **103**, 9966 (1999).

[21] D. W. Hyden and D. C. McCain, J. Chem. Phys. **57**, 171 (1972).

[22] W. H. Moores and R. McWeeny, Proc. Roy. Soc. **332**, 365 (1973).

[23] G. H. Lushington, P. Bündgen, and F. Grein, Int. J. Quantum Chem. **55**, 377 (1995).

[24] P. J. M. Geurts, P. C. P. Bouten, and A. van der Avoird, J. Chem. Phys. **73**, 1306 (1980).

[25] M. Ishii, K. Morihashi, and O. Kikuchi, J. Mol. Struct.: THEOCHEM **235**, 39 (1991).

[26] G. H. Lushington and F. Grein, Theor. Chim. Acta **93**, 259 (1996).

[27] H. Tachikawa, Chem. Phys. Lett. **260**, 582 (1986).

[28] G. H. Lushington and F. Grein, J. Chem. Phys. **106**, 3292 (1997).

[29] P. J. Bruna and F. Grein, Int. J. Quantum Chem. **77**, 324 (2000).

[30] G. H. Lushington, J. Phys. Chem. A **104**, 2969 (2000).

[31] O. Vahtras, B. Minaev, and H. Ågren, Chem. Phys. Lett. **281**, 186 (1997).

[32] M. Engström, B. Minaev, O. Vahtras, and H. Ågren, Chemical Physics **237**, 149 (1998).

[33] C. W. Bauschlicher Jr., S. R. Langhoff, and H. Partridge, J. Chem. Phys. **89**, 2985 (1988).

[34] C. W. Bauschlicher, Jr., J. Chem. Phys. **92**, 518 (1989).

[35] K. Funken, B. Engels, S. D. Peyerimhoff, and F. Grein, Chem. Phys. Lett. **92**, 518 (1990).

[36] D. M. Chipman, I. Carmichael, and D. Feller, J. Phys. Chem. **95**, 4702 (1991).

[37] I. Carmichael, J. Chem. Phys. **91**, 1072 (1989).

[38] D. Feller and E. R. Davidson, J. Chem. Phys. **88**, 7580 (1988).

[39] B. Engels, J. Chem. Phys. **100**, 1380 (1994).

[40] T. Momose, H. Nakatsuji, and T. Shida, J. Phys. Chem. **89**, 4185 (1988).

[41] H. Nakatsuji and M. Izawa, J. Phys. Chem. **91**, 6205 (1989).

[42] I. Carmichael, J. Chem. Phys. **94**, 5734 (1990).

[43] P. Kristiansen and L. Veseth, J. Chem. Phys. **84**, 2711 (1986).

[44] P. Kristiansen and L. Veseth, J. Chem. Phys. **84**, 6336 (1986).

[45] D. Feller, E. D. Glendening, E. A. McCullough, Jr., and R. J. Miller, J. Chem. Phys. **89**, 2829 (1993).

[46] W. Koch and M. C. Holthausen, *A Chemist's Guide to Density Functional Theory* (Wiley-VCH, Weinheim, 2000).

[47] G. Schreckenbach and T. Ziegler, J. Phys. Chem. A **101**, 3388 (1997).

[48] O. L. Malkina, J. Vaara, B. Schimmelpfennig, M. Munzarová, V. G. Malkin, and M. Kaupp, J. Am. Chem. Soc. **122**, 9206 (2000).

[49] F. Neese, J. Chem. Phys. **115**, 11080 (2001).

[50] C. J. Pickard and F. Mauri, Phys. Rev. Lett. **88**, 084603 (2002).

[51] V. Barone, A. Grand, C. Minichino, and R. Subra, J. Chem. Phys. **93**, 6787 (1993).

[52] L. A. Eriksson, V. G. Malkin, O. L. Malkina, and D. R. Salahub, J. Chem. Phys. **99**, 9756 (1993).

[53] L. A. Eriksson, O. L. Malkina, V. G. Malkin, and D. R. Salahub, J. Chem. Phys. **7**, 5066 (1994).

[54] N. Ishii and T. Shimizu, Chem. Phys. Lett. **235**, 614 (1995).

[55] P. Belanzoni, E. J. Baerends, S. van Asselt, and P. B. Langewen, J. Phys. Chem. **99**, 13094 (1995).

[56] P. Belanzoni, E. J. Baerends, and M. Gribnau, J. Phys. Chem. A **103**, 3732 (1999).

[57] R. Moss, *Advanced Molecular Quantum Mechanics* (Chapman and Hall, London, 1973).

[58] D. Jayatilaka, J. Chem. Phys. **108**, 7587 (1998).

[59] R. A. Pérez and D. A. Case, J. Chem. Phys. **79**, 4939 (1983).

[60] H. M. Quiney and P. Belanzoni, Chem. Phys. Lett. **353**, 253 (2002).

[61] E. van Lenthe, P. E. S. Wormer, and A. van der Avoird, J. Chem. Phys. **107**, 2488 (1997).

[62] P. Belanzoni, E. van Lenthe, and E. J. Baerends, J. Chem. Phys. **114**, 4421 (2001).

[63] M. Stein, E. van Lenthe, E. J. Baerends, and W. Lubitz, J. Phys. Chem. A **105**, 416 (2001).

[64] M. Stein, E. van Lenthe, E. J. Baerends, and W. Lubitz, J. Am. Chem. Soc. **123**, 5839 (2001).

[65] M. Douglas and N. M. Kroll, Ann. Phys. (NY) **82**, 89 (1974).

[66] B. A. Hess, R. J. Buenker, and P. Chandra, Int. J. Quantum Chem. **29**, 737 (1986).

[67] O. D. Häberlen and N. Rösch, Chem. Phys. Lett. **199**, 491 (1992).

[68] P. Knappe and N. Rösch, J. Chem. Phys. **92**, 1153 (1990).

[69] T. Belling, T. Grauschopf, S. Krüger, F. Nörtemann, M. Staufer, M. Mayer, V. A. Nasluzov, U. Birkenheuer, A. Hu, A. Matveev, A. V. Shor, M. S. K. Fuchs-Rohr, K. M. Neyman, D. I. Ganyushin, T. Kerdcharoen, A. Woiterski, and N. Rösch, ParaGauss, Version 2.2, Technische Universität München, 2001.

[70] M. Mayer, dissertation, Technische Universität München, 1999.

[71] A. V. Matveev, dissertation, Technische Universität München, 2003.

[72] K. M. Neyman, D. I. Ganyushin, A. V. Matveev, and V. A. Nasluzov, J. Phys. Chem. A **106**, 5022 (2002).

[73] K. M. Neyman, D. I. Ganyushin, Ž. Rinkevičius, and N. Rösch, Int. J. Quantum Chem. **90**, 1404 (2002).

[74] K. M. Neyman, D. I. Ganyushin, V. A. Nasluzov, N. Rösch, A. Pöppl, and M. Hartmann, Phys. Chem. Chem. Phys. **5**, 2429 (2003).

[75] N. Rösch, S. Krüger, M. Mayer, and V. A. Nasluzov, in *Recent Developments and Applications of Modern Density Functional Theory*, edited by J. M. Seminario (Elsevier, Amsterdam, 1996), p. 497.

[76] E. Engel, in *Relativistic Electronic Structure Theory — Fundamentals*, *Theoretical and Computational Chemistry Series*, edited by P. Schwerdtfeger (Elsevier, Amsterdam, 2003).

[77] N. Rösch, A. Matveev, V. A. Nasluzov, K. M. Neyman, L. Moskaleva, and S. Krüger, in *Relativistic Electronic Structure Theory — Applications*, *Theoretical and Computational Chemistry Series*, edited by P. Schwerdtfeger (Elsevier, Amsterdam, 2003).

[78] J. D. Bjorken and S. D. Drell, *Relativistic Quantum Mechanics* (Mc Graw-Hill, New York, 1964).

[79] P. Strange, *Relativistic Quantum Mechanics* (Cambridge University Press, Cambridge, 1998).

[80] W. Kutzelnigg, Int. J. Quantum Chem. **25**, 107 (1984).

[81] W. H. E. Schwarz and H. Wallmeier, Mol. Phys. **46**, 1045 (1982).

[82] R. E. Stanton and S. Havriliak, J. Phys. Chem. **81**, 1910 (1984).

[83] P. J. C. Aerts and W. C. Nieuwpoort, Int. J. Quantum Chem. Symp. **19**, 267 (1986).

[84] K. G. Dyall, J. Chem. Phys. **100**, 2118 (1993).

[85] K. G. Dyall, P. R. Taylor, K. Faegri, and H. Partridge, J. Chem. Phys. **95**, 2583 (1991).

[86] M. Mayer, S. Krüger, and N. Rösch, J. Chem. Phys. **115**, 4411 (2001).

[87] A. Matveev and N. Rösch, J. Chem. Phys. **118**, 3997 (2003).

[88] B. I. Dunlap and N. Rösch, Adv. Quantum Chem. **21**, 317 (1990).

[89] R. G. Parr and W. Yang, *Density-Functional Theory of Atoms and Molecules* (Oxford University Press, Oxford, 1989).

[90] A. S. Davydov, *Quantum Mechanics* (Pergamon, Oxford, 1976).

[91] M. Barysz and A. J. Sadlej, Theor. Chem. Acc. **97**, 260 (1997).

[92] M. Barysz and A. J. Sadlej, J. Mol. Struct.: THEOCHEM **537**, 181 (2001).

[93] V. Kelö, A. J. Sadlej, and B. A. Hess, J. Chem. Phys. **105**, 1995 (1996).

[94] R. Fukuda, M. Hada, and H. Nakatsuji, J. Chem. Phys. **118**, 1015 (2003).

[95] L. L. Foldy and S. A. Wouthuysen, Phys. Rev. **78**, 29 (1950).

[96] T. Nakajima and K. Hirao, J. Chem. Phys. **113**, 7786 (2000).

[97] W. A. de Jong, R. J. Harrison, and D. A. Dixon, J. Chem. Phys. **114**, 48 (2001).

[98] R. J. Buenker, P. Chandra, and B. A. Hess, Chem. Phys. **84**, 1 (1984).

[99] B. A. Hess, (ed.), *Relativistic Effects in Heavy-Element Physics and Chemistry* (Wiley, Chichester, 2003).

[100] A. Görling, dissertation, Technische Universität München, 1989.

[101] M. Staufer, dissertation, Technische Universität München, 1999.

[102] A. Szabo and N. S. Ostlund, *Modern Quantum Chemistry: Introduction to Advanced Electronic Structure Theory* (McGraw-Hill, New York, 1989).

[103] O. D. Häberlen, dissertation, Technische Universität München, 1993.

[104] J. D. Jackson, *Classical Electrodynamics* (Wiley, New York, 1999).

[105] N. C. Pyper, Mol. Phys. **64**, 933 (1988).

[106] V. M. Shabaev, J. Phys. B **28**, 5825 (1994).

[107] P. Chandra and B. A. Hess, Theor. Chim. Acta **88**, 183 (1994).

[108] P. A. M. Dirac, *The Principles of Quantum Mechanics* (Clarendon, Oxford, 1958).

[109] F. Jensen, *Introduction to Computational Chemistry* (John Wiley & Sons, Chichester, 1999).

[110] R. Bracewell, *The Fourier Transform and Its Applications* (McGraw-Hill, New York, 1999).

[111] E. C. Pollard, Phys. Rev. **47**, 611 (1935).

[112] W. Benenson, *Handbook of Physics* (Springer, New York, 2003).

[113] M. Mayer, O. D. Häberlen, and N. Rösch, Phys. Rev. A **54**, 4775 (1996).

[114] J. Griffith, *The Theory of Transition-Metal Ions* (Cambrige University Press, Cambrige, 1961).

[115] A. V. Luzanov, E. N. Babich, and V. V. Ivanov, J. Mol. Struct.: THEOCHEM **311**, 211 (1994).

[116] M. Schindler and W. Kutzelnigg, J. Chem. Phys. **76**, 1919 (1982).

[117] R. Ditchfield, Mol. Phys. **27**, 789 (1974).

[118] A. E. Hansen and T. D. Bouman, J. Chem. Phys. **82**, 5035 (1985).

[119] F. London, J. Phys. Radium **8**, 397 (1937).

[120] R. McWeeny, *Methods of Molecular Quantum Mechanics* (Academic Press Limited, London, 1992).

[121] G. H. Golub and C. F. V. Loan, *Matrix Computations* (Johns Hopkins University Press, Baltimore, MD, 1996).

[122] M. J. S. Dewar, J. A. Hashmall, and C. G. Venier, J. Am. Chem. Soc. **90**, 1953 (1968).

[123] V. Barone, J. Chem. Phys. **101**, 6834 (1994).

[124] A. D. Becke, Phys. Rev. A **38**, 3098 (1988).

[125] J. P. Perdew, Phys. Rev. B **33**, 8822 (1986).

[126] S. H. Vosko, L. Wilk, and M. Nusair, Can. J. Phys. **58**, 1200 (1980).

[127] N. Rösch, P. Knappe, P. Sandl, A. Görling, and B. I. Dunlap, in *The Challenge of d and f Electrons. Theory and Computation*, Vol. 394 of *ACS symposium series*, edited by D. R. Salahub and M. C. Zerner (American Chemical Society, Washington, DC, 1989), p. 180.

[128] *CRC Handbook of Chemistry and Physics*, 59 ed. (CRC Press, Boca Raton, Florida, 1978).

[129] G. Wessel and H. Lew, Phys. Rev. **92**, 641 (1953).

[130] Y. Ting and H. Lew, Phys. Rev. **105**, 581 (1957).

[131] A. J. H. Wachters, J. Chem. Phys. **52**, 1033 (1970).

[132] S. Huzinaga, J. Chem. Phys. **66**, 4245 (1977).

[133] J. P. Perdew and Y. Wang, Phys. Rev. B **33**, 8800 (1986).

[134] W. Kutzelnigg, U. Fleisher, and M. Schindler, *NMR-Basic Principles and Progress* (Springer, Heidelberg, 1990), Vol. 23, p. 165.

[135] J. R. Morton, K. F. Preston, and S. J. Strach, J. Phys. Chem. **83**, 533 (1979).

[136] A. Lund and K. Å. Thomas, Chem. Phys. Lett. **44**, 569 (1976).

[137] F. J. Adrian, B. F. Kim, and J. Bohandy, J. Chem. Phys. **82**, 1804 (1985).

[138] L. Severin, M. Richter, and L. Steinbeck, Phys. Rev. B **55**, 9211 (1997).

[139] P. Novák, J. Kuneš, W. E. Pickett, W. Ku, and F. R. Wagner, Phys. Rev. B **67**, 140403 (2003).

[140] S. Patchkovskii, J. Autschbach, and T. Ziegler, J. Chem. Phys. **115**, 26 (2001).

[141] B. J. Boland, J. M. Brown, and A. Carrington, Mol. Phys. **34**, 453 (1977).

[142] F. J. Adrian, E. L. Cochran, and V. A. Bowers, J. Chem. Phys. **36**, 1661 (1962).

[143] T. C. DeVore and W. Weltner, J. Am. Chem. Soc. **99**, 4700 (1977).

[144] W. Weltner Jr., *Magnetic Atoms and Molecules* (Van Nostrand Reinhold, New York, 1983).

[145] A. J. H. Wachters, J. Chem. Phys. **52**, 1033 (1970).

[146] M. E. Radzig and B. M. Smirnov, *Reference Data on Atoms, Molecules, and Ions* (Springer, Berlin, 1985).

[147] L. B. Knight and W. Weltner, J. Mol. Spec. **40**, 317 (1971).

[148] J. M. Brom, Jr., W. R. M. Graham, and W. Weltner, Jr., J. Chem. Phys. **57**, 4116 (1972).

[149] L. B. Knight, Jr. and W. Weltner, Jr. , J. Chem. Phys. **55**, 2061 (1971).

[150] L. B. Knight, Jr., T. A. Fisher, and M. B. Wise, J. Chem. Phys. **74**, 6009 (1981).

[151] P. H. Kasai and D. McLeod, Jr., J. Phys. Chem. **79**, 2324 (1975).

[152] M. Mayer, S. Krüger, and N. Rösch, J. Chem. Phys. **115**, 4411 (2001).

[153] S. Hassani, *Mathematical Physics. A Modern Introduction to Its Foundations* (Springer, New York, 1999).

[154] T. Belling, T. Grauschopf, S. Krüger, M. Mayer, F. Nörtemann, M. Staufer, C. Zenger, and N. Rösch, in *High Performance Scientific and Engineering Computing*, Vol. 8 of *Lecture Notes in Computational Science and Engineering*, edited by H.-J. Bungartz, F. Durst, and C. Zenger (Springer, Heidelberg, 1999), p. 439.

[155] L. B. Knight and J. Steadman, J. Chem. Phys. **77**, 1750 (1982).

[156] F. J. Adrian and V. A. Bowers, Chem. Phys. Lett. **41**, 517 (1976).

[157] J. M. Brown, T. C. Steimle, M. E. Coles, and R. F. Curl, J. Chem. Phys. **74**, 3668 (1981).

[158] R. W. Holmberg, J. Chem. Phys. **51**, 3255 (1969).

[159] G. Maier, H. P. Reisenauer, B. Rohnde, and K. Dehnicke, Chem. Ber. **116**, 732 (1983).

[160] G. Schreckenbach and T. Ziegler, J. Phys. Chem. A **101**, 3388 (1997).

[161] M. Engström, O. Vahtras, and H. Ågren, Chem. Phys. Lett. **243**, 263 (1999).

[162] P. H. Kasai, E. Hedaya, and E. B. Whipple, J. Am. Chem. Soc. **91**, 4364 (1969).

[163] J. H. Noordik, J. Schreurs, R. O. Gould, J. J. Mooij, and E. de Boer, J. Phys. Chem. **82**, 1105 (1978).

[164] O. Burghaus, M. Plato, M. Rohrer, K. Möbius, F. MacMillan, and W. Lubitz, J. Phys. Chem. **97**, 7639 (1993).

[165] J. C. Boettger, Phys. Rev. B **62**, 7809 (2000).

[166] S. Majumder, A. V. Matveev, and N. Rösch, Chem. Phys. Lett. **382**, 186 (2003).

[167] S. Patchkovskii and T. Ziegler, J. Phys. Chem. A **111**, 5730 (1999).

[168] S. Patchkovskii and T. Ziegler, J. Phys. Chem. A **105**, 5490 (2001).

[169] S. Varga, E. Engel, W. D. Sepp, and B. Fricke, Phys. Rev. A **59**, 4288 (1999).

[170] T. Belling, dissertation, Technische Universität München, 1999.

[171] M. J. Frisch, G. W. Trucks, H. B. Schlegel, G. E. Scuseria, M. A. Robb, J. R. Cheeseman, J. A. Montgomery Jr., T. Vreven, K. N. Kudin, J. C. Burant, J. M. Millam, S. S. Iyengar, J. Tomasi, V. Barone, B. Mennucci, M. Cossi, G. Scalmani, N. Rega, G. A. Petersson, H. Nakatsuji, M. Hada, M. Ehara, K. Toyota, R. Fukuda, J. Hasegawa, M. Ishida, T. Nakajima, Y. Honda, O. Kitao, H. Nakai, M. Klene, X. Li, J. E. Knox, H. P. Hratchian, J. B. Cross, C. Adamo, J. Jaramillo, R. Gomperts, R. E. Stratmann, O. Yazyev, A. J. Austin, R. Cammi, C. Pomelli, J. W. Ochterski, P. Y. Ayala, K. Morokuma, G. A. Voth, P. Salvador, J. J. Dannenberg, V. G. Zakrzewski, S. Dapprich, A. D. Daniels, M. C. Strain, O. Farkas, D. K. Malick, A. D. Rabuck, K. Raghavachari, J. B. Foresman, J. V. Ortiz, Q. Cui, A. G. Baboul, S. Clifford, J. Cioslowski, B. B. Stefanov, G. Liu, A. Liashenko, P. Piskorz, I. Komaromi, R. L. Martin, D. J. Fox, T. Keith, M. A. Al-Laham, C. Y. Peng, A. Nanayakkara, M.

Challacombe, P. M. W. Gill, B. Johnson, W. Chen, M. W. Wong, C. Gonzalez, and J. A. Pople, *Gaussian 03* Revison A.1, Gaussian Inc., Pittsburgh PA, 2003.

[172] E. van Lenthe, E. J. Baerends, and J. G. Snijders, Chem. Phys. Lett. **236**, 235 (1995).

[173] E. van Lenthe, J. G. Snijders, and E. J. Baerends, J. Chem. Phys. **105**, 6505 (1996).

[174] E. O. Steinborn and K. Ruedenberg, Adv. Quantum Chem. **7**, 1 (1973).

[175] E. O. Steinborn and K. Ruedenberg, Adv. Quantum Chem. **7**, 83 (1973).

[176] A. R. Edmonds, *Drehimpulse in der Quantenmechanik* (Bibliographisches Institut, Mannheim, 1964).

[177] E. U. Condon and G. H. Shortley, *The Theory of Atomic Spectra* (Cambridge University Press, Cambridge, 1935).

[178] D. Brink and G. Satchler, *Angular Momentum* (Oxford University Press, Oxford, 1968).

[179] L. E. McMurchie and E. R. Davidson, J. Comm. Phys. **26**, 218 (1978).

[180] A. Görling, S. B. Trickey, P. Gisdakis, and N. Rösch, in *Topics in Organometallic Chemistry*, edited by P. Hofmann and J. M. Brown (Springer, Berlin, Heidelberg, New York, 1999), Vol. 3, p. 109.

[181] Y. S. Lebedev, in *Modern Pulsed and Continuous-Wave Electron Spin Resonance*, edited by L. Kevan and M. Bowman (Wiley, New York, 1990), pp. 365–404.

[182] T. F. Prisner, Adv. Magn. Opt. Resonance **20**, 245 (1977).

[183] P. Jordan, P. Fromme, H. T. Witt, O. Klukas, W. Saenger, and N. Krauss, Nature **411**, 909 (2001).

[184] C. R. D. Lancaster, M. V. Bibikova, P. Sabatino, D. Oesterhelt, and H. Michel, Biol. Chem. **275**, 39364 (2000).

[185] B. Hales, J. Am. Chem. Soc. **98**, 7350 (1976).

[186] P. J. O'Malley, J. Phys. Chem. A **101**, 6334 (1997).

[187] P. J. O'Malley, J. Phys. Chem. A **102**, 248 (1998).

[188] P. J. O'Malley, J. Am. Chem. Soc. **120**, 5093 (1998).

[189] L. A. Eriksson, F. Himo, P. E. M. Siegbahn, and G. T. Babcock, J. Phys. Chem. A **101**, 9496 (1997).

[190] M. Kaupp, C. Remenyi, J. Vaara, O. L. Malkina, and V. G. Malkin, J. Am. Chem. Soc. **124**, 2709 (2002).

[191] M. Engström, F. Himo, A. Gräslund, B. Minaev, O. Vahtras, and H. Ågren, J. Phys. Chem. A **104**, 5149 (2000).

[192] B. Hammer, L. B. Hansen, and J. K. Nørskov, Phys. Rev. B **59**, 7413 (1999).

[193] F. Sim, A. St-Amant, I. Papai, and D. R. Salahub, J. Am. Chem. Soc. **114**, 4391 (1992).

[194] I. A. Topol, S. K. Burt, and A. A. Rashin, Chem. Phys. Lett. **247**, 112 (1995).

[195] B. Civalleri, E. Garrone, and P. Ugliengo, J. Mol. Struct.: THEOCHEM **419**, 227 (1997).

[196] F. B. van Duijneveldt, IBM Res. Rept. #16437 945 (1971).

[197] V. A. Nasluzov and N. Rösch, Chem. Phys. **210**, 413 (1996).

[198] S. Boys and F. Bernardi, Mol. Phys. **19**, 553 (1970).

[199] M. Fuchs, A. M. Shor, and N. Rösch, Int. J. Quantum Chem. **86**, 487 (2002).

[200] I. Tunon, E. Silla, and J.-L. Pascual-Ahuir, J. Am. Chem. Soc. **115**, 2226 (1993).

[201] J. H. Noordik, J. Schreuers, R. O. Gould, J. J. Mooij, and E. de Boer, J. Phys. Chem. **82**, 1105 (1978).

[202] M. C. Z. Sojka and E. Giamello, J. Phys. Chem. **101**, 4831 (1997).

[203] M. Shelef, Chem. Rev. **95**, 209 (1995).

[204] E. Giamello, D. Murphy, G. Magnacca, C. Morterra, Y. Shioya, T. Nomura, and M. Anpo, J. Catal. **136**, 510 (1992).

[205] A. Pöppl and M. Hartmann, in *Impact of Zeolites and other Porous Materials on the New technologies at the Beginning of the New Millennium, Studies in Surface Science and Catalysis*, edited by A. Aiello, G. Giordano, and F. Testa (Elsevier, Amsterdam, 2002), Vol. 142, p. 375.

[206] T. Rudolf, A. Pöppl, W. Hofbauer, and D. Michel, Phys. Chem. Chem. Phys. **3**, 2167 (2001).

[207] K. Albert, K. M. Neyman, G. Pacchioni, and N. Rösch, Inorg. Chem. **35**, 7370 (1996).

[208] A. Veillard, Theor. Chim. Acta **12**, 405 (1968).

[209] A. Pöppl, T. Rudolf, P. Manikandan, and D. Goldfarb, J. Am. Chem. Soc. **122**, 10194 (2000).

[210] J. Laane and J. R. Ohlsen, Prog. Inorg. Chem. **27**, 465 (1980).

[211] J. H. Lunsford, J. Phys. Chem **72**, 2141 (1968).

[212] W. Känzig and M. H. Cohen, Phys. Rev. Lett. **3**, 509 (1967).

[213] D. Nachtigallová, P. Nachtigall, M. Sierka, and J. Sauer, Phys. Chem. Chem. Phys. **1**, 2019 (1999).

[214] W. F. Schneider, K. C. Hass, R. Ramprasad, and J. B. Adams, J. Phys. Chem. **100**, 6032 (1996).

[215] H. V. Brand, A. Redondo, and P. J. Hay, J. Phys. Chem. B **101**, 7691 (1997).

[216] P. Treesukol, J. Limtrakul, and T. N. Truong, J. Phys. Chem. B **105**, 2421 (2001).

[217] I. V. Yudanov, V. A. Nasluzov, and N. Rösch, unpublished.

Publications

1 D. I. Ganyushin, K. M. Neyman, N. Rösch, *Calculation of Hyperfine Coupling Constants Using a Relativistic Density Functional Douglas-Kroll Method*, in preparation.

2 K. M. Neyman, D. I. Ganyushin, V. A. Nasluzov, N. Rösch, A. Pöppl, M. Hartmann, *Electronic g-Values of Na^+–NO and Cu^+–NO Complexes in Zeolites: Analysis Using a Relativistic Density Functional Method*, Phys. Chem. Chem. Phys., **5**, 2429 (2003).

3 K. M. Neyman, D. I. Ganyushin, Ž. Rinkevičius, N. Rösch, *Hydrogen-Bonding Effects on Electronic g-Tensor of Semiquinone Anion Radicals: Relativistic Density Functional Investigation*, Int. J. Quantum Chem., **90**, 1404 (2002).

4 K. M. Neyman, D. I. Ganyushin, A. V. Matveev, V. A. Nasluzov, *Calculation of Electronic g-Tensors Using a Relativistic Density Functional Douglas-Kroll Method*, J. Phys. Chem. A, **106**, 5022 (2002).

Acknowledgements

This work has become possible due to the generous and outgoing support of many people, it is hardly accomplishable to name all of them here.

First and foremost, I would like to thank Prof. Dr. Notker Rösch, for constant support and guidance, in scientific matters and beyond, and for helping me to make this thesis much better than its first version.

I would like to thank my supervisor Dr. K. M. Neyman for his patience, stimulation, fruitful discussions, and productive cooperations.

Of course, I would like to thank Dr. A. V. Matveev, for his everyday help.

I would like to express my gratitude to my other friends, colleagues, and guests of Prof. Rösch's research group, past and present:

Dr. W. Alsheimer, A. Basha, S. Bosko, Dr. C. Bussai, Dr. S.-H. Cai, Dr. Z. Chen, P. Chuichay, Dr. N. Cruz Hernández, A. Deka, Dr. R. Deka, Dr. D. Egorova, Dr. M. Fuchs-Rohr, Dr. M. Garcia Hernández, Dr. M. Gelin, A. Genest, M. Girju, Dr. A. Gordienko, Dr. V. Igoshin, C. Inntam, R. Kosarev, Dr. S. Krüger, K.-H. Lim, Dr. S. Majumder, Dr. D. Mamaluy, Dr. L. Moskaleva, Dr. V. Nasluzov, Ž. Rinkevičius, F. Schlosser, Dr. A. Shor, E. Shor, K. Siriwong, M. Suzen, Dr. G. Vayssilov, E. Vladimirov, Dr. A. Voityuk, Dr. A. Woiterski, Dr. I. Yudanov, and many others.

Finally, I would like to thank my family and Inga Khristoforova for their patience, forbearance, and encouragement.